ALLOSTERIC INHIBITION OF LRRK2-MEDIATED PARKINSON'S DISEASE WITH CONSTRAINED PEPTIDES

by

LEAH HELTON

(Under the Direction of Eileen Kennedy)

ABSTRACT

Parkinson's Disease (PD) is the second most common neurodegenerative disease affecting nearly 10 million people worldwide. Leucine Rich Repeat Kinase 2 (LRRK2) is the most common genetic contributor to disease pathogenesis, and LRRK2-mediated PD is indistinguishable from the sporadic form of the disease. Understanding how LRRK2-mediated PD functions could provide valuable insight into molecular pathways that are common between both familial and sporadic forms of the disease. Efforts to inhibit the catalytic activity of pathogenic LRRK2 have yielded effective and potent small molecule kinase inhibitors, yet these drugs have been limited in therapeutic potential due to adverse side effects. As an attempt to more subtly and specifically modulate LRRK2 activity, we have designed and developed stapled peptide allosteric inhibitors of LRRK2.

Efforts to inhibit the catalytic activity of LRRK2 were previously limited to the kinase domain, yet protein-protein interactions have frequently been identified as largely involved in the disease-causing pathology of LRRK2. Specifically, LRRK2 dimerization, association with Fas Associated Death Domain (FADD), and localization with Rabs were all identified as upregulated with mutant-LRRK2 expression. We sought to disrupt these interactions using constrained peptides.

All-hydrocarbon stapled peptides bridge the gap between small molecules and biologics. By identifying peptide sequences that are major contributors to the binding site of interest, we can synthetically mimic these regions and reinforce the secondary structure via the introduction of a hydrocarbon constraint. We designed distinct peptides for downregulating LRRK2 dimerization, disrupting LRRK2 association with FADD, and inhibiting LRRK2 recruitment by Rab proteins. While these constrained peptides are distinct in nature, they all serve the common goal of allosterically regulating LRRK2 to downregulate its pathogenic activity *in vitro.* This work represents first-in-class allosteric inhibition of LRRK2, which can serve as a tool for researchers aiming to understand LRRK2 pathogenesis and highlights the long-term therapeutic potential of allosteric inhibition of LRRK2.

INDEX WORDS: Stapled Peptide, Leucine Rich Repeat Kinase 2, Dimerization, Allosteric Inhibitor, Parkinson’s Disease, Protein Kinase

ALLOSTERIC INHIBITION OF LRRK2-MEDIATED PARKINSON'S DISEASE WITH CONSTRAINED PEPTIDES

by

LEAH HELTON

B.S., University of Tennessee at Chattanooga, 2016

A Dissertation Submitted to the Graduate Faculty of The University of Georgia in Partial Fulfillment of the Requirements for the Degree

DOCTOR OF PHILOSOPHY

ATHENS, GEORGIA

2022

ALLOSTERIC INHIBITION OF LRRK2-MEDIATED PARKINSON'S DISEASE WITH CONSTRAINED PEPTIDES

by

LEAH HELTON

Major Professor:	Eileen Kennedy
Committee:	Shelley Hooks
	Natarajan Kannan
	Eva Strauch

Electronic Version Approved:

Ron Walcott
Vice Provost for Graduate Education and Dean of the Graduate School
The University of Georgia
May 2022

DEDICATION

To Anna, who is my most fervent advocate and biggest challenger- I could not have done this without you. To my parents, who believed in me before I believed in myself. So much of where I am and what I accomplish is due to the love and support provided by the three of you. Thank you.

ACKNOWLEDGEMENTS

First and foremost, I would like to thank Dr. Kennedy, who has always been a source of inspiration. Thank you for believing in me, trusting me, challenging me, and supporting me. I am eternally grateful to have you in my life as a mentor and a friend.

To Ameya Limaye and Dr. George Bendzunas, my work brother and work husband. You two have taught me more than any class ever could. I'm grateful I was able to learn from you and alongside you throughout this process- thank you for everything.

I would like to thank Dr. Arjan Kortholt, who graciously provided me with the opportunity to spend a summer working in his lab at the University of Groningen, during which time I developed a foundational understanding of cellular biology pertaining to LRRK2.

I would like to thank Dr. Hardy Rideout, who has served as both a mentor and a collaborator throughout my time at UGA. I have the utmost respect for you as both a scientist and person, and I am grateful to have met along my journey.

To Julie Simmons, who kept my head above water throughout this journey. Thank you for listening and providing a safe space- I'm eternally indebted to you.

To my committee members, Dr. Shelley Hooks, Dr. Natarajan Kannan, and Dr. Eva Strauch, for providing guidance and input on my project over the past 4 years. You all gave me the space to think deeper and more critically about my work, which made me a better scientist.

To Brinck- the PhD is great, but our friendship is undoubtedly the best thing to come out of my time in Athens. Thanks for listening to my presentations before I had any idea what I was talking about.

TABLE OF CONTENTS

Page

LIST OF FIGURES

Page

CHAPTER 1

CONSTRAINED PEPTIDES AS ALLOSTERIC REGULATORS OF PROTEIN-PROTEIN INTERACTIONS

1.1 Statement of Purpose

Protein-Protein Interactions (PPIs), which were long considered "undruggable", have an expansive role within human disease[1-3]. While small molecules are being developed to disrupt these interactions due to their favorable drug-like properties, some PPIs are composed of elongated surfaces ill-suited to small molecule inhibition (reviewed here: [4, 5]). These interfaces, which are often composed of alpha helices, are well suited to peptide therapeutics due to their ability to mimic the endogenous PPI[6, 7]. Efforts to develop peptides as therapeutics are limited in part by the poor solubility of peptides, their inability to permeate cells, and short half-life. The development of chemical modifications to improve the properties of peptides as therapeutics resulted in the development of all-hydrocarbon stapled peptides[8-10]. By introducing non-natural amino acids along the non-binding interface and chemically constraining these amino acids to form a "staple", these constrained peptides can permeate cells, resist proteolytic cleavage, and retain their secondary structure longer than native peptides[9, 10].

1.2 Protein-Protein Interactions as a Therapeutic Target

Intracellular Protein-Protein Interactions are an essential component of many disease-associated cellular pathways, and the network of PPIs driving disease pathogenesis continues to expand[11-13]. Unlike traditional therapeutic targets such as receptors and enzymes, which contain a distinct ligand binding site well suited to small molecules, PPIs are composed of an elongated contact area that is typically hydrophobic and difficult to outcompete[4, 14]. Efforts to

develop modulators of PPIs have yielded compounds falling into three main categories: small molecules, peptides, and biologics[4, 5]. Each of these distinct types of modulators have both advantages and disadvantages. Small molecule inhibitors, which are typically ill-suited to the large hydrophobic interfaces composing most PPIs, are capable of disrupting PPIs when the interface of interest maintains a "pocket" or if the binding region is relatively small in area[1, 11, 14, 15]. Further, small molecule inhibitors have favorable oral bioavailability and can permeate cell membranes, but these advantages are offset by the wide range of proteins small molecules often bind. Due to the engagement of few amino acids, small molecules are likely to exhibit off-target effects due to low selectivity for one specific protein of interest. On the other end of the spectrum lies biologics, most commonly in the form of antibody therapeutics. The major limitation in development of antibodies as inhibitors of protein-protein interaction is the fact that they are unable to permeate cells to target intracellular PPIs[16].

1.3 Potential for Peptides as Therapeutics

Peptides represent a unique opportunity for drug development as they bridge the gap between small molecule therapeutics and biologics. While the original utilization of native peptides, such as insulin and vasopressin, incited excitement within the peptide field, the limitations of native, non-modified peptides quickly tampered that enthusiasm[17-19]. Due to the poor oral bioavailability, short half-life, lack of desired secondary fold, and susceptibility to proteolytic cleavage, many of the opportunities within the field of peptide therapeutic development faced a mountain of challenges[17]. While optimizing peptide length and modifying amino acid sequences to improve stability yielded peptides with improved therapeutic properties (reviewed here [20]), work to introduce chemical constraints to improve the therapeutic potential of peptides resulted in the development of constrained or "stapled"

peptides[21, 22]. By modifying the peptide sequence to introduce a constraint, constrained peptides can permeate cells and target intracellular protein interfaces that were previously considered “undruggable” due to their inaccessibility for biologics[22-24].

1.4 Allosteric Regulation of Protein Kinases with Constrained Peptides

The human kinome, which is composed of over 540 protein kinases, is one of the major therapeutic targets due to the involvement in kinases across a wide range of cellular events[25]. As the involvement of protein kinases in human diseases is often directly linked to their catalytic activity, direct inhibition of the ATP-binding pocket is generally considered a favorable approach. Indeed, of the 68 FAD-approved therapeutics that target protein kinases, fewer than eight are considered “allosteric” inhibitors[26-28]. However, due to both the high conservation of the ATP-binding pocket and the complex signaling networks involving protein kinases, abolishing the catalytic activity of a protein kinase of interest is not always a trivial or valid therapeutic approach.

“As a strategy for selective kinase inhibition, allosteric disruption of protein kinases may offer a more selective form of regulation by targeting unique regions or surfaces that are imperative for overall kinase function. Protein-protein interaction surfaces, whether intramolecular or intermolecular, often require relatively large, shallow, and hydrophobic surfaces that are particularly well suited for peptide targeting. However, native peptides are inherently susceptible to various processes including proteolytic cleavage, lack of solubility, and loss of the secondary structural fold that may be required for PPIs[9]. In order to circumvent the issues seen with native peptides, constrained peptides were developed to “lock” the peptide in a favorable conformation and embed the backbone, which makes the peptide resistant to

proteolytic cleavage[29]. In addition, various chemical modifications can be made to improve the hydrophilicity, specificity, and biological relevance of the compound[30].

One synthetic strategy for constraining peptides is hydrocarbon stapling [31]. In this approach, non-natural olefinic amino acids are incorporated into a peptide sequence of interest during solid-phase synthesis, and the olefinic side chains are subsequently joined together to form an all-hydrocarbon staple using ring-closing metathesis chemistry. In the case of peptide helices, the secondary structural fold of the helix can be synthetically reinforced by incorporation of a staple by positioning the olefinic amino acids around one or two helical turns. Hydrocarbon stapled peptides possess the potential to have multiple favorable properties including reinforced helical conformation, resistance to proteolytic degradation, and enhanced cell permeability through an active transport mechanism [8, 9].”[1] In this dissertation, we will discuss how hydrocarbon stapled peptides have been utilized to allosterically inhibit Leucine Rich Repeat Kinase 2 (LRRK2).

[1] Helton, L.G., Limaye, A.J., Bendzunas, G.N., & Kennedy, E.J. “Novel Stabilized Peptide Inhibitors of Protein Kinases.” Next Generation Kinase Inhibitors. *Springer*, **2020**, p. 141-167.
Portions of this chapter reprinted here with permission from publisher.

CHAPTER 2

LEUCINE RICH REPEAT KINASE 2 (LRRK2) PEPTIDE MODULATORS: RECENT ADVANCES AND FUTURE DIRECTIONS[2]

[2] Helton, L.G., Rideout, H.J., Herberg, F.W., & Kennedy, E.J. *Peptide Science* **2021**, e24251. Reprinted here with permission from publisher.

2.1 Abstract

Leucine rich repeat kinase 2 (LRRK2) is the most common genetic contributor to Parkinson's disease (PD), a complex neurodegenerative disorder affecting nearly 10 million people worldwide. Pathogenic mutations within LRRK2 often induce increased kinase activity, an effect that can be abolished with many small molecule inhibitors; however, these small molecule inhibitors are currently limited by their toxicities. Given the large and complex nature of LRRK2, more recent efforts have focused on protein–protein interactions (PPIs) involving LRRK2 and how they can contribute to PD. Here, we review recently resolved structures of LRRK2 and highlight unique interfaces driving both catalytic and non-catalytic activities. Combining new structural information with established *in vitro* and *in vivo* data clarifies the role of PPIs in driving LRRK2-mediated disease pathogenesis. Since constrained peptides and peptidomimetics have the potential to engage with elongated, hydrophobic interfaces that were previously considered “undruggable,” they may provide a unique handle for LRRK2 targeting. Here, we discuss the use of constrained peptides and peptidomimetics to target LRRK2 as a strategy to downregulate its pathological activity.

2.2 Introduction

Affecting over 10 million people worldwide, Parkinson's disease is the second most common neurodegenerative disorder after Alzheimer's disease. Current treatment options consist of dopamine therapy, lifestyle changes, invasive cell replacement therapies or deep brain stimulation, and the effectiveness of these therapies vary on a case-by-case basis[32, 33]. The limited number of therapeutic options is due, in part, to the complex and elusive nature of the disease. Work to understand how aging, genetics, and environmental factors contribute to disease progression is ongoing, and the identification of genetic mutations as causative for the disease

has garnered significant interest[34]. Since its link to PD was definitively established in 2004, PARK8 encoding for leucine rich repeat kinase 2 (LRRK2) has been identified as a major genetic contributor to Parkinson's disease[35-37]. However, the clinical picture of LRRK2 patients is often indistinguishable from the sporadic form of the disease, making its mechanism of disease pathogenesis particularly intriguing. Further, LRRK2 kinase hyperactivation can also be present in the absence of LRRK2 mutations, indicating underlying signaling pathways could be driving pathogenesis in the idiopathic disease state[38]. In addition to the role of LRRK2 mutations in PD pathogenesis, identical and novel mutations have also been identified in Crohn's disease[39-41], leprosy[42-45], tuberculosis[46], and cancer[47-49] (reviewed here[50]). While the association between LRRK2 and these diseases is less clear than its association with PD[51-54], the identified similarities in terms of mechanisms of disease pathogenesis warrant attention.

LRRK2 is composed of seven domains which are depicted in **Figure 2.1**. The Ras of complex proteins (Roc) and COR (C-terminal of Roc) domains, although distinct in structure, form the RocCOR tandem domain. The Roc domain is responsible for GTP binding and hydrolysis, where the COR domain has been experimentally and structurally linked to driving protein dimerization [55, 56]. This tandem domain is a defining characteristic of Roco family proteins, which are present in bacteria, archaea, metazoans, and plants[57]. The surrounding scaffolding and/or catalytic domains are what distinguish the Roco proteins from one another. In LRRK2, the serine/threonine kinase domain directly follows the RocCOR tandem domain and is responsible for driving both autophosphorylation and downstream substrate phosphorylation[58]. While the remaining four domains lack catalytic activity (armadillo repeat, ankyrin repeat, leucine-rich repeat region, and WD40 domain), they are essential for mediating protein–protein

and scaffolding interactions, as well as regulating the activities of the catalytically active domains[59, 60].

The relatively recent identification of a subset of Rab GTPases as downstream substrates of LRRK2 has helped clarify the understanding of how pathogenic mutations affect catalytic activity[58, 61] as well as provide better understanding for the normal functions of LRRK2. Previous work to understand the catalytic activity of LRRK2 utilized peptide substrate mimetics, LRRKtide and NICtide, which were critical in early-stage identification of kinase inhibitors of LRRK2[62, 63]. As cell or tissue source can greatly impact the levels of endogenous Rab phosphorylation, LRRKtide and NICtide are commonly used in in vitro kinase assays as a means of measuring the intrinsic kinase activity of LRRK2 (reviewed here[64]). LRRK2 phosphorylation of downstream Rab GTPases can subsequently alter their association with effector proteins, leading to alterations in ciliogenesis, lysosomal function, immune responses, and other essential cellular functions[65, 66].

Mutations that contribute to PD pathogenesis are primarily localized to the RocCOR GTPase domain (N1437H, R1441G/C/H, Y1699C) and the protein kinase domain (G2019S, I2020T)[67] (**Figure 2.1**), with the G2019S mutation being the most common. Both the I2020T and G2019S mutations were found to enhance LRRK2 kinase activity, although the relative scale of this effect is largely context dependent based on cell line and model system[68-71]. The mutations found within the RocCOR GTPase domain have a more controversially discussed effects on LRRK2 kinase activity[59], but they have been repeatedly shown to reduce GTPase activity and promote GTP binding[66, 72]. Understanding how point mutations may contribute to LRRK2 activity has been limited, in part, by the lack of structural knowledge regarding LRRK2. Fortunately, recent work has led to the determination of a low resolution *in situ* full-

length cryo-ET structure[73], a high resolution cryo-EM structure of the Roc, COR, Kinase, and WD40 (RCKW) domains[74], and most recently, a full-length cryo-EM structure[75]. Here, we will discuss insights gleaned from these structures with regards to potential mechanisms of allosteric regulation and the potential for development of peptidomimetics and/or constrained peptides targeting these allosteric regulatory mechanisms.

2.3 Determining the Structure-Function Relationship of LRRK2

Most attempts to target LRRK2 have focused on inhibition of the ATP-binding pocket using small molecule (kinase) inhibitors. Early work to develop a selective LRRK2 inhibitor yielded LRRK2-IN-1, which inhibited both WT and G2019S-LRRK2 in the low nanomolar range and demonstrated limited off-target effects[76]. However, its clinical usage was limited by its inability to cross the blood-brain barrier (BBB) and off-target effects on inflammatory pathways[77]. Two more early stage LRRK2 inhibitors, CZC-25146 and TAE684, were similarly limited by poor brain penetration and limited effects on LRRK2 in the central nervous system (CNS), respectively[78, 79]. The challenge to selectively target LRRK2 with small molecules paired with minimal effects on the CNS triggered a shift in research toward the development of brain-permeable small molecules that could inhibit LRRK2 in the CNS. This resulted in the development of multiple compounds which demonstrated nanomolar affinity, excellent selectivity, and the ability to cross the BBB and the potential to inhibit LRRK2 in vivo[80-82]. Such compounds, MLi-2[83], PF-475, and PF-360[84] have been used both in cellular models as well as *in vivo*[85]. Initial concerns pertaining to small molecule kinase inhibition inducing notable toxicities in the lung and kidneys of nonhuman primates were recently shown to be a reversible phenotype[86, 87]. Further, some compounds induced filament formation where cytoplasmic skein-like filaments were found to co-localize with microtubules in

WT LRRK2 following application of kinase inhibitors, in the context of some pathogenic mutations[88, 89] or by removing the N-terminal non-catalytic domains (RCKW-only, Schmidt et al. [59]). Interestingly, genetic ablation of LRRK2 kinase activity is insufficient to induce filament formation, pointing to a more complex relationship between kinase inhibition and this overt cellular re-localization. It is critical to point out, however, that this phenotype has only been reported with over-expressed LRRK2. With the availability of better antibodies for immunohistochemical detection of endogenous LRRK2, it might be possible to observe such structures at endogenous levels in tissues, such as the lung, where expression levels are high.

Further efforts to develop potent and selective small molecule inhibitors of LRRK2 with limited toxicity are ongoing, and there are multiple inhibitors that exhibit potential as therapeutics[87, 90], with some compounds in clinical trials. However, given the complexity of LRRK2 and the difficulty in developing small molecule inhibitors to effectively target LRRK2, allosteric inhibitors of LRRK2 may serve as a unique avenue for the development of LRRK2-targeting therapeutics. Further, a better understanding of how structural changes are driving catalytic activity may be advantageous for the development of multiple inhibitor classes including ATP- or GTP-competitive inhibitors and allosteric effectors, for example peptide inhibitors or peptidomimetics.

Early attempts to characterize the structure of LRRK2 relied predominantly on bacterial homologs of LRRK2, namely Roco proteins. Characterized by the Roc domain directly preceding the COR domain, this family of proteins was first discovered in Dictyostelium discoideum, but, as noted above, Roco family members have since been identified in bacteria, archaea, metazoans, and plants[55, 91]. All members of the Roco protein family contain a RocCOR tandem domain, but the presence or absence of various additional catalytic and

scaffolding domains may serve to diversify RocCOR function. Since LRRK2 mutations were first associated with PD, it attracts substantial attention among all the Roco proteins; however, LRRK2 is also one of the largest family members (with 2527 amino acids), making crystallization and characterization difficult.

A major hurdle in the LRRK2 field that significantly slowed structural advancements was related to protein production. Due to the size and complexity of LRRK2, expressing and purifying full-length or truncated constructs of LRRK2 were extremely challenging. Alternatively, attempts were made to structurally study LRRK2 homologs from other species, however, protein expression and purification of these homologs were also not straightforward[92, 93]. Until recently, the available crystal structures pertaining to LRRK2 were primarily truncated forms of the protein, crystal structures of less complex bacterial homologs, or structural models[92, 94-96]. These structures provided valuable insight into potential structural motifs present in LRRK2, but the biological relevance could not be fully elucidated with these incomplete or modeled forms.

More recently, three structures of human LRRK2 have been solved using either cryo-ET[73] or cryo-EM[74, 75]. Using a combination of Cryo-ET and integrative modeling, a 14 Å full-length structure of LRRK2 revealed that LRRK2 oligomerizes around microtubules when pathogenically mutated. This formation of a right-handed helix around microtubules was determined using the I2020T mutant form of LRRK2, and only the C-terminal domains (Roc, COR, kinase, and WD40) were involved in microtubule association which is consistent with previous cell-based data[88]. This structure of the active form of the kinase highlighted a few key interfaces driving localization of LRRK2 around the microtubules: dimerization of WD40 domains and the COR:COR dimer interface. The GTPase domain is essential for driving the

interaction of LRRK2 with microtubules and is topologically adjacent to the kinase domain, indicating they may serve to regulate one another. Further, they were able to identify the WD40: WD40 interface as being a key driver of filament formation, which highlights a potential area of allosteric regulation to eliminate the formation of toxic oligomers around microtubules in the presence of Type I kinase inhibitors[73].

Separately, a higher resolution (3.5 Å) cryo-EM structure of a truncated form of the protein bearing the C-terminal half of wildtype LRRK2 containing the Roc, COR, Kinase and WD40 domains ($LRRK2^{RCKW}$) was solved[74]. In this structure of a most likely artificial trimer, they found that the kinase domain was in the open, inactive conformation. Deniston et al. combined their structure with the previously discussed 14 Å *in situ* structure of LRRK2 bound to microtubules and concluded that the kinase domain needs to be in a closed conformation to dock to microtubules[74]. Further, they resolved two potential conformations for the microtubule bound LRRK2: one mediated by WD40 dimerization and one mediated by COR dimerization. This is consistent with recent cell data showing that LRRK2-inhibitor induced filaments are populated with dimeric LRRK2[97].

In addition, structures of kinase-inactive forms of both full-length monomeric and dimeric LRRK2 were solved via cryo-EM at resolutions of 3.7 and 3.5 Å, respectively[75]. In both the monomeric and dimeric form, the N-terminal region of LRRK2 was flexible, which may explain previous difficulties with both protein purification and crystallization. The reported difference (in RMSD) between the RCKW region of this full-length structure and the Cryo-EM LRRK2RCKW structure was 5.2 Å, with the largest difference being a shift in the RocCOR domains, although this could be attributed to purification conditions. This structure confirms the importance of the COR domain for mediating dimerization as well as the importance of a C-

terminal helix, while also identifying new mechanisms of self-regulation that were not previously appreciated (**Figure 2.2**).

Taken together, these structures revealed multiple new interfaces and structural motifs that may allow us to better understand LRRK2 function. Here, we will discuss in detail these protein-protein interaction interfaces, how they may be functioning and regulated, and why using peptide-based molecules or peptidomimetics may be an effective strategy for targeted PPI disruption.

2.4 Potential Targeting Allosterically Regulated Sites

Attempts to inhibit the ATP-binding pocket of LRRK2 activity have yielded a library of both Type I and Type II inhibitors with high levels of selectivity and binding affinity, but both classes have several limitations[98]. While inhibition of LRRK2 kinase activity with certain small molecules yields neuroprotective effects and prevents aberrant endolysosomal function, all currently available kinase inhibitors have reached a clinical roadblock[99]. (Reviewed here[100]). Several Type I inhibitors were found to trigger the re-localization of LRRK2 microtubules, a notable pitfall when considering therapeutic viability, whereas many Type II inhibitors demonstrated a lack of specificity for pathogenic forms of LRRK2 and did not alter LRRK2 biomarker phosphorylation[101]. More recent efforts were focused on the development of small molecule inhibitors with specificity toward only the pathogenic G2019S mutant, however, these compounds were found to be poorly brain penetrant[102]. The development of ATP-competitive catalytic inhibitors is rapidly expanding and yielding many exciting novel inhibitors that may be able to overcome some major challenges in the field including target selectivity, selectivity for pathogenic forms of LRRK2 and brain penetrance. The pros and cons of catalytic vs allosteric inhibition of LRRK2 remain undefined, and thus efforts to allosterically

modulate LRRK2 may serve as a complementary strategy for both therapeutic and research purposes.

Protein kinases often contain a highly conserved ATP-binding region, which makes selective targeting of specific kinases a difficult task[103]. As altered kinase activity has been directly associated with over 200 diseases, developing strategies to allosterically inhibit protein kinases is of critical importance[104]. One opportunity for more selective inhibition of kinase activity lies in disrupting both intra- and intermolecular protein–protein interactions (PPIs) that regulate catalytic activity. While inhibition of PPIs can be achieved with a wide range of tools, including small molecules, PROTACs, and nanobodies, the profile of constrained peptides makes them an attractive tool for PPI perturbation. This offers a unique opportunity for peptide-based molecules, which could help to bridge the gap in knowledge regarding how protein–protein interactions drive disease pathogenesis. Many of the interfaces that are of interest in LRRK2 are elongated surfaces that rely on the engagement of multiple residues, thereby making these regions ill-suited for targeting by small molecule inhibitors. Peptidomimetics and constrained peptides, on the other hand, can target extended surfaces with a high degree of specificity and potency in many different disease states[8, 9]. Further, developing peptide-based allosteric inhibitors of LRRK2 could allow for a better understanding of the subtle changes within the ATP-binding pocket during its activation cycle and thus glean insight into small molecule design. By relying on the engagement of many amino acid residues, peptide-based inhibitors have the potential to selectively target mutant forms of LRRK2 over the wild type. By developing mutant specific inhibitors, we could better understand how LRRK2 activity and localization is being affected, thus expanding our understanding of LRRK2-mediated PD beyond its kinase activity. Here, in combination with recent structural developments, we discuss how

larger molecules such as constrained peptides or peptidomimetics may be utilized to target LRRK2.

The development of both Type I and Type II kinase inhibitors and the stark difference in effect on filament formation highlighted the need to better characterize the ATP binding pocket of LRRK2 and how it is distinguishable from typical protein kinases. By comparing the kinase domain of the three structures, notable similarities and differences can be seen.

he $LRRK2_{RCKW}$ structure revealed a unique characteristic present in LRRK2 that distinguishes it from typical protein kinases, which is that the phenylalanine in the classical DFGψ motif is a tyrosine residue in LRRK2[105]. The hydroxyl group of this tyrosine (Y2018) binds to the backbone of an isoleucine (I1933) and destabilizes the regulatory triad, which typically provides a pocket for ATP and Mg2+ binding[60]. When Y2018 is mutated to a phenylalanine, LRRK2 is hyperactive and docks onto microtubules[105]. The function of the DYGψ motif, accompanied by the fact that G2019S is the most common pathogenic mutation in LRRK2, highlights the importance of this region for controlling the catalytic activity of LRRK2. In the full-length cryo-EM structure, the activation segment was revealed to form an alpha helix (**Figure 2.3a**, cyan). When comparing the two structures, there is a significant difference in the orientation of the DYG residues (**Figure 2.3a**).

Looking beyond the DYGψ motif, there are other features of the kinase domain that make it an attractive target for allosteric regulation (reviewed here [29]). The αC helix, a highly conserved helix within the active site of the kinase domain, is capped by regions that are susceptible to mediating protein–protein interactions. The αC helix is particularly interesting due to the duality of its function: one portion of the helix contributes to the active site, while the other portion of the helix interacts with the C-terminal helix extending from the WD40 domain,

which directly docks onto the αC-β4 loop in the inactive conformation (**Figure 2.3b**)[60, 74]. This C-terminal helix likely forms an extensive interface with the backbone of the kinase domain and may function to allosterically regulate the conformation and subsequent activation of the kinase domain. Further, the C-terminal helix also forms interactions with the COR domain (**Figure 2.3b**), which could help regulate its role in LRRK2 dimerization (discussed below). The identification of the C-terminal helix and the better understanding of the complexity of the DYG motif will allow for the development of improved allosteric and/or competitive inhibitors of LRRK2 kinase activity.

Dimerization of LRRK2 has long been implicated as major regulator of LRRK2 activity and subcellular localization, but efforts to inhibit dimerization have remained elusive. The COR domain of LRRK2 is believed to be a major energetic contributor of dimerization, but the interface that composes this protein–protein interaction is inconsistent across different structures. In bacterial homologs and early models of LRRK2, both the COR:COR interaction and Roc:Roc interaction were thought to be largely driven by a small alpha-helix in the CORB domain along with another helix in the Roc domain[92, 106, 107]. Based on this model, all-hydrocarbon stapled peptides were designed to mimic these helices and disrupt dimerization. This work produced a first-in-class allosteric inhibitor of LRRK2 dimerization LRRK2 Roc Inhibiting Peptide (LRIP4)[107]. LRIP4 binds LRRK2 in the nanomolar range, permeates cells, disrupts dimerization, decreases kinase activity, reduces ROS production, and decreases neuronal apoptosis[107]. This work highlights the importance of LRRK2 dimerization in mediating catalytic and pathogenic activity and sets the stage for future constrained peptide development with regards to LRRK2.

Recently released structures have revealed that while the LRRK2RCKW structure existed largely as a monomer in solution, they identified a COR:COR interface when $LRRK2_{RCKW}$ is mapped onto the full-length cryo-ET structure. In line with previously solved structures and models, the recently released full-length cryo-EM structure of LRRK2 identifies COR:COR interactions as being the major contributor to dimerization (**Figure 2.4a**)[75]. Contrary to previously released structures, the COR:COR interface appears to be chiefly composed of loops and beta-sheets as compared to the previously identified helical interactions. Further, the monomeric and dimeric structures of LRRK2 demonstrate no significant structural changes within the COR domain when comparing the monomeric and dimeric states. The dimer interface is composed of overlapping beta-sheets resulting in an interaction interface composed entirely of strands and loops (**Figure 2.4b**). Although this structure represents the inactive LRRK2 dimer, it may provide crucial insights into the development of disruptors of dimerization, as mimicking one or more of the beta strands may be sufficient to inhibit dimerization of full-length LRRK2.

Another interesting feature of the solved full-length dimer are the armadillo repeats and ankyrin domain, which form a large portion of the dimer interface[75]. The armadillo repeat of one monomer interacts with the ankyrin domain of the other monomer, and these interfaces are mostly composed of alpha helices. Previous work identified the ankyrin domain of LRRK2 as the binding region for Rab29, a small GTPase that acts upstream of LRRK2 to recruit it to the trans Golgi network (TGN)[72]. Further, pathogenic mutations that promote GTP binding further exacerbate the recruitment of LRRK2 to the TGN, making the binding of Rab29 to LRRK2 an interesting therapeutic target[72]. Three residues within the ankyrin domain of LRRK2, C727, L728, and L729, were found to serve as essential mediators for the successful recruitment and subsequent activation of LRRK2. These residues are within an embedded helix that does not

contribute to dimerization and is highly conserved in both the monomeric and dimeric forms (**Figure 2.4c**). Mimics of this helix might provide an opportunity to disrupt binding of Rab29 to LRRK2 and reduce downstream pathogenic effects in cells. Lastly, the armadillo repeat, which influences vesicular trafficking, interacts with Fas associated death domain (FADD) to trigger extrinsic apoptosis, and binds to Rab32, was partially resolved in the full-length structure[108-110]. The C-terminal region of the armadillo repeat is believed to contribute to these interactions, but unfortunately this region was not resolved in the full-length LRRK2 structure. These extramolecular protein–protein interactions may serve as an alternate mechanism for allosteric regulation of LRRK2 by affecting pathways relevant to PD pathogenesis including ER stress/mitochondrial dysfunction and apoptotic neuronal death[111, 112].

Collectively, the significance of the COR domain in mediating dimerization is consistent through all currently available structures of LRRK2. The Roc domain, on the other hand, appears to have a role in dimerization when considering smaller Roco proteins and bacterial homologs of LRRK2, but its role in LRRK2 dimerization appears to be reduced. GTP/GDP binding and turnover is intricately linked to dimerization[113], so the conformational changes in the Roc domain of LRRK2 may greatly contribute to conformational changes within the COR domain to consequently affect dimerization. Further, the pathogenic mutations found within the RocCOR tandem domain are centrally located at the Roc-COR interface, which may underscore the importance of this interface for LRRK2 function. While the full-length cryoEM structure did not identify any unique characteristics in terms of Roc involvement in dimerization, the 14 Å cryo-ET structure identified the Roc domain as mediating microtubule interactions in the presence of kinase inhibitors[73]. A better understanding of how this domain associates with microtubules might allow for the development of disruptors of microtubule association and

subsequent filament formation of LRRK2. It is important to note, however, that the role of the microtubule bound LRRK2 filaments in PD pathogenesis, or LRRK2 signaling in general, remains to be determined.

2.5 Protein-Protein Interactions Driving LRRK2 Regulation

To date, efforts to allosterically inhibit LRRK2 are limited due to the complex nature of characterizing protein–protein interactions and difficulty in targeting these interfaces with traditional small molecules[114]. Recently, cell penetrating peptides were designed to effectively disrupt the interaction between LRRK2 and protein phosphatase 1 (PP1), which dephosphorylates LRRK2[115]. Initial work determined that these peptides were able to permeate cells, resist proteolytic degradation, and block the interaction between LRRK2 and PP1. These peptides can be utilized to better understand how this PPI drives LRRK2 pathogenicity, but there are multiple PPIs involving LRRK2 that are known to directly regulate LRRK2 activity. Here, we will discuss how known PPIs regulate LRRK2 and the potential for peptides to disrupt these interactions and thus alter cellular effects.

Rab GTPases are a small family of GTPases with diverse functions within and beyond the category of membrane trafficking. A subset of Rab GTPases were identified from phosphoproteomic analyses as downstream substrates of LRRK2. Within that family, Rab29 (also named Rab7L1) was also identified as an upstream regulator of LRRK2 localization and activity. Rab29, when prenylated, has been shown to recruit LRRK2 to the TGN and upregulate its kinase activity[72, 116]. Further research indicates that Rab29 overexpression also leads to LRRK2 recruitment to the mitochondrial membrane and overloaded lysosomes, indicating the importance of membrane association rather than membrane identity[117, 118]. To our knowledge, disruptors of Rab29 recruitment to LRRK2 have not been developed, but residues

within the Ankyrin domain of LRRK2 have been identified as being essential for mediating this interaction[72] (**Figure 2.5**). The development of PPI inhibitors targeting this interaction could allow one to dissect the role of Rab29-mediated localization and activation of LRRK2 and how this mechanism contributes to disease pathogenesis. In addition to Rab29, Rab32 has also been identified as an upstream regulator of LRRK2, with its predicted binding interface being in the armadillo region of LRRK2[110] (**Figure 2.5**). Peptide-based inhibitors may provide a unique opportunity to selectively disrupt each of these interactions to characterize how Rab-mediated regulation of LRRK2 could be utilized to mitigate the progression of Parkinson's disease.

14-3-3 proteins are a family of alpha-helical rich proteins consisting of seven isoforms (β, γ, ε, η, ζ, σ, and τ) capable of homo- or heterodimerizing[119-121]. 14-3-3 proteins contain a positively charged binding groove, which is known to directly interact with pSer/pThr motifs in over 200 proteins implicated in a wide range of diseases[122-124]. Two residues (S910 and S935) were identified in the multiphosphorylation cluster that are critically involved in 14-3-3 binding[125]. The interaction of LRRK2 with 14-3-3 proteins can prevent dephosphorylation of S910/S935 and stabilize LRRK2 structure, potentially influencing the dimerization of LRRK2[126]. Stabilization of the interaction between LRRK2 and 14-3-3 with either small molecules or constrained peptides could highlight the importance of this interaction in providing neuroprotection[127].

Furthermore, 14-3-3 interactions correlate with the pattern of intracellular LRRK2 distribution. Interestingly, the pathogenic mutation Q930R, also located in the multiphosphorylation cluster of LRRK2, drastically increases binding affinity to a peptide encompassing pS935[121]. Furthermore, this mutation generates a novel PKA phosphorylation site at S933 which in turn reduces binding affinity of 14-3-3 proteins. This is a common theme

also described for the second most common pathogenic PD mutation, R1441 C/G/H/S, where this mutation destroys a PKA phosphorylation site and thereby a 14-3-3 interaction site on the ROC domain[128]. Overexpression of some 14-3-3 isoforms has been shown to increase survival in PD models, triggering an increased interest in underlying signaling pathways[129, 130]. Five common PD-linked mutations of LRRK2 result in a notable decrease in phosphorylation at S910 and S935, which disrupts the interaction between LRRK2 and 14-3-3, altering localization, and reducing neuroprotection[125, 130]. Recent work to determine 14-3-3 isoform specificity identified three binding motifs within LRRK2: the previously mentioned S910/S935 motif preceding the leucine-rich repeat, S1443/S1444 within the Roc domain, and T2524 in the C-terminal helix[121, 128] (**Figure 2.5**). Collectively, these 14-3-3 interactions provide potentially important regulatory mechanisms and may reveal sites for therapeutic opportunities. Phosphomimic peptides designed to imitate each of these 14-3-3 binding sites on LRRK2 could prove to be a useful strategy to dissect the role of each site on LRRK2 regulation and may also give insights into 14-3-3 isoform specificity and activity.

2.6 Conclusion and Future Opportunities

Allosteric inhibition of protein–protein interfaces that were previously considered "undruggable" with constrained peptides and peptidomimetics has been applied to a broad array of diseases ranging from cancer to malaria to Alzheimer's disease[131-134]. By incorporating synthetic constraints, the secondary structure of the peptide can be reinforced with the intent to promote binding of the target protein, improve proteolytic stability of the peptide, and optimize cell-based characteristics as needed. Further, the choice of constraint is dependent on the interface of interest and advances in peptide chemistry have yielded a wide array of constraints, some of which are highlighted in Figure 6. When considering protein–protein interfaces, they are

predominantly composed of alpha helical or beta sheet content and rely on the engagement of specific amino acids for high affinity interactions[135]. Depending on the secondary structure, different constraints can be applied to the peptide to effectively mimic the secondary structure of interest, and a few examples are depicted in **Figure 2.6**.

Recently, efforts were made to disrupt dimerization of LRRK2 with stapled peptides. In this work, they identified a lead compound with the ability to bind LRRK2, disrupt dimerization, downregulate kinase activity, downregulate neuronal apoptosis, and decrease ROS production[107]. Further, this peptide, termed Lrrk2 Roc Inhibiting Peptide (LRIP4), was able to elicit this effect without resulting in mislocalization of LRRK2 to the microtubules (yet still triggered dephosphorylation of S935-LRRK2 in primary neurons), a common deficit seen with Type I kinase inhibitors. The identification and development of LRIP4 as an allosteric inhibitor of LRRK2 could serve as a tool to allow better understanding of LRRK2 function and sets the precedence of peptides as modulators of LRRK2 activity. Specifically, the ability of LRIP4 to downregulate pathogenic activity by disrupting dimerization highlights the importance of LRRK2 dimerization and endorses the notion that allosteric inhibition may be a valid therapeutic target for LRRK2.

Here, we highlight unique motifs identified in recently solved structures that show potential for allosteric regulation with peptides/ peptidomimetics. Efforts to advance small molecule kinase inhibitors to clinical trials are ongoing but given the complex and varying relationship between kinase activity and pathogenesis, allosteric regulation could provide a complimentary form of modulation to downregulate hyperactivated forms of LRRK2. Beyond the ATP-binding pocket of the kinase domain, its proximity and interaction with both the WD40 and COR domains reveals multiple PPI interfaces that help to regulate the positioning of the

DYG motif and αC helix. Mimicking portions of these interfaces with peptides could yield molecules that regulate the activation state of the kinase and subsequent downstream cellular signaling.

LRRK2 consistently shows a propensity for dimerization across cellular and *in vivo* model systems, and the recently solved structures helped clarify which portions of LRRK2 drive this dimerization. Consistent with earlier structures and models, the COR domain was identified as being largely responsible in the most recent cryo-EM structure of full-length LRRK2. Contrary to crystal structures of bacterial homologs and structures of isolated domains, this cryo-EM structure identified a unique beta sheet stacking that makes up the entire interface. Previous efforts to develop beta sheet mimetics have yielded a library of selective, high affinity binders[136-138]. Parallel approaches could be utilized to design a COR-targeting dimerization disruptor for LRRK2. Alternatively, the N-terminal region of LRRK2 was also shown to contribute to dimerization in the full-length dimer structure, but these domains are primarily helical. Selective disruption of dimerization within the Ankyrin and Armadillo domain could be targeted with chemically constrained alpha-helical peptides which have been extensively explored synthetically for a wide variety of disease states[9, 132]. Further, several LRRK2 substrates are known including multiple Rab proteins and this may provide an alternative avenue to downregulating LRRK2-mediated substrate phosphorylation. A concern with this strategy is off-target effects for other kinases that may have overlapping substrate specificities. In addition, interactions between Rab GTPases and their effector proteins may be another avenue to disrupt LRRK2 activity.

Looking beyond the catalytic activity of LRRK2 and its autoregulatory mechanisms, multiple scaffolding interactions are implicated in LRRK2-mediated disease pathogenesis. As

structural advances continue to be made, discerning the residues and interfaces that drive these interactions could allow for the development of constrained peptides or peptidomimetics to disrupt key interactions. By specifically targeting PPIs that are upregulated in the disease state, one could selectively target pathogenic pathways rather than endogenous LRRK2 function. The potential for allosteric regulation of LRRK2 is overflowing, and initial efforts provided a proof-of-concept that allosteric modulation can indeed downregulate PD-associated cellular effects[107]. With recent advances in structural characterization of LRRK2, the door was opened to reveal a myriad of interfaces well-suited for targeting by peptidomimetics and constrained peptides.

2.7 Chapter 2 Figures

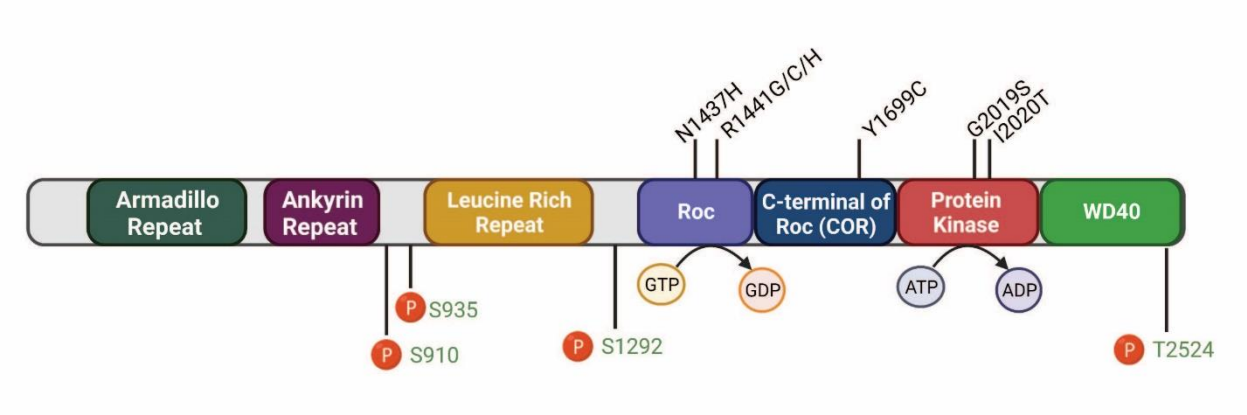

Figure 2.1 Schematic of LRRK2. Shown are the seven domains that make up LRRK2. Pathogenic PD-relevant mutations (black, top) and LRRK2 phosphorylation sites (green, bottom) on are highlighted. LRRK2 catalytic activities in the Roc and Kinase domains are shown. Image created using Biorender.

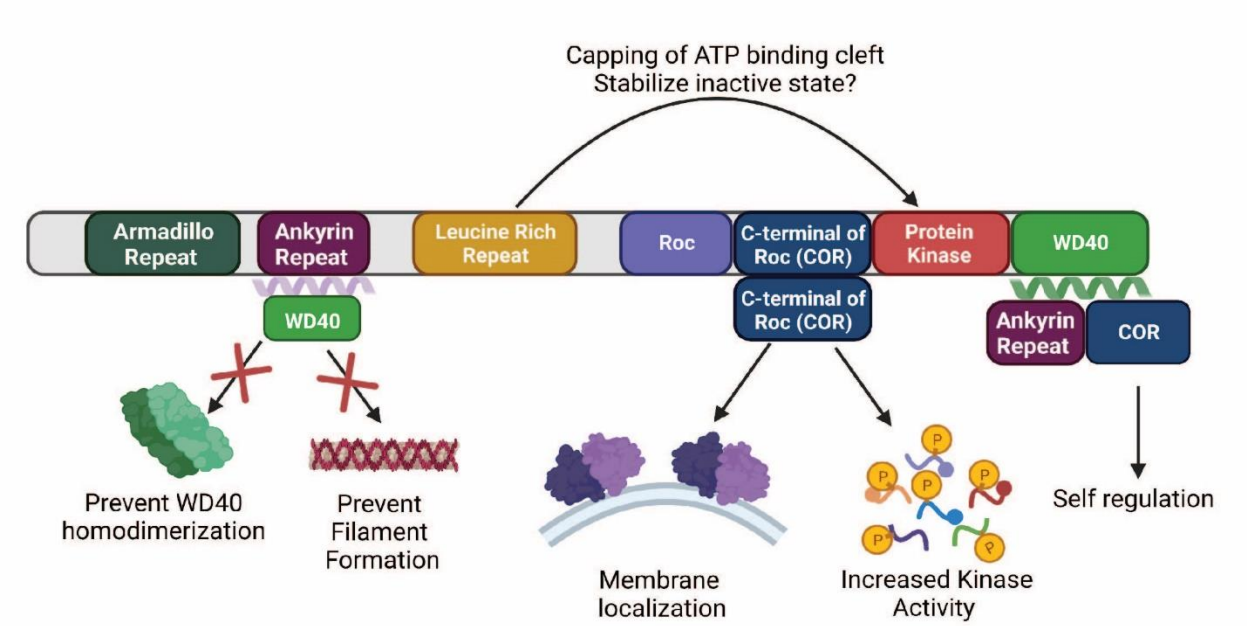

Figure 2.2 Self-regulating mechanisms of LRRK2. Recent structures of LRRK2 expose multiple mechanisms of self-regulation and reveal possible strategies for allosteric inhibition. Image created using Biorender.

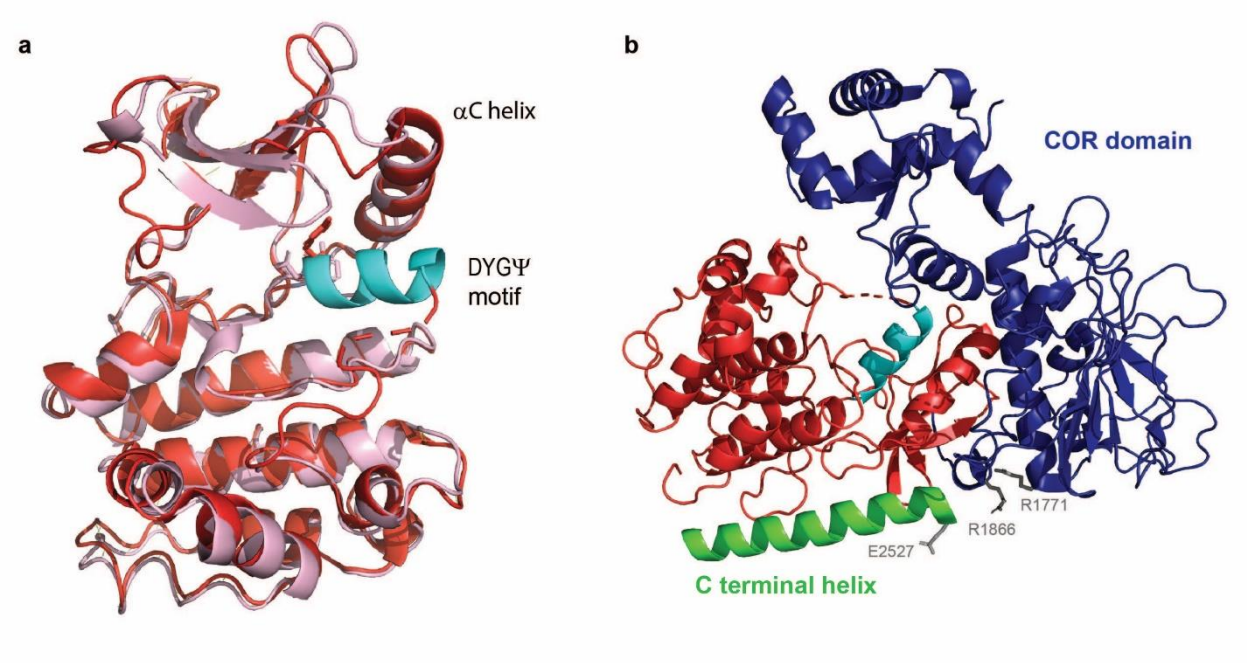

Figure 2.3 Key components of the kinase domain of LRRK2. (a) Overlay of the LRRK2RCKW(pink, PDB: 6VNO)[43]and full-length cryo-EM structures (red, PDB: 7LHW)[44]reveal different orientations of the DYG motif. The position of theαC helix is highly conserved. (b) The kinase(red), COR (blue), and WD40 domain all interact through the C-terminal helix of the WD40 domain (green). Key residues mediating the interaction between the C-terminal helix and the COR domain are highlighted. The C-terminal helix forms an elongated protein-protein interface with the backbone of the kinase domain.

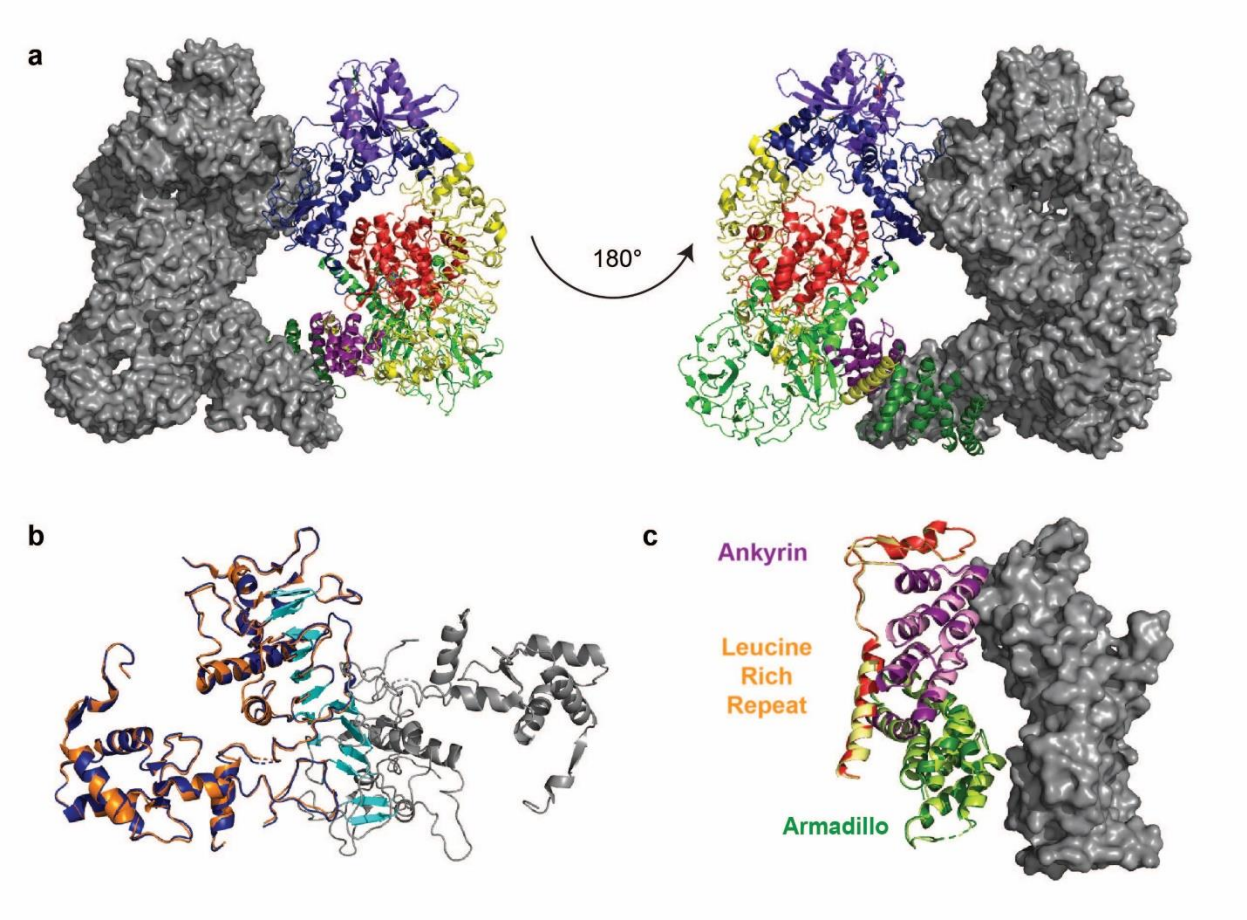

Figure 2.4 Recent cryo-EM structure of full-length LRRK2 highlights unique interaction interfaces. (a) Full-length dimeric LRRK2 structure (PDB:7LHT). One monomer of dimer depicted as gray surface, while other monomer is colored by domain: armadillo (forest green), ankyrin (deep purple), leucine-rich repeat (yellow), Roc (orange), COR (navy), kinase (red), andWD40 (bright green). (b) Overlay of the COR domain from the monomer structure (PDB: 7LHW, orange) and from the dimer structure (navy) show little structural differences. The beta-strand dimer interface is highlighted in cyan. (c) Overlay of the armadillo, ankyrin, and N-terminal region of the leucine-rich repeat domains from the dimer (PDB: 7LHT, dark purple, dark green, orange, respectively) and monomer (PDB: 7LHW, pink, light green, yellow, respectively) show minimal structural changes within these domains.

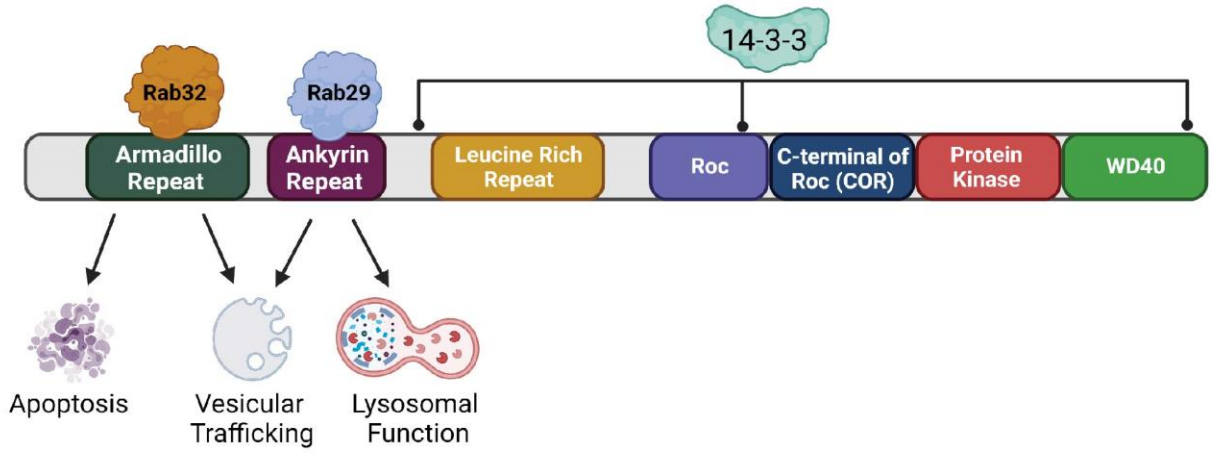

Figure 2.5 Protein-protein interactions involving LRRK2. Schematic illuminating which regions of LRRK2 are currently thought to contributeto disease-relevant PPIs. Image made using Biorender.

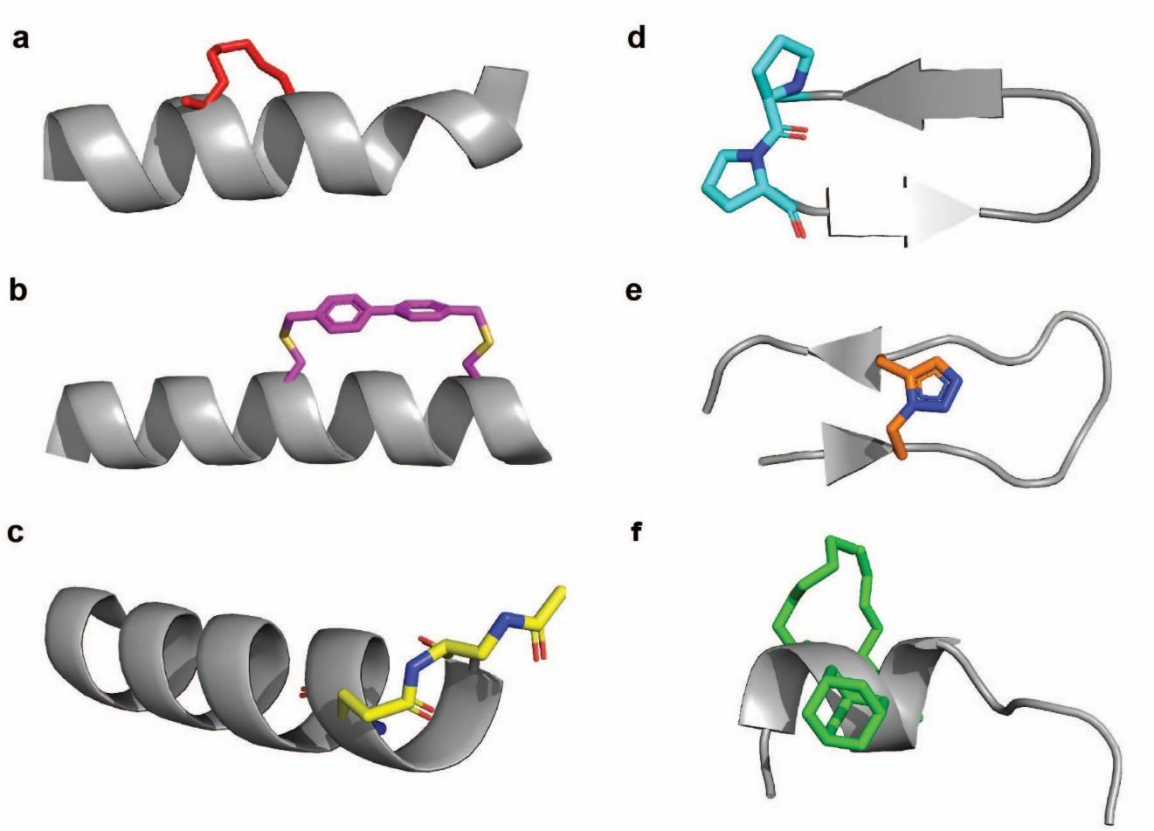

Figure 2.6 Examples of constrained peptides and peptidomimetics. a) All-hydrocarbon stapled peptide (PDB: 4NGH) SAH-MPER mimicsnative antigenic peptide secondary structure in neutralizing HIV antibodies.[139](b) Biphenyl cross-linked peptide Bph-Noxa2 (PDB: 4G35) bindsMcl-1.[140](c) N-locking stabilization improves solubility and target affinity of BH3 peptide (PDB: 6rjp).[141](d) Cyclin b-hairpin peptide 78A (PDB:2AXI) inhibits the interaction between p53 and HDM2.[142](e) Triazole bridged plasmin inhibitor (PDB: 6U7X) mimic disulfide bridgedpeptides.[143](f) Macrocyclic peptide incorporating nonnatural amino acids binds 14-3-3zeta (PDB: 5JM4)[144].

CHAPTER 3

ALLOSTERIC INHIBITION OF PARKINSON'S-LINKED LRRK2 BY CONSTRAINED PEPTIDES[3]

[3] Helton, L.G.*, Soliman, A.*, Zweydorf, F., Kentros, M., Manschwetus, J.T., Hall, S., Gilsbach, B., Ho, F.Y., Athanasopoulos, P.S., Singh, R.K., LeClair, T.J., Versées, W., Raimondi, F., Herberg, F.W., Gloeckner, C.J., Rideout, H., Kortholt, A., & Kennedy, E.J. *ACS Chem. Biol.* **2021**, 16, 2326-2338.

* Indicates authors contributed equally

https://pubs.acs.org/doi/10.1021/acschembio.1c00487

1.1 Abstract

Leucine-Rich Repeat Kinase 2 (LRRK2) is a large, multidomain protein with dual kinase and GTPase function that is commonly mutated in both familial and idiopathic Parkinson's Disease (PD). While dimerization of LRRK2 is commonly detected in PD models, it remains unclear whether inhibition of dimerization can regulate catalytic activity and pathogenesis. Here, we show constrained peptides that are cell-penetrant, bind LRRK2, and inhibit LRRK2 activation by downregulating dimerization. We further show that inhibited dimerization decreases kinase activity and inhibits ROS production and PD-linked apoptosis in primary cortical neurons. While many ATP-competitive LRRK2 inhibitors induce toxicity and mislocalization of the protein in cells, these constrained peptides were found to not affect LRRK2 localization. The ability of these peptides to inhibit pathogenic LRRK2 kinase activity suggests that disruption of dimerization may serve as a new allosteric strategy to downregulate PD-related signaling pathways.

1.2 Introduction

Parkinson's Disease (PD) is the second most common neurodegenerative disorder worldwide, with over 10 million active cases globally and at least 60 000 new diagnoses in the US each year[145]. PD can result in bradykinesia, resting tremor, postural instability, rigidity, and memory loss, with the severity of the disease varying among individuals[146]. While aging remains the largest risk factor for PD, the relatively recent identification of over 20 genes associated with familial PD highlights potential signaling pathways involved in disease pathogenesis[147-152]. Despite only 5−10% of PD cases exhibiting a genetic basis, identifying pathways altered in the genetic form of the disease could provide insight into innovative therapeutic targets and treatment strategies[153].

Missense mutations in Leucine-Rich Repeat Kinase 2 (LRRK2) are the most common cause of genetic PD and are also present in a significant portion of idiopathic PD (iPD) cases[154]. LRRK2 mutations are relatively common, accounting for 5−6% of familial PD cases and 1−2% of sporadic PD cases; this prevalence is significantly larger in specific ethnic groups[155]. Containing an armadillo domain (ARM), an ankyrin repeat (ANK), a leucine-rich repeat (LRR), a Ras-like GTPase (RocCOR) domain, a Ser/Thr kinase domain, and a C-terminal WD40 domain, the large 2527 amino acid structure and complex activation mechanism of LRRK2 have incited investigation into the underlying mechanism(s) driving its pathogenesis[156, 157]. PD-associated LRRK2 mutations are most abundant in the catalytic core of the protein: the RocCOR GTPase domain (R1437H, R1441G/H/C, Y1699C) and the protein kinase domain (G2019S, I2020T)[158]. Each mutation results in altered GTPase and/or kinase activity, and this aberrant activity triggers alterations in vesicular trafficking, cytoskeletal dynamics, autophagy, lysosomal function, oxidative stress, neurotransmission, and mitochondrial function[159]. Importantly, a common noncoding variation in LRRK2 modulates risk for PD[153]. Moreover, elevated LRRK2 kinase activity, independent of mutations, was even reported in iPD[38], indicating that targeting LRRK2 is not only beneficial for the population who carry pathogenic LRRK2 coding variants but might also be relevant for iPD patients carrying a wild-type version of this gene.

Successful inhibition of the kinase domain of LRRK2 using ATP-competitive small molecule inhibitors leads to downregulated kinase activity, reduced oxidative stress, and limited neuronal toxicity[98]. However, a major shortcoming of these small molecule inhibitors is that they also induce mislocalization of LRRK2, resulting in altered vesicular trafficking and lysosomal function, mitochondrial dysfunction, and lung and kidney abnormalities[38, 86].

Therefore, this has severely limited the translational potential of currently available small molecule inhibitors of LRRK2 and underscores the need for alternative targeting strategies to inhibit LRRK2 function. One possible strategy would be to take advantage of the different states of LRRK2 cycles between, as part of the regulation of its kinase function. Structural and functional assays have shown LRRK2 cycles between the cytoplasm and membranous organelles[160-162]. In the cytosol, LRRK2 appears to be mostly monomeric and has low kinase activity, while it is predominantly dimeric and active when localized at membranes. Furthermore, several LRRK2 PD variants result in an impaired monomer−dimer equilibrium. These data thus suggest that dimer formation and kinase activation are directly linked[160-166]. Furthermore, recent structural work[73-75] and molecular dynamics simulations[59] indicate that changes in the kinase domain allosterically signal back and forth throughout the entire molecule[60]. This could potentially be exploited as an effective strategy for allosteric inhibition of LRRK2 kinase activity.

In order to analyze the role of LRRK2 dimerization on kinase regulation, we designed peptides modified to contain an all-hydrocarbon constrained macrocycle to serve as protein-protein interface (PPI) disruptors to block the dimer interface. In contrast to small molecule inhibitors, which rely on hydrophobic pockets and the engagement of a few key amino acids for binding, peptides can target elongated binding surfaces that are typically ill-suited to small molecules[9]. Incorporation of the hydrocarbon staple into the desired peptide sequence was done as a strategy to create cell permeable peptides. The design and synthesis of peptides to effectively disrupt protein-protein interactions has been applied to a diverse array of targets across multiple diseases (for example, see refs [24, 132, 136, 167-169]). Here, we developed constrained peptides designed to target the LRRK2 RocCOR dimerization interface. These

peptides permeate cells, bind to LRRK2, and reduce kinase activity and reactive oxygen species (ROS) production. Furthermore, the peptides reduce the toxic cellular effects seen with pathogenic LRRK2 in primary cortical neurons. Additionally, the allosteric inhibitors do not appear to induce mislocalization of LRRK2 to the microtubules that is frequently seen with small molecule inhibitors. This work supports the hypothesis that dimerization is an important regulator of kinase activity, and dimerization disruption may serve as a new therapeutic strategy for the treatment of LRRK2-mediated PD pathogenesis.

3.3 Results and Discussion

Until recently (see refs [73-75]), purification and structure elucidation of LRRK2 constructs have proven elusive, in large part due to the large, complex nature of the protein; therefore, structural studies have initially focused on characterization of bacterial homologs, namely, “Roco” proteins[170, 171]. As the RocCOR GTPase domain is considered essential for mediating LRRK2 dimerization[113, 172, 173], we analyzed a structural model of this dimer interface to identify components of the interface that may contribute to dimer formation[92]. We identified two key sequences, one in the Roc domain and one in the COR domain, that appear to contribute to the dimerization interface by binding along large hydrophobic clefts [**Figure 3.1A**]. Newly released cryo-EM structures[74, 75] confirm the helical nature of LRIP, but the contribution of this helix to the dimer interface is unclear. Differences in these structures depending on activation state of LRRK2 reveal that the Roc and COR domains may adopt multiple conformations, and the Roc inhibitors may interfere with the dimer interface in either a direct or an indirect manner as LRRK2 transitions between inactive and active conformers. Sequence alignment of these peptide sequences across the family of human Roco proteins

indicates that these sequences in the protein−protein interface are unique to LRRK2 [**Figure 3.1B**].

From this model, we sought to determine which amino acids may be essential for dimer formation. After analyzing the sequence, homologous protein structures[171], and the structural model of LRRK2[92], amino acids that were predicted to be involved in mediating the protein−protein interaction (PPI) were identified [**Figure 3.1C**, red and orange]. Peptides were derived from these regions where the amino acids predicted to comprise the PPI remained unchanged while olefinic amino acids were introduced in positions that were not predicted to contribute to dimerization [**Figure 3.1C**, black]. The olefinic amino acid Fmoc-(S)-2-(4- pentenyl)alanine was incorporated at *i, i+4* positions along the nonbinding interface[174] to form hydrocarbon macrocycles with the intent to improve cell permeability as compared to the native, unmodified peptide sequence. In addition, we designed a small library of Roc domain-derived peptides with shifted stapled positions to identify the ideal position for minimal interference with target binding. The COR-targeting peptide was much shorter, so olefinic amino acids were incorporated at the only *i, i+4* positions that were suitable for replacement [**Figure 3.1C**]. Peptides were synthesized using Fmoc-based solid phase peptide synthesis (SPPS) on solid support, and the olefinic amino acids were cyclized using Grubbs I Catalyst while on solid support to yield the constrained peptide products [**Figure 3.1D**]. Further modification included incorporation of an N-terminal PEG3 linker to improve hydrophilicity of the peptide and additional N-terminal labeling with either biotin or 5,6-carboxyfluorescein (FAM) for biochemical and cellular assays. Recently released structures[74, 75] identified the LCIP1 sequence as being predominantly nonhelical; therefore, we performed circular dichroism and

determined that LCIP1 is not in a purely helical or beta-sheet conformation but instead adopts a mixture of different secondary structural elements [Figure S1].

Peptides designed to target the Roc domain (LRRK2 Roc Interacting Peptides, LRIP) and COR domain (LRRK2 COR Interacting Peptides, LCIP) were first passed through a preliminary screen to determine whether they had any inhibitory effects LRRK2 dimerization [Figure S2] by assessing coimmunoprecipitation of differently tagged LRRK2 constructs. From this screen, LRIP3, LRIP4, and LCIP1 appeared to partly downregulate dimerization. The peptide libraries were also screened by fluorescence polarization (FP) to determine whether they bound their target domains of LRRK2 [**Figures 3.2A,B** and S3]. Two MBP-tagged protein constructs, COR and RocCOR, were purified and plated in concentrations ranging from 5 μM to 1 nM along with 10 nM FAM-labeled peptides. While most of the peptides demonstrated no appreciable binding curves to these protein constructs, LRIP4 exhibited a binding affinity in the mid-nanomolar range (~60 nM) while LCIP1 bound to the CORB construct with significantly weaker interaction in the low micromolar range (~1 μM; **Figures 3.2A,B** and S3). The weak binding of LCIP1 to its target domain may be due, at least in part, to its secondary structural conformation, which differs from that in the newly released full-length structure of LRRK2. To ensure that the detectable binding by the lead peptides, LRIP4 and LCIP1, was toward their target domain and not the MBP tag, FP assays were performed with MBP alone. Both peptides exhibited no binding to this construct [Figure S4], indicating that they appear to bind their targeted domains in LRRK2.

Next, we sought to determine whether the lead peptides could bind their target, LRRK2, from cell lysates. To test this, HEK293 cells overexpressing GFP-tagged LRRK2 were lysed and incubated with biotin-labeled peptides. Peptide pulldowns were performed using avidin-coated

resin. As compared to DMSO and scrambled controls, LRIP4 and LCIP1 pulled down LRRK2 [**Figure 3.2C**]. Of note, LRIP4 pulled down considerably more LRRK2 as compared to LCIP1, which may correlate with this peptide binding LRRK2 with a higher affinity. To further confirm these results, pull-down experiments from cell lysates were performed and analyzed by protein mass spectrometry [Table S1]. In this experiment, LRRK2 was detected in pulldowns with either LRIP4 or LCIP1 but not their scramble controls. Both LCIP1 and LRIP4 exhibit binding to other human protein kinases including nucleoside diphosphate kinases A/B, pyruvate kinase PKM, and ribose-phosphate pyrophosphokinase 1. However, none of these kinases contain RocCOR domains and homologous proteins to LRRK2, such as LRRK1, were not found to interact with the peptides.

To determine whether LCIP1 and LRIP4 could effectively disrupt LRRK2 dimerization, we monitored disruption of dimerization using two different tagged versions of LRRK2. This was achieved by cotransfecting HEK293 cells with GFP-tagged and streptagged full-length LRRK2. Next, a GFP-trap immunoprecipitation (IP) was performed using lysates that were treated with or without 10 μM peptide. Western blotting was performed to detect the level of strep-tagged LRRK2. In the absence of peptide treatment, strep-tagged full-length LRRK2 coprecipitated with GFP-LRRK2, indicating a background level of dimer formation [**Figures 3.3A**, S5]. Quantification of these IP experiments [Figure S5] revealed that LRIP4 and LCIP1 both downregulated LRRK2 dimerization with statistical significance as demonstrated by reduced levels of strep-tagged LRRK2. LRIP4 had the most pronounced effect with approximately 70% reduction, albeit neither peptide yielded complete inhibition of dimer formation.

To establish whether LCIP1 and LRIP4 would be suitable for cell-based experiments, cell permeation of the peptides was evaluated. Flow cytometry revealed dose-dependent uptake of both lead peptides [Figure S6]. At the 6-h time point, both peptides demonstrated considerable permeability as measured by a shift in fluorescence detection by flow cytometry [**Figures 3.3B**, S6]. To determine whether the peptides could reach the cytosol, confocal microscopy was performed. While both peptides were detected in the cytoplasm, LRIP4 had greater cytoplasmic fluorescence intensity as well as some nuclear localization, while LCIP1 appeared to partly localize within vesicles [**Figure 3.3C**].

We next sought to assess whether these peptides could also inhibit LRRK2 dimer formation in cells. We used a previously published in situ LRRK2 proximity biotinylation approach[97] where HEK293T cells expressing either wild-type or G2019S mutants of LRRK2 fusions, either with the biotin ligase BirA or the acceptor peptide AP, were treated with increasing concentrations (0.1, 1, and 10 μM) of each fluorescently labeled peptide. The ROC domain-targeting peptide, LRIP4, caused a statistically significant reduction in both G2019S/ G2019S and G2019S/wild-type LRRK2 dimers at 10 μM peptide treatment [**Figures 3.3D**, S7−S9. In this assay, LCIP1 failed to consistently lead to a reduction in LRRK2 dimerization [Figures S7, S8] which may be due to relatively weaker cell permeation and weaker target binding as compared to LRIP4. Further, only partial inhibition could be observed, and this may be due to many other interfaces involved in LRRK2 dimerization derived from other domains of the protein that may still influence and induce dimerization.

Autophosphorylation at site S1292 is correlated with LRRK2 kinase activity[69]. To test whether impaired LRRK2 dimerization may result in LRRK2 kinase activity, we therefore measured the effects of LRIP4 and LCIP1 on LRRK2 S1292 phosphorylation. In these

experiments, HEK293 cells were transfected with GFP-tagged LRRK2. Cells were then treated with 10 μM of either LRIP4 or LCIP1 prior to immunoblotting. Western blots of pS1292-LRRK2 revealed that both peptides caused a significant reduction of autophosphorylation by 50−70% as compared to the DMSO control, although neither was as potent as the ATP-competitive LRRK2 inhibitor MLi-2 [**Figure 3.4A,B**].

LRRK2 kinase activity was also measured as a function of Rab10 phosphorylation[61, 175]. To test whether disruption of LRRK2 dimerization can also reduce Rab phosphorylation, a hyperactive LRRK2 mutant (R1441G) and Rab29 were overexpressed in HEK293T cells[72, 116]. Overexpression of Rab29 induces recruitment of LRRK2 to the trans-golgi network (TGN) where it becomes activated. After transfection, cells were then treated with 10 μM peptide, followed by immunoblotting of pT73 Rab10. In these experiments, treatment with LRIP4 or LCIP1 reduced Rab10 phosphorylation with LRIP4 inducing a more pronounced effect [**Figure 3.4C**]. We performed a homologous experiment in cells transfected with LRRK2 G2019S and show that LRIP4 reduced Rab10 phosphorylation and LRRK2 autophosphorylation at pS1292; however, LCIP1 had no effect [Figure S10]. To test the effect of the dimerization inhibitors on endogenous LRRK2 function, we performed a similar experiment using nontransfected A549 cells which natively express detectable levels of both LRRK2 and Rab10. In these cells, LRIP4 caused a significant reduction in phosphorylation of Rab10 as compared to the DMSO control [**Figures 3.4D**, S11]. On the other hand, LCIP1 had a modest effect on Rab10 phosphorylation. This may be due to variances in different cell lines for the different experiments, the extent of permeation by the compound, or differences in LRRK2 localization and expression levels. To measure whether disruption of dimerization would alter the GTPase activity of LRRK2, full-length wild type LRRK2 was incubated with 10 μM of peptide and GDP production was

measured via reversed phase HPLC. The peptides did not induce a change in the intrinsic hydrolysis of the monomer, indicating no effect on GTPase activity [Figure S12]. Together, it appears that disrupted dimerization may lead to reduced LRRK2 activation as assessed by autophosphorylation of LRRK2 and subsequent Rab10 phosphorylation. This demonstrates that LRRK2 dimerization may control LRRK2 kinase activation and disruption of dimerization may allosterically inhibit LRRK2 activity.

Next, we analyzed the effects of these inhibitor peptides on LRRK2 localization. Classical ATP-competitive LRRK2 kinase inhibitors induce cellular recruitment of LRRK2 to microtubules and block kinesin and dynein-1-mediated transport[74, 88]. To investigate whether the dimerization-blocking peptides would induce a similar phenotype, the localization of GFP-tagged LRRK2 was analyzed by confocal microscopy [**Figures 3.4E,F**]. Consistent with previous studies, the LRRK2 ATP-competitive inhibitor MLi-2 induced altered localization to filament-like structures. This is also consistent with previous work demonstrating that kinase inhibitor-induced filaments are populated with dimeric LRRK2[161]. In contrast, LRRK2 maintained its cytoplasmic distribution after 12-h treatments with 10 μM of either LRIP4 or LCIP1. On the basis of this observation, it is possible that allosterically inhibited monomeric LRRK2 may be adopting a different conformation as compared to catalytically inhibited LRRK2.

We subsequently sought to evaluate how these peptide inhibitors of LRRK2 impact PD-linked cellular effects. Although the exact physiological function of LRRK2 is still elusive, and in particular the mechanism(s) by which mutant forms induce neuronal death, pathogenic LRRK2 mutants were shown to impair lysosomal function and therefore account for increased levels of ROS production[50] in both neuronal[176, 177] and peripheral immune cells[178, 179].

Further, inhibition of LRRK2 kinase activity was reported to alleviate such enhanced oxidative stress[176, 178, 179]. Consistent with these observations, incubation of cells with LRIP4 resulted in a significant reduction of zymosan induced ROS production to an extent comparable to MLi-2 [**Figure 3.5A**]. The effect of LCIP1 on ROS production produced highly variable results, similar to its effects on dimerization in cells, thereby yielding no statistically significant consequence.

Finally, we used primary cortical neurons to assess the neuroprotective ability of LRIP4 and LCIP1. It has been shown that LRRK2-mediated neuronal toxicity is kinase-dependent[180]. To determine if peptide-treated cortical neurons maintained cellular integrity, fluorescence imaging was performed[181]. Cortical neurons transfected with wild-type LRRK2 maintained proper cellular morphology, with no evidence of nuclear changes typical of apoptotic death, whereas neurons expressing G2019S LRRK2 exhibited aberrant LRRK2 distribution and apoptotic nuclear condensation and fragmentation and activation of the late-stage protease caspase-3 [**Figure 3.5B,C**]. Importantly, upon treatment with the peptides, there was a sharp decline in neurons undergoing apoptosis, especially for LRIP4 treated cells [**Figure 3.5D**]. Furthermore, we sought to determine whether pharmacodynamic markers of kinase inhibition are evident in primary neurons treated with the peptides, expressing endogenous levels of LRRK2. After overnight treatment with LRIP4 or LCIP1, we saw a statistically significant decrease in pS935 relative to the scramble treated control, similar to what is seen following treatment with MLi2 [Figure S13]. Together, these results indicate that disruption of dimerization with LRIP4 can effectively downregulate LRRK2-mediated ROS production, kinase activity, and neuronal apoptosis.

3.4 Discussion

Although the normal function of LRRK2 is not fully understood, elevated kinase activity in both PD-linked mutations and idiopathic PD leads to neuronal degeneration[147-155]. Further, inhibition of abnormally elevated activity of PD-associated LRRK2 can result in neuroprotection[156]. Although LRRK2 has been sought after as a therapeutic target for PD, the ATP-competitive LRRK2 kinase inhibitors reported to date have largely led to altered LRRK2 localization as well as kidney and lung abnormalities in *in vivo* toxicological studies[86, 182, 183]. Thus, alternative strategies to downregulate LRRK2 activity could present new opportunities for targeted therapeutic intervention.

LRRK2 was previously shown to alternate between monomeric and dimeric species where LRRK2 exists primarily as a dimer with enhanced kinase activity is associated with the dimeric fractions of LRRK2[97, 184]. Further, LRRK2 dimers were also shown to exist inside cells and are enriched at membranous structures with proportionally little dimeric LRRK2 in the cytosol[72, 160]. In addition, LRRK2 kinase activity was found to be induced upon dimerization[162], which is at least partly mediated by intermolecular interactions between the RocCOR tandem domains of two LRRK2 monomers. The mechanism regulating the balance between the monomer/ dimer population is not known[92, 162, 185], although it is clear that GDP/GTP binding to the RocCOR domain plays a role in regulating this equilibrium[113, 186]. While most pathogenic variants of LRRK2 are associated with either increased kinase or decreased GTPase activity, it was also recently shown that wild-type LRRK2 kinase activity was enhanced in midbrain DA neurons of patients with idiopathic PD[38]. Therefore, allosteric targeting of LRRK2 to regulate dimerization may serve as a strategy to shift from the dimer to monomer population and may be a viable alternative strategy for targeted inhibition of kinase

activity, without altering its localization. We previously showed that disruption of dimerization using nanobodies can increase the GTPase activity in a bacterial homologue of LRRK2[186].

Here, we report the design, synthesis, and characterization of a peptide-based PPI inhibitor of LRRK2 dimerization, namely LRIP4. LRIP4 was shown to permeate cells, inhibit dimerization, and inhibit kinase activity both in vitro and in cells. Although the exact physiological function of LRRK2 is still elusive, and in particular the mechanism(s) by which mutant forms induce neuronal death, pathogenic LRRK2 mutants were shown to impair lysosomal function and therefore account for increased levels of ROS production[50] in both neuronal[176, 177] and peripheral immune cells[179]. Consistently, inhibition of dimerization also led to reduced ROS production and neuronal apoptosis. In addition, we demonstrate for the first time that this inhibition strategy can downregulate kinase activity without inducing LRRK2 mislocalization that was previously shown by ATP-competitive kinase inhibitors of LRRK2. To our knowledge, this study is the first report of allosteric inhibition of LRRK2 dimerization and provides pharmacological evidence that LRRK2 dimerization regulates kinase activity. Our second compound, LCIP1, which targeted the COR domain, showed limited cell uptake and binding affinity when compared to LRIP4. Although this compound showed some inhibitory activity in early biochemical assays, it had little to no activity in cells. Previous reports indicate that the COR domain is essential for mediating dimerization[162, 171]; therefore, optimization of this targeting site based on recent structural advances could result in a more potent disruptor of dimerization. Several limitations exist for studying allosteric inhibitors of LRRK2 including low LRRK2 expression levels in many cell lines and the need to transfect some cell lines to promote detectable levels of phospho-Rab10. Further, biochemical experiments with LRRK2 remain difficult due to challenges with stable expression and purification of full-length or

truncated constructs of LRRK2 as well as the tendency of LRRK2 protein to dimerize in solution.

To further explore the potential for targeting LRRK2 dimerization, high-resolution structural insights into LRRK2 are required. Even though the exact function of the RocCOR domain is unknown, our results demonstrate that disruption of RocCOR-mediated dimerization attenuates LRRK2 kinase activity. Recently published structures reveal many new interfaces that are critical for LRRK2 dimerization and may also serve as viable targets for LRRK2 inhibition[73-75]. In addition, allosteric disruptors will be invaluable tools to dissect the different functions of the many domains of LRRK2 as we seek to better understand the significance of each domain on LRRK2 activity and regulation.

3.5 Methods

Constructs

Cloning of the Strep-FLAG (SF) tagged LRRK2 (pDEST(N)SF.LRRK2 constructs has been described previously[92]. The generation of N-terminal Flag-tagged LRRK2 for the transfection of neuronal cultures has been described in ref [187]. N-terminal GFP-tagged LRRK2 (pcDNA3.1_GFP.LRRK2) has been generated by Gateway cloning. For the proximity biotinylation assay, two constructs were created encoding LRRK2 fusions with biotin ligase (BirA; N-term, Flag-tagged) and an acceptor peptide (AP, N-term; c-Myc tagged)[97]. The cDNAs encoding Rab10 and Rab29 were ordered as synthetic genes and subcloned via the Gateway system into the pcDNA3.0-based pDEST N-HA/FLAG vector, generated in-house.

Cell Culture

LRRK2 parental RAW 264.7 cells (ATCC, SC-6003) were cultured in Dulbecco's Modified Eagle's medium (DMEM, ATCC, 30-2002) supplemented with 10% FBS and 1%

penicillin-streptomycin (Gibco, 15070063). HEK293(T) cells (ATCC, CRL-1573, and CRL-3216) and A549 cells (ATCC, CCL-185) were grown in Dulbecco's Modified Eagle's medium (DMEM, Gibco, 11960044) supplemented with 10% FBS and 1% penicillin-streptomycin-Glutamine (Gibco, 10378016).

Peptide Synthesis

Peptide synthesis was performed using standard Fmoc solid phase peptide synthesis on Rink amide MBHA resin using standard N-α-Fmoc amino acids. All synthesis reagents and solvents were purchased from Fisher, Sigma-Aldrich, or Acros. Deprotection was performed using 25% (v/v) piperidine in 75% (v/v) *N*-methylpyrrolidinone (NMP) for 25 min with agitation. After each deprotection, resin was washed three times for 30 s with NMP and agitation. Standard amino acids were coupled by adding 10 equiv of amino acids followed by the addition of 9.9 equiv of 2-(6-chloro-1H-benzotriazole-1-yl)-1,1,3,3-tetramethylaminium hexafluorophosphate (HCTU in NMP). Twenty equivalents of N,N-diisopropyl ethylamine (DIEA, Fisher) was added to catalyze the addition of the amino acid. This solution was agitated for 45 min. For S_5 ((S)-N-Fmoc-2-(4-pentenyl) alanine, Sigma-Aldrich) and PEG_3 (Fmoc-11-amino-3,6,9-trioxaundecanoic acid, ChemPep), we added 4 equiv of S_5 or PEG_3, followed by the addition of 3.9 equiv of HCTU. For LRIP4, Methionine 1466 was mutated to norleucine to improve synthetic yield. This substitution was contingent on evidence suggesting the methionine was not essential for mediating dimerization.

To cyclize the olefinic amino acids and form the staple, we performed ring closing metathesis (RCM) using a first-generation Grubbs catalyst. This reaction was performed on resin with 1,2-dichloroethane (DCE) using 0.4 equiv of a first-generation Grubbs catalyst for two separate 1-h time periods. Upon completion of the sequence and closing of the staple, we made

modifications to the N-terminus based on experimental needs. These modifications included the addition of a PEG_3 linker (previously described [24]) and labeling with either 5,6-carboxyfluorescein (FAM, Sigma-Aldrich) or D-biotin (GoldBio). For FAM labeling, 2 equiv of FAM were added with 1.8 equiv of HCTU and 4.6 equiv of DIEA overnight in dimethylformamide (DMF) with agitation. For biotin labeling, 10 equiv of biotin were added with 9.9 equiv of HCTU and 20 equiv of DIEA in a 1:1 mixture of dimethyl sulfoxide (DMSO) and DMF overnight with agitation. After overnight labeling, the peptides were cleaved from resin using 95% (v/v) trifluoroacetic acid (TFA), 2.5% (v/v) triisopropylsilane, and 2.5% (v/v) water then rotated for 5 h at RT. Peptides were then precipitated in methyl-*tert*-butyl ether at 4 °C via centrifugation.

Peptide Characterization

Following cleavage from resin, peptides were separated via RP-HPLC using a Zorbax analytical SB-C18 column. The mobile phase linear gradient was 10–100% water to acetonitrile with 0.1% TFA at a flow rate of 0.5 mL/min. Peptides were then characterized via ESI-MS (Agilent 6120 Single Quadrupole) following separation over a Zorbax analytical SB-C18 column via HPLC (Agilent 1200). Peptide purification was performed using the same conditions over a semipreparatory column with a flow rate of 4 mL/min. To confirm peptide purity, products were analyzed by ESI-MS over a Zorbax analytical SB-C18 column.

To quantify peptides, intrinsic qualities of the N-terminal labels were used. For FAM labeled peptides, quantification was based on the absorbance at 495 nm in 10 mM Tris (pH 8) using an extinction coefficient of 69 000 $M^{-1}cm^{-1}$. Biotin-labeled peptides were quantified by measuring decreased absorbance of the 2-hydroxyazobenzen-4′-carboxylic acid (HABA)-avidin complex at

500 nm. Final M/S for all peptides are included in the Supporting Information (norleucine is abbreviated Nle; Figures S14-21).

The peptide sequence for FAM-labeled LRIP1 is 5(6)FAM-PEG_3-DEK*RKA*(Nle)SKITKELLNKR, and the mass is 2967.0 (expected = 2967.5).

The peptide sequence for FAM-labeled LRIP2 is 5(6)FAM-PEG_3-DEKQRKA*(Nle)SK*TKELLNKR, and the mass is 2981.4 (expected = 2982.4).

The peptide sequence for FAM-labeled LRIP3 is 5(6)FAM-PEG_3-DEKQRKAC(Nle)SK*TKE*LNKR, and the mass is 2972.0 (expected = 2972.4).

The peptide sequence for FAM-labeled LRIP4 is 5(6)FAM-PEG_3-DEKQRKAC(Nle)SKITKE*LNK*, and the mass is 2928.0 (expected = 2929.4).

The peptide sequence for Biotin-labeled LRIP4 is D-Biotin-PEG3-DEKQRKAC(Nle)SKITKE(S5)LNK(S5), and the mass is 2796.6 (expected = 2797.4).

The peptide sequence for FAM-labeled LRIP4 scramble is 5(6)FAM-PEG_3-Q(Nle)DKAESKNKERKLC*TIK*, and the mass is 2928.9 (expected = 2929.4).

The peptide sequence for Biotin-labeled LRIP4 scramble is D-Biotin-PEG_3-Q(Nle)DKAESKNKERKLC*TIK*, and the mass is 2796.9 (expected = 2797.4).

The peptide sequence for FAM-labeled LCIP1 is 5(6)FAM-PEG_3-KGEGE*LLK*WK, and the mass is 1983.6 (expected = 1984.3).

The peptide sequence for Biotin-labeled LCIP1 is D-Biotin-PEG_3-KGEGE*LLK*WK, and the mass is 1851.6 (expected = 1852.3).

The peptide sequence for FAM-labeled LCIP1 scramble is 5(6)FAM-PEG_3-GKWEK*GEL*KL, and the mass is 1983.6 (expected = 1984.3).

The peptide sequence for Biotin-labeled LCIP1 scramble is D-Biotin-PEG_{3}- GKWEK*GEL*KL, and the mass is 1851.6 (expected mass = 1852.3).

The peptide sequence for FAM-labeled LRIP Native is 5(6)FAM-PEG3-DEKQRKAC(Nle)SKITKELLNKR, and the mass is 2946.9 (expected = 2948.4)

Fluorescence Polarization Assays

Direct binding of our lead compounds (LRIP4 and LCIP1) to LRRK2 constructs was assessed via FP assays. For LRIP4, we measured binding with purified MBP-tagged RocCOR LRRK2 protein in the presence of 2 mM GTP and 10 mM $MgCl_2$. For LCIP1, we measured binding to purified MBP-tagged CORB. Each FAM-labeled peptide was plated at a final in-well concentration of 10 nM in 384-well microtiter plates. 1:2 dilutions of the protein were then performed from a concentration range of 5 μM to 1 nM. For each peptide/protein interaction, we had a range of at least 10 protein concentrations, and each concentration was performed in triplicate. The assay was performed in FP buffer (20 mM MOPS pH 7, 150 mM NaCl, and 0.005% CHAPS) at RT. The peptide/protein mixture was incubated at RT for 2 h with readings taken every 30 min. The final readings were obtained at 2 h.

Protein Mass Spectrometry Analysis of Binding Interactors in Cells

Proteins interacting with biotin-labeled LRIP4, LRIP4 Scramble, LCIP1, or LCIP1 Scramble peptides were captured by magnetic strep-beads as described in pulldown experiments. The samples were denatured with 1.6 M urea, reduced with 5 mM TCEP (37 °C, 1h), alkylated with 10 mM iodoacetamide (RT, 45 min in dark), and digested with sequencing grade modified trypsin (37 °C, overnight). After digestion, the magnetic beads were removed from the samples, and the tryptic peptides were extracted by solid phase extraction using C18 tips (Pierce). The cleaned peptides were then subjected to LC-MS analysis using an Easy-nLC II LC system

coupled to a LTQ Orbitrap XL mass analyzer (Thermo Scientific). The data acquisition was set at data-dependent mode for 60 min elution gradient, with full scan MS spectra (*m*/*z* 300–1650) at a resolution of 30 000. The raw data were imported into PEAKS Studio X+ (Bioinformatics Solutions Inc.) and analyzed against all reviewed human proteins in the Uniprot database. The peptide false discovery rate (FDR) was set to 0.1% using the target-decoy method. Protein entries with at least one unique peptide found in the analysis were regarded as positive hits and tabulated.

Pulldown Experiments

Fresh lysate of HEK293 cells overexpressing GFP-tagged LRRK2 was mixed and incubated with biotin-labeled peptide (added to a final concentration of 10 μM) and incubated at 4 °C overnight. The mixture was then applied to Magnetic Strep-beads (MagStrep “Type3” XT Beads (IBA, Göttingen, Germany)), and the immune complex was washed twice (10 mM Tris/HCl pH 7.5, 150 mM NaCl) and subjected to immunoblot analysis. Samples were separated on 6% Tris-Glycine gels, transferred onto a nitrocellulose membrane (GE Lifesciences), and processed for western analysis. Membranes were blocked in 5% dry milk in Tris-buffered saline plus Tween-20 for 1 h and probed with rat monoclonal anti-LRRK2 (clone 24D8 1:1000, Gloeckner lab[188]) and incubated overnight at 4 °C with gentle shaking. Membranes were then washed three times for 10 min at RT in PBS containing 0.1% or 0.05% Tween-20 and then incubated for 1 h with antirat IgG-HRP (sc-2750, Santa Cruz Biotechnology). Membranes were again washed three times for 10 min at RT in PBS containing 0.1% or 0.05 Tween-20. The membranes were coated with an enhanced chemiluminescent (ECL) reagent (WesternSure PREMIUM, Li-COR biosciences), and proteins were detected using the C–Digit Imaging System (Li-COR Biosciences).

In vitro Dimerization Assay

HEK293 cells were cotransfected using JetPEI reagent (Polyplus transfection) with pcDNA3.1_GFP.LRRK2 and pDEST(N)SF.LRRK2. Cells were cultivated for 48 h. The cells were then lysed with 200 μL of ice-cold lysis buffer (10 mM Tris/HCl pH 7.5; 150 mM NaCl; 0.5 mM EDTA; 0.5% NP-40), complete EDTA-free protease inhibitor cocktail (Sigma–Aldrich Cat # 11836170001), and Protease Inhibitor Cocktail, Sigma (cat. no. P-2714). The mixture was incubated and rotated on ice for 30 min with extensive pipetting every 10 min. Lysate was cleared by centrifugation for 10 min at 14 000*g* for 10 min at 4 °C. The supernatant was transferred to a precooled tube, and 300 μL of dilution buffer (same as lysis buffer without NP-40) was added to the lysate. Peptides were added to a final concentration of 10 μM, and the mixture was allowed to rotate at 4 °C overnight. GFP-LRRK2 was immunoprecipitated with Magnetic GFP nanotrap beads (ChromoTek). Immune complexes were washed twice with 10 mM Tris/HCl at pH 7.5 and subjected to immunoblot analysis by boiling samples in sample buffer with a reducing agent. Samples were separated on 6% Tris-Glycine gels, transferred onto a nitrocellulose membrane (GE Healthcare), and processed for western analysis. Membranes were blocked in 5% dry milk in Tris-buffered saline plus Tween-20 for 1 h and probed with mouse anti-Strep tag LRRK2, 1:1000 (34850, Qiagen), or rabbit anti-GFP antibodies, 1:2500 (MA5–15256, Invitrogen), and incubated overnight at 4 °C with gentle shaking. Membranes were then washed three times for 10 min at RT in PBS containing 0.1% or 0.05% Tween 20 and then incubated for at least 1 h (light protected) with secondary antibodies: mouse IgG kappa binding protein (m-IgGκ BP) conjugated to horseradish peroxidase (HRP; sc-516102, Santa Cruz Biotechnology, 1:5000) or antirabbit HRP conjugated (#7074, Cell Signaling, 1:500). Membranes were again washed three times for 10 min at RT in PBS containing 0.1% or 0.05%

Tween-20. The membranes were coated with the enhanced chemiluminescent (ECL) reagent (WesternSure PREMIUM, Li-COR biosciences), and proteins were detected using the C–Digit Imaging System (Li-COR Biosciences).

Flow Cytometry

HEK293 cells were plated in 96-well plates (50 000/well) and allowed to grow 24 h in complete growth medium (DMEM supplemented with 10% fetal bovine serum, L-glutamine). DMEM was carefully aspirated, and cells were treated with fresh prewarmed complete growth medium supplemented with 10 μM of peptide or DMSO. After 6 h, cells were analyzed on a Beckman Cytoflex flow cytometer (Beckman Coulter). Using forward and side scattered light, a gate for intact, nonaggregated cells was defined, and the fluorescence of 10 000 events was collected within this cell gate. The fluorescent channel for FITC (488 nm excitation [ex], 525 nm emission [em]) was used. Data were analyzed using FlowJo software, and the reported fluorescent intensity values represent arithmetic means of the results determined for the analyzed cells.

Confocal Microscopy

HEK293 cells were plated (40 000/well) on μ-Slides (chambered coverslip, tissue-culture treated, 80826, Ibidi) and cultured for 24 h in complete growth medium (DMEM supplemented with 10% fetal bovine serum and L-glutamine). Then, DMEM was carefully aspirated, and cells were treated with fresh prewarmed growth medium (DMEM supplemented with FAM-labeled stapled peptide (10 μM) or DMSO). After 6 h, cells were washed three times in warm PBS to remove excess peptide from the cell surface and left in prewarmed low fluorescence imaging medium (FluoroBrite DMEM, Gibco). Cells were immediately analyzed under an LSM800 confocal laser scanning microscope with a prewarmed incubation chamber (37 °C). By scanning

through the *z* planes of each cell, the outer plasma membrane borders were determined. Images were taken between the plasma membrane *z* planes to obtain signals from internalized peptides and to minimize artificial signals from cell surface adhered peptides. The distribution of FAM-labeled peptides was analyzed using a 63X Plan-Apochromat oil-immersion objective (Zeiss). Image analysis of z-scan was done using the Zeiss microscope software ZEN.

Proximity Biotinylation of Dimeric LRRK2

To purify LRRK2 dimers, we relied on the proximity biotinylation technique recently described[97, 189]. Briefly, two cDNAs were created encoding LRRK2 fusions with biotin ligase (BirA; N-term, Flag-tagged) and an acceptor peptide (AP, N-term; c-Myc tagged) and overexpressed in HEK293T cells grown in biotin-depleted medium (OptiMEM+2% FBS). The following day, the cells were treated with the indicated concentrations of the stapled peptides: LRIP4 and LCIP1. Stock peptides, fluorescently tagged, were diluted in serum-free medium and added every 24 h after transfection. After 48 h, following the initiation of treatment (i.e., 72 h of total expression), the cells were extensively washed in PBS, given a brief biotin pulse (50 μM, 5 min, 37°C), followed by another three washes in PBS, and centrifuged and the pellet snap frozen in a dry ice/MeOH bath. In some experiments, the cells were treated with peptides for a total of 24 h before collection. Following lysis, extracts were diluted in TBST/BSA (10 mM Tris HCl, pH 7.6; 100 mM NaCl; 0.1% Triton X-100; 1% BSA) and 2.5 μg of protein loaded in parallel ELISA plates, coated with streptavidin (SA; to capture biotinylated LRRK2 dimers) and anti-LRRK2 (to quantify LRRK2 overexpression). To detect and quantify dimeric LRRK2, SA-coated plates were incubated with HRP-conjugated anti-Flag antibodies (1 h, RT). Since the biotin tag is only present on AP-LRRK2 fusions, and the flag epitope tag is located on the BirA-LRRK2 fusion, by using HRP-Flag as our detector reagent, we are specifically labeling dimeric

LRRK2 present in the ELISA plates. On the parallel anti-LRRK2 coated plates (clone c41–2), total overexpressed LRRK2 was quantified using HRP-LRRK2 antibodies (clone N241) and used to normalize the relative amounts of dimeric LRRK2. We assessed the following LRRK2 dimers: WT/WT homodimers, WT/G2019S, and G2019S/G2019S homodimers.

LRRK2 Immunoblotting

Protein content per sample was determined by a bicinchoninic acid colorimetric assay (BCA), using bovine serum albumin as a standard (23225; Life Technologies). Next, 100 μg of protein was resolved on 6% Tris-glycine gels and transferred to a nitrocellulose membrane (GE Lifesciences). Membranes were then blocked in 5% dry milk in Tris-buffered saline plus Tween-20 for 1 h and probed with rabbit anti-LRRK2-pSer1292 (1:1000, ab203181, Abcam) overnight at 4 °C. Membranes were washed three times for 10 min at RT in PBS containing 0.1% or 0.05% Tween 20 and then incubated for 1 h with antirabbit HRP conjugated (1:500, #7074, Cell Signaling). The membranes were coated with the enhanced chemiluminescent (ECL) reagent (WesternSure PREMIUM, Li-COR biosciences), and proteins were detected by C–Digit Imaging System (Li-COR Biosciences). For total LRRK2 detection, membranes were subsequently stripped (0.2 M Glycine pH 2.2, 0.1% SDS, 1% Tween-20), reblocked as above, and probed with rat monoclonal anti-LRRK2 (clone 24D8, 1:1000, Gloeckner lab[188]) overnight at 4 °C. Membranes were then incubated with antirat IgG-HRP (sc-2750, Santa Cruz Biotechnology). Membranes were again washed three times for 10 min at RT in PBS containing 0.1% or 0.05 Tween 20. The membranes were coated with enhanced chemiluminescent (ECL) reagent (WesternSure PREMIUM, Li-COR biosciences), and proteins were detected with a C–Digit Imaging System (Li-COR Biosciences). For quantification, images were analyzed with Image

Studio (Li-COR), and signals were normalized to total LRRK2 and expressed as percentage of within-gel DMSO controls.

Rab10 Immunoblotting

HEK293T cells were cotransfected at a confluency of 50–60% with Strep-FLAG tagged LRRK2 R1441G and Rab29 as well as Rab10 (both HA-FLAG tagged) using polyethylenimine (PEI, Polyscience) as previously described[92]. At a confluency of approximately 80%, cells were treated with either 1 μM MLi-2, DMSO, or 10 μM of LRIP4 or LCIP1. After an additional 15 h, cells were lysed twice, first in lysis buffer (30 mM Tris-HCL (pH7.4), 150 mM NaCl, 0.5% NP-40, complete protease Inhibitor cocktail, and phosphatase inhibitor cocktail II and III (Sigma-Aldrich), and again after centrifugation in 1% SDS. Cleared lysates were adjusted to 2 μg/μL with 5 × Laemmli Buffer and lysis buffer. Samples were used for denaturating electrophoresis using 10% Bis-Tris gels (NuPAGE) and for Western blotting onto PVDF membranes. Membranes were blocked with 5% nonfat dry milk dissolved in TBS-T (30 mM Tris-HCL (pH 7.4), 0.1% Tween 20) and separated horizontally at 140 kDa. Primary antibodies were added TBS-T with 5% BSA (pT73 Rab10) 1:2000 (ab230261) and pS1292 LRRK2 1:2000 (ab203181)) or total protein antibodies (Rab10(ERP13424) 1:5000 (ab181367) or LRRK2(clone 24D8) 1:5000 (Gloeckner lab)), respectively. Membranes were incubated with HRP-conjugated secondary antibodies diluted in TBS-T with 5% milk prior to imaging using ECL Plus (Pierce) with exposure to photometric films (Hyperfilms, GE Healthcare).

In Vitro GTPase Assay

Different concentrations of full-length wild-type LRRK2 (0.1 μM and 1 μM) were incubated with 10 μM of peptide either for 30 min at 20 °C or on ice overnight. Then, 500 μM GTP was added, and the production of GDP was monitored at 20 °C. To determine the amount

of GDP and GTP, we used a reversed phase HPLC using a Hypersil Gold column (Thermofisher) with 10 mM tetra-*n*-butylammonium bromide, 50 mM phosphate buffer, and 14% ACN containing buffer. Data were integrated with Chromeleon 7 (Thermofisher) and fitted with Grafit 5 (Erithacus Software).

ROS Production Assay

Flow cytometry was used to measure reactive oxygen species (ROS) through fluorescence emission of the CellROX deep red dye (Life Technologies). RAW264.7 cells (ATCC SC-6003) were plated at 120 000/well in a 96-well low-adherence tissue culture plate (Costar). Cells were preincubated with stapled peptide or DMSO for 9 h then stimulated with Zymosan for 30 min (50 μg/mL). The CellROX staining was done according to the manufacturer's instructions; the CellROX reagent was added to the cell cultures at a final concentration of 2.5 μM, and the mixture was incubated for an additional 30 min. Cells were lifted, kept on ice, and analyzed immediately. Cells were then analyzed on Beckman Cytoflex flow cytometer (Beckman Coulter). The fluorescent channel was APC (638 nm excitation [ex], 660 nm emission [em]). Reported fluorescent intensity values represent arithmetic means of the results determined for analyzed cells.

Preparation of Primary Mouse Neuronal Cultures and Assessment of Neuronal Death

Embryonic day 16 (E16) pregnant C57BL mice were used in this study, with primary cortical neurons prepared as described[109]. Briefly, under aseptic conditions, cortices were removed and cut into small pieces before enzymatic digestion (trypsin 0.05% and 100 μg/mL DNase) and mechanical dissociation. Cells were centrifuged and counted and plated at a density of 150 000/cm^2 in BrainPhys neuronal culture medium (StemCell Technologies) supplemented with SM1 Neuronal Supplement (StemCell Technologies), L-glutamine (0.5 mM), and

penicillin/streptavidin. After 3–4 DIV, neurons were transfected using Lipofectamine 2000 (Thermo Scientific) per the manufacturer's instructions. Neurons were transfected with Flag-tagged WT or mutant (G2019S) human LRRK2 (as described previously [109]). The following day, we initiated the treatment of neurons with fluorescently labeled peptides (at 10 μM final concentration). We replenished the peptides in the neuronal medium after 24 h and at the indicated concentrations. After 3 days following transfection, and 2 days of treatment, the coverslips were washed in PBS and fixed in 3.7% paraformaldehyde for 20 min at 4°C. The neurons were processed for immunofluorescence labeling with the following antibodies: GFP (chicken; Abcam), Flag (M2 mouse; Sigma-Aldrich), active caspase-3 (rabbit; R&D Systems), and DAPI nuclear stain. Mounted coverslips were imaged on a Leica TSP5 multiphoton confocal microscope and the Z-stacks processed in ImageJ and Adobe Photoshop. For quantification of apoptotic neuronal profiles, we used the approach described by Antoniou and colleagues[109].

Statistical Analysis

GraphPad Prism was used for statistical analysis. One-way ANOVA and Dunnett's multiple comparisons test were used for the analysis of western blots and ROS production. n.s. = not significant, *$p < 0.05$, **$p < 0.01$, ***$p < 0.001$, and ****$p < 0.0001$. For neuronal apoptosis assay and *in vitro* dimerization assays, a one-way ANOVA with Tukey posthoc tests was performed. All experiments were performed in triplicate, at minimum. Unless otherwise stated, graphed data are presented as means ± SEM.

3.6 Chapter 3 Figures

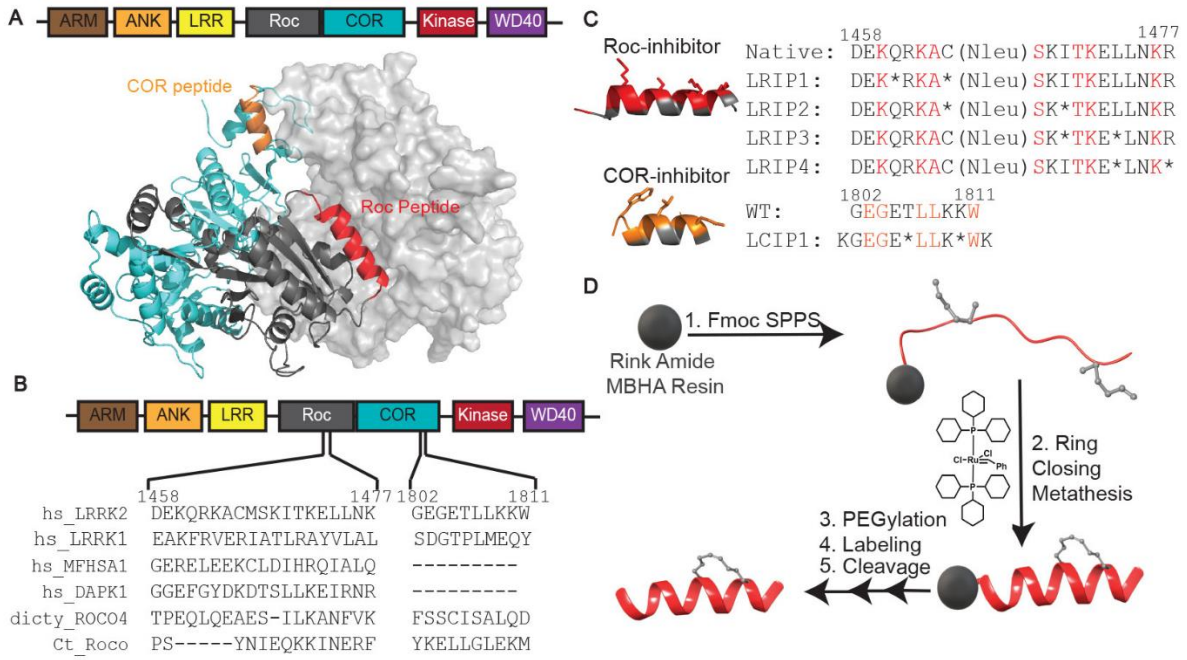

Figure 3.1 Design and synthesis of stapled peptide dimerization disruptors of LRRK2. a, Domain architecture of LRRK2 and homology model of the RocCOR dimer interface. The Roc domain is shown in dark gray and the COR domain is shown in cyan. The Roc peptide is highlighted in Red and the COR peptide is highlighted in orange. The dimer interface is indicated by the light grey surface. **b**, Sequence alignments of LRRK2 to other Roco proteins at the indicated interfaces. **c**, Peptide library sequences were designed to preserve amino acids at the predicted interface (red/orange). Non-natural amino acids were substituted on the predicted non-binding interface (grey). **d**, Schematic of Fmoc-based Solid Phase Peptide Synthesis (SPPS) and ring-closing metathesis.

A

Compound	MBP-RocCOR
LRIP Native	n.d.[1]
LRIP 1	n.d.
LRIP 2	n.d.
LRIP 3	n.d.
LRIP 4	58.2 ± 19.7 nM
Scramble	n.d.

B

Compound	MBP-COR
LCIP 1	1.1 ± 0.5 μM
Scramble	n.d.[1]

C

Figure 3.2 LCIP1 and LRIP4 bind LRRK2 *in vitro* and downregulate LRRK2 dimerization. a, Table depicting binding affinities of each peptide in the LRIP library to MBP-RocCOR. **b**, Table depicting binding affinities of LCIP1 and scramble to MBP-COR. **c**, Lysates derived from HEK293 cells overexpressing GFP-tagged LRRK2 were treated with 10 μM biotin-labeled peptides (LCIP1 and LRIP4) and pulldowns were performed using avidin-coated resin. LRRK2 was detected via immunoblotting, demonstrating that both peptides pulled down LRRK2. Blot is representative of n=3.

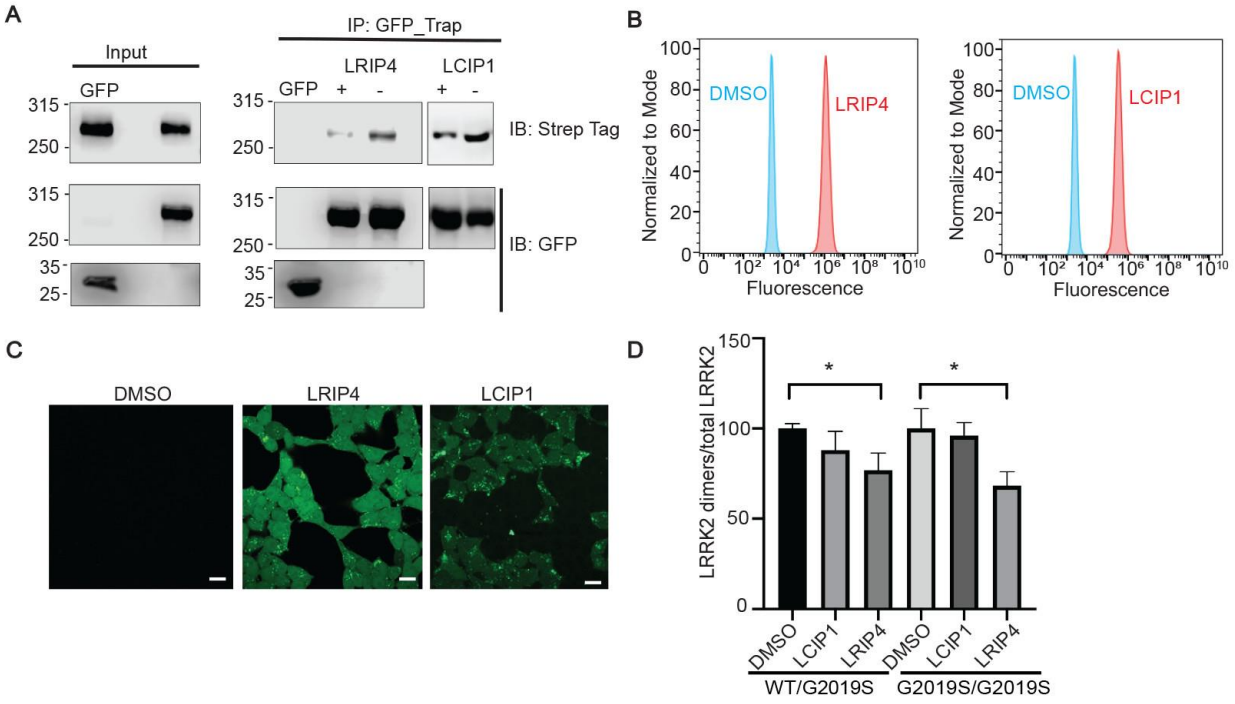

Figure 3.3 LCIP1 and LRIP4 permeate cells and are detected in the cytoplasm. a, HEK293 cells were transiently transfected with Strep-tagged LRRK2 and GFP or GFP-tagged LRRK2. Whereas Strep-LRRK2 did not bind non-specifically to GFP, it was pulled down with GFP-LRRK2. Incubation with inhibitory peptides LRIP4 and LCIP1 resulted in reduced dimerization. GFP alone is indicated in the bottom panel. Blot is representative of n=3. **b**, HEK293 cells were treated with 10 μM FAM-labeled LRIP4 or LCIP1 for 6 hours at 37 ℃. Flow cytometry experiments demonstrate that both peptides yielded an increased shift in fluorescence. **c**, Confocal fluorescence microscopy images indicate that LRIP4 and LCIP1 can be detected in the cytosol with LRIP4 demonstrating greater cytosolic accumulation. Scale bar corresponds to 20 μm. **d,** LRRK2 dimerization was measured in cells using a proximity biotinylation ELISA-based assay. Dimeric LRRK2 was biotinylated *in situ* and purified on streptavidin-coated ELISA plates. LRIP4 was found to inhibit dimerization of both wild-type/G2019S LRRK2 heterodimers or G2019S LRRK2 homodimers in HEK293 cells. *$p < 0.05$. Blot is representative of n=3.

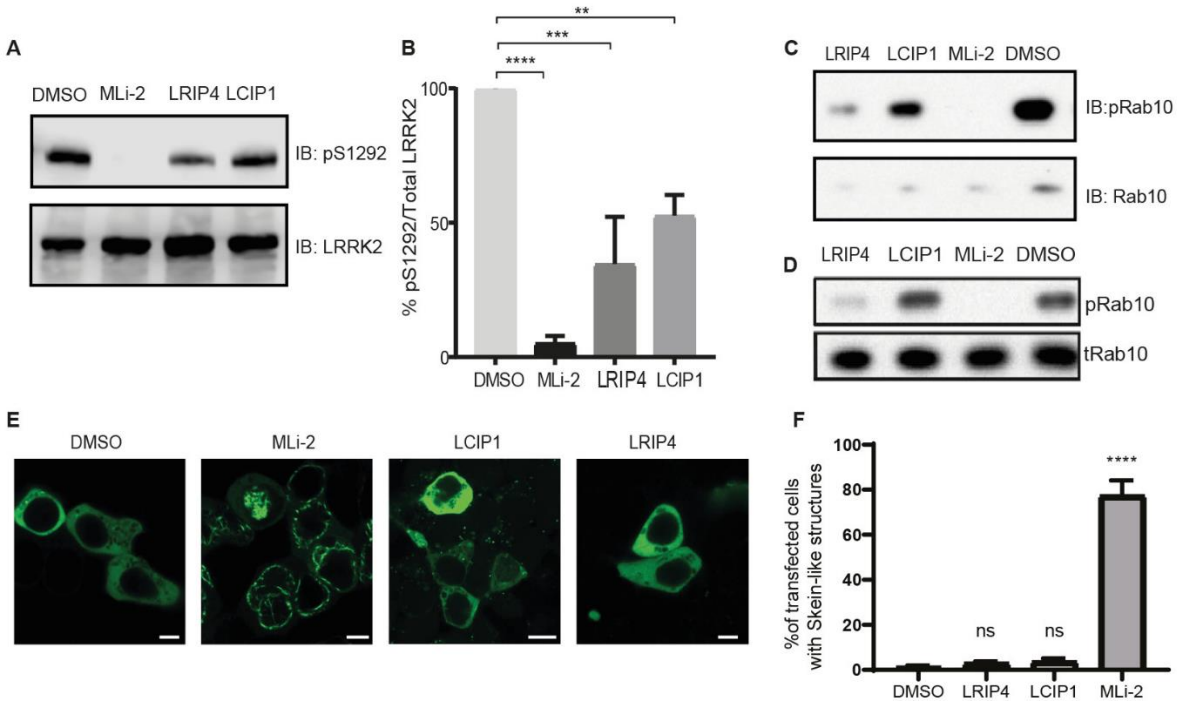

Figure 3.4 Figure 4. LRIP4 inhibits LRRK2 autophosphorylation and Rab10 phosphorylation. a, Autophosphorylation of LRRK2 (pS1292) was monitored in HEK293 cells in the presence of inhibitor peptides (10 μM) or the ATP-competitive LRRK2 inhibitor MLi-2 (100 nM). Both peptides inhibited LRRK2 autophosphorylation as compared to the DMSO control. Blot is representative of n = 3. **b,** Quantification of **a** by densitometric analysis. Levels of pS1292-LRRK2 were normalized to total LRRK2 expression and shown as LRRK2 activity relative to the DMSO control. Data was averaged from three independent experiments and are shown as means ± SD. The inhibitor peptides downregulated autophosphorylation by 50-70% but not as potently as MLi-2. **c**, HEK293T cells were transfected with SF-tagged LRRK2 (R1441G) and FLAG-HA-tagged Rab29 and treated with 10 μM of inhibitor peptides for 12 h prior to lysis. Endogenous Rab10 phosphorylation was reduced after treatment with LRIP4 or LCIP1, with LRIP4 having a larger inhibitory effect. **d**, Untransfected A549 cells were used to investigate the inhibitory effect of LRIP4 and LCIP1 (10 μM) on endogenous LRRK2 kinase

activity as measured by Rab10 phosphorylation. LRIP4 downregulated Rab10 phosphorylation. **e,** HEK293 cells were transiently transfected with GFP-tagged LRRK2 and treated with biotin-labeled peptides (10 μM of LRIP4 or LCIP1) for 12 h. As a control, cells were treated with 100 nM MLi-2. Unlike cells treated with MLi-2, LRIP4 and LCIP1 did not induce mislocalization of LRRK2 in cells. Scale bar represents 5 μm. Images are representative of n = 3. **f**, Quantification of the results in **e** is shown. A minimum of 200 transfected cells were analyzed under each condition for filamentous structures of GFP-LRRK2. The average percentage of cells showing skein-like structures and standard errors of the mean (SEM) for three biological replicates are shown. **** $p<0.0001$

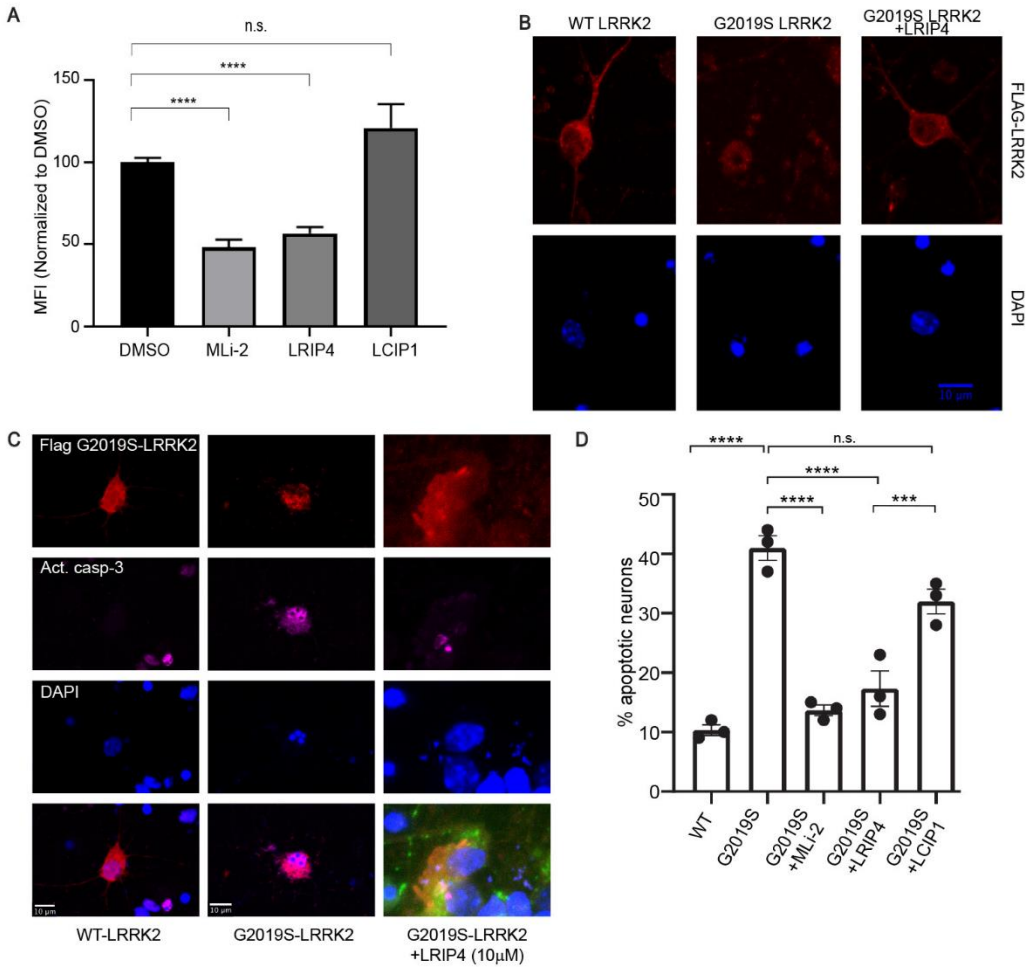

Figure 3.5 LRIP4 downregulates ROS production and neuronal apoptosis. a, Reactive oxygen species (ROS) was measured via fluorescence emission of the CellROX deep red dye. RAW 264.7 cells were treated with 10μM of each peptide for 9 hours then stimulated with Zymosan for 30mins (50 μg/mL). LRIP4 significantly downregulated ROS production. n=4. **b**, Cultured primary cortical neurons transiently overexpressing WT or G2019S-LRRK2 were treated with 10 μM of each peptide for 48h, or 200 nM of MLi-2. Fixed neurons were immunostained for flag-LRRK2 and counterstained with DAPI. Scale bar represents 10 μm. n=3. **c**, Primary neurons were transiently transfected with Flag-LRRK2 (WT, G2019S) and then

treated with following day with 10 μM LRIP4 for a total of 48hr (72hr total transgene over-expression). Neurons were fixed and immunostained for Flag and an active form of caspase-3, which strictly co-localizes in neurons with condensed/fragmented (2 or more) nuclei.**d**, Quantification of apoptotic neurons from **c**, Neurons from three biological replicates (independent transfections) were counted in a blinded manner. n=3. * $p<0.05$; ** $p<0.01$; *** $p<0.001$; **** $p<0.0001$.

CHAPTER 4

DOUBLY CONSTRAINED PEPTIDES AS ALLOSTERIC INHIBITORS OF LRRK2-MEDIATED PARKINSON'S DISEASE[4]

[4] Helton, L.G., Kentros, M., LeClair, T.J., Moore, T.T., Hall, S. Herberg, F.W., Rideout, H.J., & Kennedy, E.J. (In preparation) To be submitted to *Chemical Sci* **2022.**

4.1 Abstract

Leucine Rich Repeat Kinase 2 (LRRK2) is a protein kinase commonly mutated in Parkinson's Disease. Increased kinase activity of LRRK2 is a hallmark feature of LRRK2-mediated PD yet attempts to inhibit the kinase activity with ATP-competitive small molecule inhibitors has yielded molecular with significant off-target effects and inhibitor-induced protein mislocalization. As an alternative, allosteric inhibitors of LRRK2 dimerization were previously developed based on homology models of the Roc (Ras of Complex Proteins) COR (C-terminal of Roc) dimer interface, but initial targeting of COR-mediated dimerization yielded an underwhelming lead compound. Here, based on recently released crystal structures, we designed and a doubly constrained peptide that mimics a peptide within the COR domain believed to drive dimerization. We designed a helix-turn-helix peptide with the intention of destabilizing COR-mediated dimerization. Here we show that lead compounds can permeate cells, bind to LRRK2, and downregulate kinase activity *in vitro*. To our knowledge, an all-hydrocarbon double stapled helix-turn-helix peptide with the ability to permeate cells and elicit inhibition *in vitro* has not been reported, making this a first-in-class constrained peptide.

4.2 Introduction

Leucine Rich Repeat Kinase 2 (LRRK2) is a multi-domain protein kinase commonly mutated in Parkinson's Disease (PD). Composed of 2527 amino acids, LRRK2 contains a catalytic core (Ras of complex proteins (Roc) domain and Serine/Threonine Protein Kinase domain) surrounded by protein scaffolding domains (Armadillo Repeat Region (ARM), Ankyrin Repeat Region (ANK), Leucine Rich Repeat Region (LRR), C-terminal of Roc (COR), and WD40 region)[157]. Pathogenic mutations are localized to the Roc, COR, and kinase domains and typically result in hyperactivation of the kinase activity[38]. Early attempts to develop

therapeutics targeting LRRK2 were designed to inhibit the ATP-binding pocket of the kinase domain and abolish associated kinase activity[98]. While this target yielded multiple small molecules with high specificity and nanomolar binding, the diverse expression profile of LRRK2 resulted in LRRK2 mislocalization and toxicities[81, 82, 86, 87, 98].

As an alternative approach, we sought to disrupt LRRK2 dimerization as a means of downregulating kinase activity. We previously reported the successful design, synthesis, and characterization of all-hydrocarbon stapled peptides mimicking key helices within the Roc and COR domains of LRRK2 to allosterically inhibit LRRK2[107]. While the lead peptide candidate, LRRK2 Roc Inhibiting Peptide (LRIP4) demonstrated an ability to bind LRRK2 and elicit subsequent cellular effects in the nano- or micromolar range, the LRRK2 COR Inhibiting Peptide (LCIP1) was limited in its potency[107]. Previous work identified the COR region of LRRK2 as being the major energetic contributor of LRRK2 dimerization; therefore, we sought to develop a peptide able of disrupting this interface[92, 113, 190].

The first-generation inhibitors of LRRK2 dimerization, LRIP4 and LCIP1, were based on a homology model developed using single domain crystal structures, bacterial homologues, and integrative molecular modelling[92]. Recent efforts to determine the structure of LRRK2 have yielded multiple structures of LRRK2 in varying conformations. Intriguingly, both the full-length cryo-EM structure and the cryo-EM structure of the C-terminal RCKW portion of LRRK2 identified the COR domain of LRRK2 as essential in mediating dimerization[73-75]. This interface is predominantly composed of beta sheet and loops, with the beta sheets forming an overlapping interaction driven by hydrophobic content[74, 75]. Previous efforts to design dimerization disruptors identified a helix within the COR domain from a structural model, but this peptide showed inconsistent effects in cells[107].

Here, we report the design and development of a doubly constrained peptide mimicking a 30 residue peptide composing a key portion of the COR:COR dimer interface, as identified in recent crystal structures. Importantly, cryo-EM data indicates that this region of LRRK2 adopts a beta sheet confirmation, which is in direct contrast to previous reports indicating this region of LRRK2 was helical[74, 75, 92]. With the intention of designing peptides capable of permeating cells and disrupting the beta sheet stacking that stabilizes dimerization, we design a double constrained helix-loop-helix with key amino acids poised to bind a hydrophobic interface in the COR domain. Here we show the successful design and characterization of a doubly constrained peptide capable of permeating cells and downregulating pathogenic LRRK2 activity *in vitro*.

4.3 Results and Discussion

Previous work identified a short helical portion within the COR domain of LRRK2 as a a minor driver of dimerization[92, 107]. A constrained peptides designed based on this 10 amino acid sequence had a modest effect on downregulating dimerization but exhibited vast room for improvement[107]. Interestingly, when more recent structures of LRRK2 were solved, including the full-length dimer[75] and catalytic portion of LRRK2 (RocCor, Kinase, and WD40 domains, "RCKW"[74]), this helical region exhibited primarily sheet and loop content [**Figure 4.1A**]. When considering only the sequence of interest, peptide-modeling predictors indicated a propensity for helix-loop-helix for the selected sequence. Further, when docking the peptide sequence to both monomeric LRRK2 and LRRK2RCKW, the helix was predicted to adopt a similarly helical conformation with the loop contributing to binding. It is possible that the beta sheet stacking identified in the dimeric structure is a highly stabilized conformation; further, this dimeric structure was resolved in the absence of ATP[75]. We predict that the LRRK2 dimer exists in a series of conformations, which is consistent with previous work identifying a helix

within the Roc domain as a major inhibitor of dimerization[107]. This is in direct contrast to the new structures of LRRK2 and indicates the potential for more variability than current structures indicate[74].

Based on these results, we designed a 29 amino acid peptide [**Figure 4.1B**] and performed docking experiments with both LRRK2 RCKW and monomeric LRRK2 to identify which amino acids contributed significantly to binding using BUDE Alanine Scanning software. We identified a hydrophobic bundle within the loop region as a major contributor to binding across multiple models [**Figure 4.1C**]. The primary concerns in general when designing a peptide are the proteolytic stability, preference of the peptide for the intended secondary structure, and ability of the peptide to permeate cells[17]. When considering a 29 amino acid sequence, our primary concern was the ability of this peptide to permeate cells to reach its intracellular target. All-hydrocarbon stapling, where olefinic amino acids are incorporated into the sequence and metathesized to form a covalent "staple", is effective in improving many of the drawbacks seen with native peptides[9]. Seminal work performed by Bird, G.H. et al. identified double stapling as capable of improving proteolytic stability, but there is limited work focusing on doubly constrained peptides and their ability to permeate cells[191]. Given the length, size, and complex secondary structure of this sequence, we sought to introduce two staples along the nonbinding interface of both the C- and N-terminal helices while conserving the native sequence of the loop region believed to be essential for binding [**Figure 4.1D, E**]. To promote the ability of the loop region to adopt a loop conformation, we introduced a glycine mutation at position 1812A, which would promote the adaptation of the helix-loop-helix conformation. To further analyze the contributions of the double staple, we designed analogous single stapled peptides to discern both the biochemical and cellular impact [**Figure 4.1D, E**]. The **E**longated **COR** peptide

library (“ECOR”) consists of one native peptide, two single stapled (“SS”) peptides, and two double stapled peptides [**Figure 4.1E**]. Further, the amino acid following 1812 indicates whether there was a glycine substitution, indicated “ECOR12G” [**Figure 4.1E**].

Our first aim was to characterize the secondary structure of all our peptides to better compare how the native, single, and double stapled peptides. Further, we aimed to identify if and how the A1812G mutation altered secondary structure. Circular dichroism results show that all peptides exhibit some helicity, as indicated by minima at 208nm and 222nm; however, as expected, the native peptide exhibits minimal helical content when compared to the stapled peptides. Both double stapled peptides, ECOR12A and ECOR12G, exhibited high helical content, with ECOR12G being predominately helical [**Figure 4.2A**]. The helicity exhibited by ECOR12A and ECOR12G, however, did not improve the proteolytic stability of the peptide when compared to the single stapled peptide. While the native peptide was degraded within 30 minutes of exposure to mouse serum, all stapled peptides exhibited long-term stability up to six hours [**Figure 4.2B**].

Biochemical characterization revealed that while the double stapled did not embed improved stability, it did contribute to higher levels of helicity. We next sought to determine the ability of the peptides to permeate cells to identify which compounds, could move forward with *in vitro* and target-specific assays. RAW macrophages were treated with 10μM fluorescently labelled peptide for eight hours, washed with PBS, stained with Hoechst, and fixed with paraformaldehyde prior to imaging via fluorescent microscopy. As expected, the native unstapled peptide exhibited no uptake, whereas all the stapled peptides exhibited some level of uptake [**Figure 4.3A**]. The degree of uptake was significantly higher with the double stapled peptides when compared to the single stapled [**Figure 4.3A**]. While we do see small peptide

aggregates in some cases, this could likely be mitigated with lower dosing. Due to the higher level of uptake with double stapled peptides, we proceeded to binding affinity assessment and *in vitro* analysis with both ECOR12A and ECOR12G.

To determine if the ECOR peptides were able to bind LRRK2, we first performed fluorescence polarization (FP) assay using FAM labelled peptides and purified RocCOR or RCKW constructs. Due to the elusive native of purified full-length LRRK2, we first sought to determine if the peptides could bind to the predicted RocCOR dimer interface. Both ECOR12A and ECOR12G exhibited binding to RocCOR in the low nanomolar range, which is comparable to first-generation inhibitors of LRR2 dimerization. We then wanted to determine how the presence of the kinase domain and WD40 domain would affect peptide binding by using purified RCKW. Interestingly, both ECOR12A and ECOR12G were able to bind to the RCKW construct in the low nanomolar range, confirming the importance of C-terminal domains in dimerization and subsequent peptide binding [**Figure 4.4**].

We next sought to assess whether these peptides could also inhibit LRRK2 dimer formation in cells. We used a previously published *in situ* LRRK2 proximity biotinylation approach[97](chapter 3). Both ECOR12A and ECOR12G disrupt dimerization of LRRK2 in cells in the low micromolar range [**Figure 4.5**]. LRRK2 dimerization is directly associated with increased kinase activity; therefore, we sought to determine if our lead compounds could downregulate phosphorylation of downstream substrates[107, 187]. Recently, a subset of Rab GTPases was identified as downstream substrates of LRRK2[61]. To determine how ECOR12A and ECOR12G would affect LRRK2 kinase activity, we utilized A549 cells, which endogenously express both LRRK2 and Rab10. At 2.5μM, both ECOR12G and ECOR12A were able to significantly downregulate WT LRRK2 kinase activity [**Figure 4.6 A,B**]. We anticipate

that at higher concentrations, ECOR12A and ECOR12G are aggregating, which is decreasing their ability to directly interact with LRRK2. Here we show that doubly constrained peptides can permeate cells, bind their intended target, and downregulate associated pathways. This work serves as a proof-of-concept for both allosteric inhibition of COR-mediated dimerization of LRRK2 and the development of doubly constrained peptides with *in vitro* potential and relevance.

4.4 Methods

Circular Dichroism. CD experiments were performed as previously described[192]. Briefly, FAM labelled peptides were diluted to 5-40 μM in diH_2O and readings taken using the Jasco J-710 CD Spectrometer. Blanks were measured and used as a baseline for each peptide concentration measurement. The path length was 0.1 cm, sensitivity was 100 mdeg, and scanning mode was continuous at 50 nm/min. Savitzky-Golay smoothing was applied to all measurements. Mean residue ellipticity was calculated using JASCO software and known molecular weights and concentrations.

Proteolytic Stability. Proteolytic stability assessment was performed as previously described[192]. Briefly, peptides were incubated at a concentration of 0.2mM in a stability cocktail composed of 50% mouse serum, 0.4% benzoic acid, and 15% DMSO in PBS at 37C with agitation. At the indicated time period, aliquots were drawn and serum was precipitated using an equal volume of 0.1% TFA acetonitrile. The precipitate was centrifuged at 14k rpm for five minutes and the supernatant was collected for analysis. Degradation was monitored as a ratio of peptide to control at 280nm using HPLC-MS with the same flow rates as previously described. This process was repeated in triplicate for each time point.

Cell Culture LRRK2 parental RAW 264.7 cells (ATCC, SC-6003) were cultured in Dulbecco's Modified Eagle's medium (DMEM, ATCC, 30-2002) supplemented with 10% FBS and 1% penicillin-streptomycin (Gibco, 15070063). A549 cells (ATCC, CCL-185) were grown in Dulbecco's Modified Eagle's medium (DMEM, Gibco, 11960044) supplemented with 10% FBS and 1% penicillin-streptomycin-Glutamine (Gibco, 10378016).

Peptide Synthesis. Peptide synthesis was performed as previously described[107] (chapter 3).

Peptide Characterization. Peptides were purified, quantified, and characterized as described in chapter 3 of this dissertation.

The peptide sequence for FAM labelled ECOR Native is 5(6)-carboxyfluorescein-PEG_3-GEGETLLKKWALYSFNDGEEHQKILLDL, and the mass is 3948.8 (expected = 3949.5)

The peptide sequence for FAM labelled ECOR12A is 5(6)-carboxyfluorescein-PEG_3-KGEGE*LLK*WALYSFNDGEKH*KKL*KL, and the mass is 3978.9 (expected = 3979.6)

The peptide sequence for FAM labelled ECOR12A SS is 5(6)-carboxyfluorescein-PEG_3-KGEGE*LLK*WALYSFNDGEKHQKKLLKL, and the mass is 4099.2 (expected = 4099.7)

The peptide sequence for FAM labelled ECOR12G is is 5(6)-carboxyfluorescein-PEG_3-KGEGE*LLK*WGLYSFNDGEKH*KKL*KL, and the mass is 3965.4 (expected = 3965.6)

The peptide sequence for FAM labelled ECOR12G SS is 5(6)-carboxyfluorescein-PEG_3-KGEGE*LLK*WGLYSFNDGEKHQKKLLKL, and the mass is 4085.2 (expected = 4085.7)

Cell Uptake. RAW Macrophages cells were seeded at 20,000 cells/well on 8-well chamber slides (BD Biosciences). Cells were grown overnight in complete DMEM (10% Fetal Bovine Serum and 1% Penicillin Streptomycin). 10μM of FAM labelled peptides were added once cells reached 70% confluence and incubated at 37 °C for 8 hours before staining with Hoechst and fixation

with 2% paraformaldehyde. Slides were imaged using an Olympus 1X71 microscope, and three independent uptake experiments were completed.

Fluorescence Polarization Assays Direct binding of our lead compounds (ECOR12A and ECOR12G) to LRRK2 constructs was assessed via FP assays. We measured binding with purified MBP-tagged RocCOR LRRK2 protein in the presence of 2 mM GTP and 10 mM $MgCl_2$. Each FAM-labeled peptide was plated at a final in-well concentration of 10 nM in 384-well microtiter plates. 1:2 dilutions of the protein were then performed from a concentration range of 5 μM to 1 nM. For each peptide/protein interaction, we had a range of at least 10 protein concentrations, and each concentration was performed in triplicate. The assay was performed in FP buffer (20 mM MOPS pH 7, 150 mM NaCl, and 0.005% CHAPS) at RT. The peptide/protein mixture was incubated at RT for 2 h with readings taken every 30 min. The final readings were obtained at 2 h. The FP assays completed with the RCKW construct were same as above, with the addition of 2 mM ATP.

Proximity Biotinylation Assay was performed as previously described [107] (chapter 3).

4.5 Chapter 4 Figures

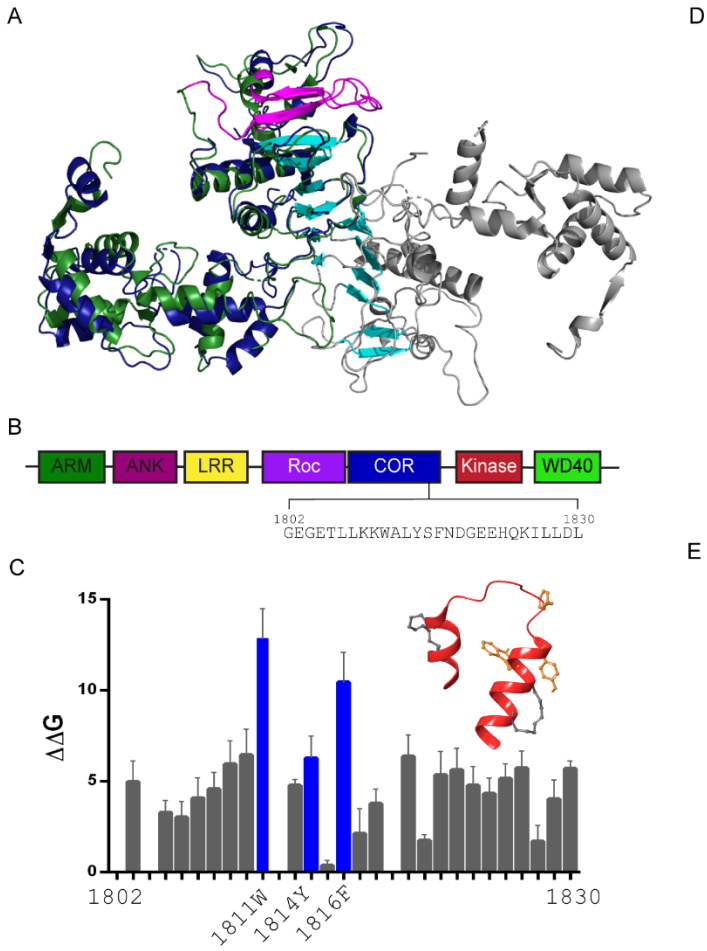

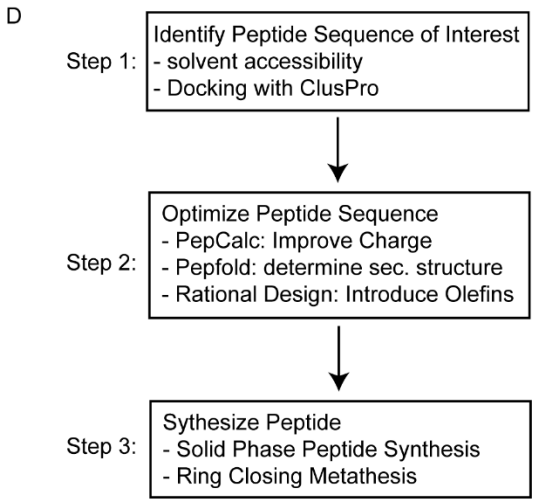

E

Peptide Name	Peptide Sequence
NATIVE	GEGETLLKKWALYSFNDGEEHQKILLDL
ECOR12A	KGEGE*LLK*WALYSFNDGEKH*KKL*KL
ECOR12ASS	KGEGE*LLK*WALYSFNDGEKHQKKLLKL
ECOR12G	KGEGE*LLK*WGLYSFNDGEKH*KKL*KL
ECOR12GSS	KGEGE*LLK*WGLYSFNDGEKHQKKLLKL

Figure 4.1 Rational Design of Doubly Constrained Helix-Loop-Helix Peptides. a, Overlay of the COR dimer interface with LRRK2 RCKW shown in navy and full-length dimeric LRRK2 shown in green and grey. 7+1 beta sheet stack is shown in cyan and ECOR sequence is shown in magenta. **b**, Schematic of LRRK2 and location of ECOR sequence **c**, Results of Alanine scanning with n=10 models. Shown in blue are the hydrophobic triad. Theoretical helix-loop-helix designed based on these results is shown in red with hydrophobic triad in orange. **d**, Workflow for the design of ECOR peptides. **e**, Peptide names and sequences. Shown in pink are Lysine substitutions that were added to improve charge. Shown in blue is the Glycine mutation.

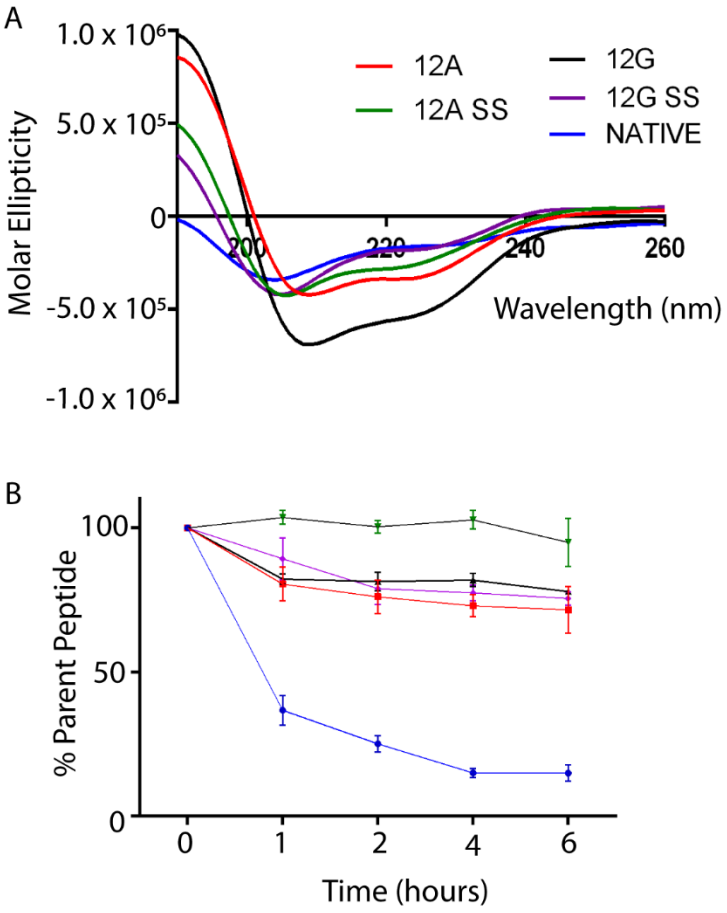

Figure 4.2 Biochemical Characterization of ECOR library. a, Circular Dichroism results with peptides color coded based on the legend. Minima at 208nm and 222 nm indicate the presence of helical content. Measurements were taken at 5μM in diH_20 and molar ellipticity was calculated using JASCO software. **b,** 0.2mM peptide was incubated in mouse serum for 0, 1, 2, 4, and 6 hours with agitation. At the designated time points, serum was separated using an acetonitrile cocktail. Supernatant was run on RP-HPLC and analyzed with ESI-MS using benzoic acid as a control.

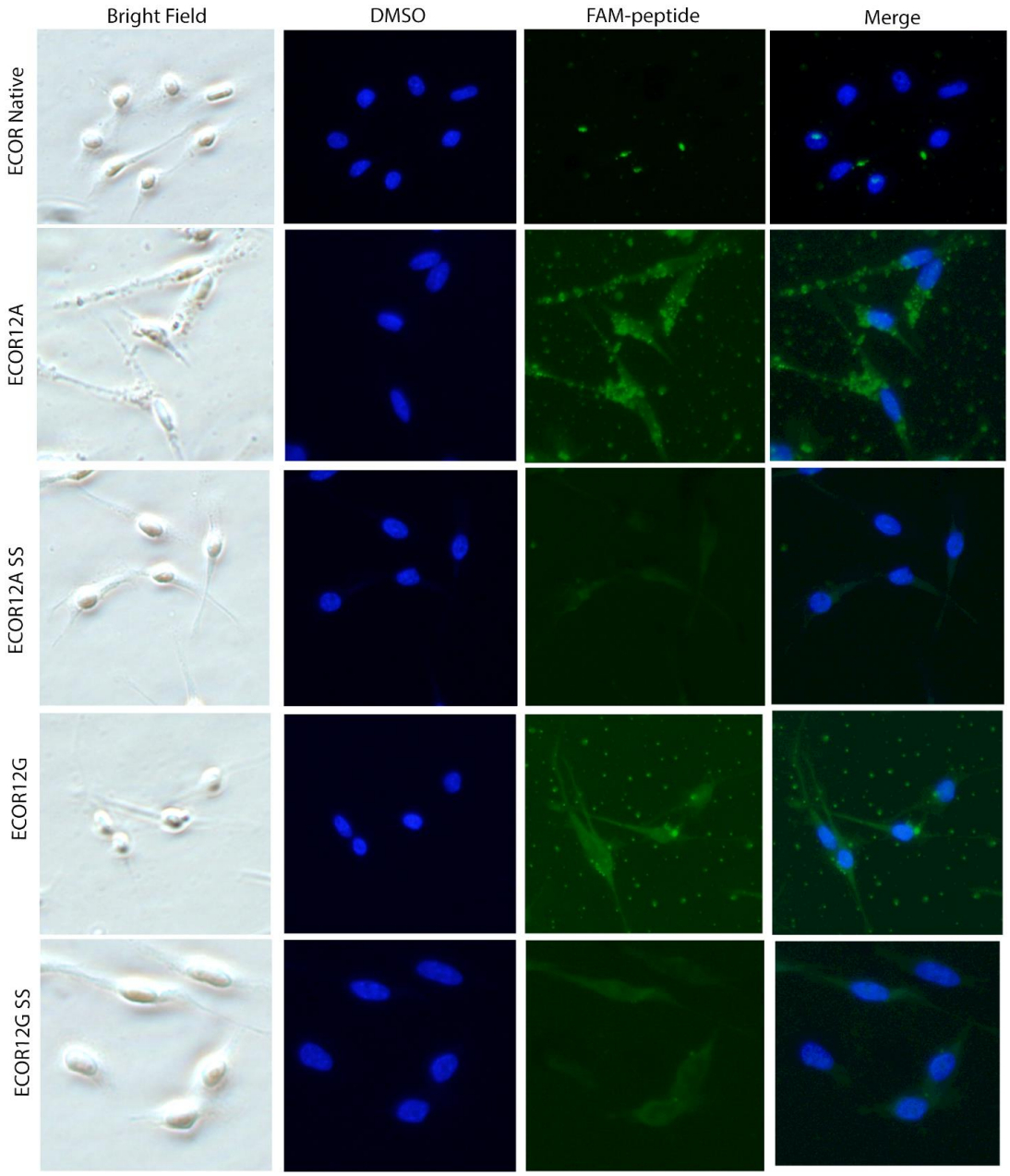

Figure 4.4 Double Staple Improves Cell Permeability of Peptides. RAW 264.7 Macrophages (20,000 cells/well, 8 chamber well slide) were treated with 10μM peptide for 8 hours prior to nuclear staining with Hoechst and fixation. Cells were images via fluorescence microscopy and cells were counted using ImageJ.

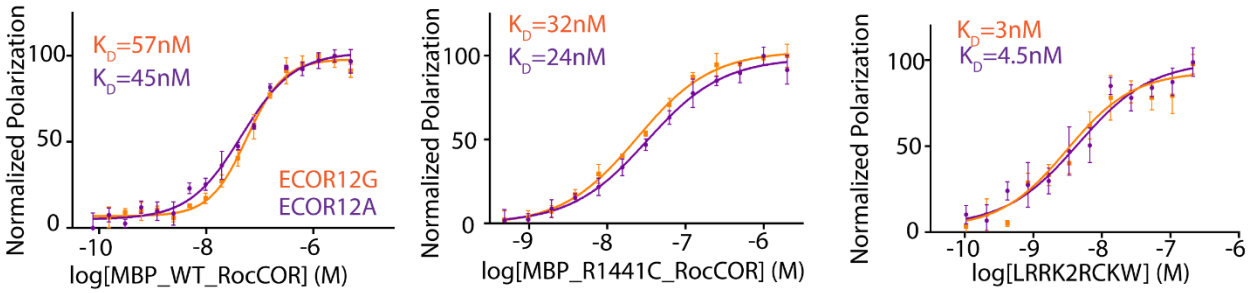

Figure 4.4 ECOR12A and ECOR12G bind to LRRK2 constructs. Fluorescence Polaization assays indicated that ECOR12G and ECOR12A bound the RocCOR construct with a K_D of 57nM and 45nM, respectively. Both ECOR12G and ECOR12A exhibited slightly higher affinity for the pathogenic mutant R1441C RocCOR protein with K_D values of 32nM and 24nM. Both peptides demonstrated the highest affinity for the C-terminal RCKW portion of LRRK2 at K_D values of 3nM and 4.5nM. Each data point is representative of n =3 and K_D was determined using GraphPad Prism.

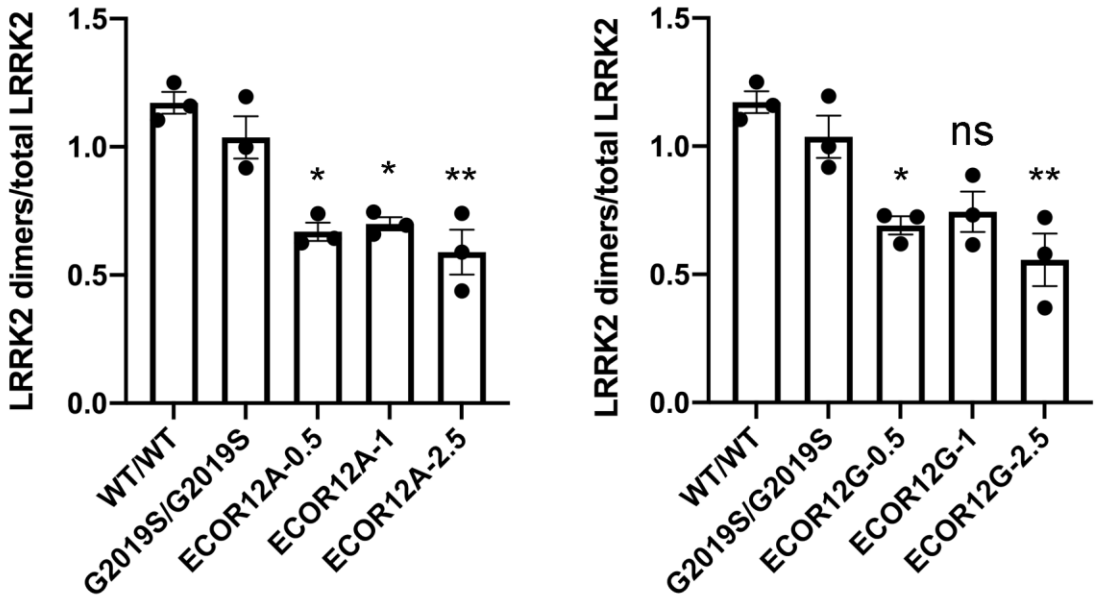

Figure 4.5 ECOR12 peptides disrupt dimerization in cells. LRRK2 dimerization was measured in cells using a proximity biotinylation ELISA-based assay. Dimeric LRRK2 was biotinylated *in situ* and purified on streptavidin-coated ELISA plates. ECOR12 was found to inhibit dimerization of G2019S LRRK2 homodimers in HEK293 cells. *$p < 0.05$ **$p<0.005$.

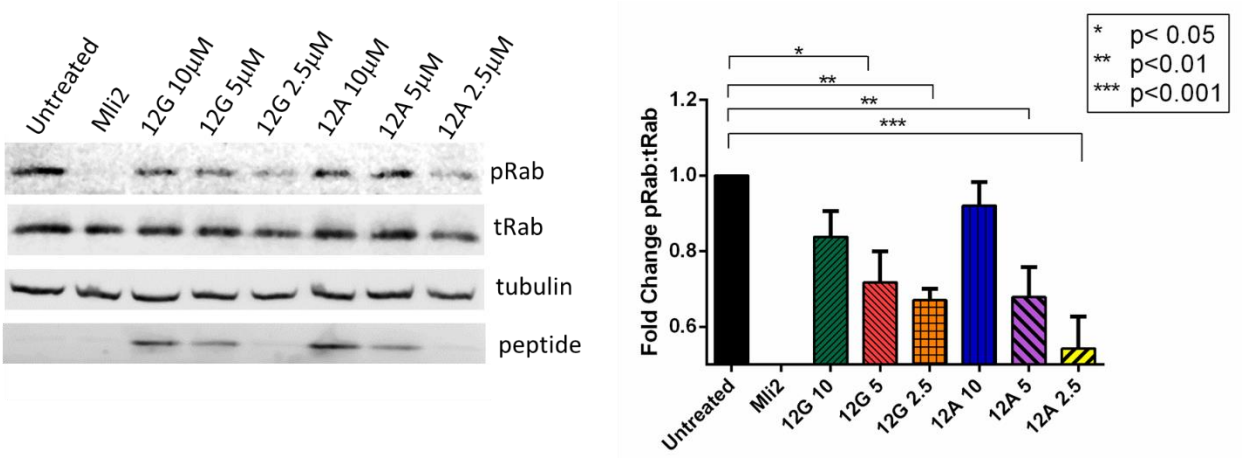

Figure 4.6 ECOR12A and ECOR12G decrease LRRK2 kinase activity. A549 cells were treated with varying concentrations of peptide for 8 hours prior to lysis. Mli-2 treatment was 100nM for 90 minutes prior to lysis. At low concentrations, both ECOR12A and ECOR12G deplete LRRK2 kinase activity by 30-40%. n=3.

CHAPTER 5

MIMICKING FAS ASSOCIATED DEATH DOMAIN (FADD) TO ALLOSTERICALLY INHIBIT LRRK2-MEDIATED APOPTOSIS AND PROVIDE NEUROPROTECTION[5]

[5] Helton, L.G., Kentros, M., Tantis-Tapeinos, D., Polissidis, A.V., Kennedy, E.J., & Rideout, H.J. (In Preparation) To be submitted to *npj Parkinson's Disease* **2022**

5.1 Abstract

Parkinson's Disease-linked mutations in the gene encoding Leucine rich repeat kinase 2 (LRRK2) are the most common genetic form of the disease. Kinase inhibition of LRRK2 effectively blocks neuronal death, and Type I inhibitors are proceeding in clinical trials. The toxic interaction between mutant LRRK2 and Fas Associated Death Domain (FADD) lies downstream of its kinase activity and is required to induce neuronal death. Our goal in the present study was to determine if constrained peptides could disrupt the interaction between LRRK2 and FADD to provide neuroprotection. We designed all-hydrocarbon stapled peptides mimicking the alpha-helical portion of FADD that directly forms the protein interaction interface with the LRRK2 armadillo region. *In vitro* peptide treatment significantly reduced this interaction and blocked the apoptotic death of primary neurons expressing mutant LRRK2 in a kinase-independent manner. Our work has identified novel constrained peptides capable of disrupting mutant LRRK2 induced neuronal death in an allosteric manner, thus providing a potential alternative therapeutic approach.

5.2 Introduction

Neuronal death induced by mutant forms of leucine-rich repeat kinase 2 (LRRK2), either in viral *in vivo* models or cellular over-expression models, requires a complex series of signaling events dependent on both intact kinase activity and the presence of specific components of various cell death pathways[88, 112, 181, 193-195]. We have previously shown that the baseline interaction between wild type (WT) LRRK2 and the death adaptor protein FADD is strengthened by most pathogenic mutant forms of LRRK2, and this interaction serves to recruit and activate caspase-8[112]. We further showed that the increased interaction between mutant LRRK2 and FADD was downstream of LRRK2 kinase activity, as genetic ablation of kinase activity

normalized the interaction with FADD to endogenous levels[112]. Subsequently, we went on to show that in addition to activating these components of the extrinsic death pathway, FADD/caspase-8 signaling in neurons activated downstream mitochondrial death cascades involving Bid and Bax translocation to the mitochondria[109].

We mapped the binding domain of LRRK2 that mediated the interaction with FADD to the armadillo region within the large N-terminal domain of LRRK2[109]. Homology modeling of this region of LRRK2, coupled with molecular docking techniques, further refined the domain mapping to identify candidate residues that mediate this interaction. Targeting the LRRK2-FADD interaction using genetic or dominant negative approaches successfully reduced the PPI and was neuroprotective in primary cultured cortical neurons[109]. Deletion of the FADD-binding region within the ARM domain of LRRK2 reduced the recruitment of WT LRRK2 to overexpressed FADD death-effector filaments and prevented the induction of neuronal death by mutant LRRK2. Similarly, co-expression of a dominant negative fragment of the FADD death-domain together with mutant LRRK2, prevented the binding of LRRK2 with full-length FADD, and was also neuroprotective[109]. In the current study, our goal was to design and develop constrained peptides to destabilize the LRRK2-FADD complex.

By designing peptides to mimic the LRRK2-binding region of FADD, we sought to disrupt the PPI via direct inhibition of the binding interface. We utilized the crystal structure of the FADD death domain and the model we previously generated of the LRRK2-ARM region to identify which residues are essential for mediating the interaction and which non-interacting residues could be substituted in favor of olefinic amino acids that permit chemical constraint of the peptide. This chemical constraint, or “staple”, is introduced along the non-binding interface

of the peptide, improves peptide stability, decreases proteolytic cleavage, improves overall target binding, and increases cell permeability of the peptide[9, 107, 168].

Here, we show that mimicking the alpha helical nature of the LRRK2-binding region of FADD with constrained peptides effectively disrupts the interaction and results in neuroprotection in a cellular model of mutant LRRK2-PD. We demonstrate cellular uptake of the candidate peptides in both HEK293T cells and primary cortical neurons, where the PPI between LRRK2 and FADD is disrupted. Critically, as we have previously shown, blocking the interaction between mutant LRRK2 and FADD in primary neurons can prevent the initiation of a FADD-dependent cell death pathway and subsequent apoptotic neuronal death. Identifications of peptides that are capable of downregulating PD-linked cellular effects in vitro validates disruption of the FADD:LRRK2 complex as a therapeutic target.

5.3 Results and Discussion

We have previously designed all hydrocarbon stapled peptides that disrupt LRRK2 dimerization, downregulate kinase activity, and decrease neuronal apoptosis in vitro[107]. Since validating allosteric modulation of LRRK2 as a means of downregulating LRRK2-mediated pathogenesis, we sought to apply the same technique to disruption of the LRRK2:FADD interaction. Homology modeling identified a helical region within FADD as responsible for driving its association with LRRK2 [**Figure 5.1A, cyan**][109]. The identification of both the helical region of FADD and peptide binding interface of LRRK2 revealed a few potential interactions between the proteins that we aimed to conserve [**Figure 5.1B**]. Native peptides often exhibit poor solubility, lack of secondary structure, poor target engagement, and inability to diffusely permeate cells[17]. To overcome these barriers in the development of peptides as therapeutics, the introduction of non-natural amino acids and chemical constraints has yielded a

wide variety of potential modifications that can be utilized on a case-by-case basis[196]. Here, we introduced non-natural amino acids along the non-binding interface at the *i, i+4* positions. These olefinic amino acids were cyclized to form a "staple" via ring closing metathesis [**Figure 5.1C**]. The staple reinforces the helical nature of the peptide, embeds the hydrophobic peptide backbone, reduces the susceptibility to proteolytic cleavage, and enhances the ability of the peptides to permeate cells[9]. Based on the availability of non-interacting residues, we designed an initial library of five FADD mimicking Armadillo-binding peptides (FARM1-5) [**Figure 5.1D**]. The peptide sequence was flanked with lysines to improve the charge from 0 to +2, and olefinic amino acids were introduced at shifting positions along the non-binding interface.

We have previously shown that deletion of an N-terminal region within LRRK2 disrupts the interaction with FADD and is neuroprotective[109]. Here, we take an alternative approach to disrupting the PPI by competitive binding with short, conformationally constrained peptides predicted to bind the same motif within the N-terminal region of LRRK2. We first determined the ability of the peptides to disrupt the interaction between LRRK2 and FADD in vitro via co-immunoprecipitation. While FARM2 and FARM3 both exhibited a clear ability to disrupt the interaction, FARM5 produced the greatest and most consistent reduction in co-immunoprecipitation [**Figure 5.2**].

After identifying our lead compound, we next sought to determine if FARM5 could permeate cells by treating cells with a fluorescently-labeled peptide and visualizing via confocal microscopy. As the interaction between LRRK2 and FARM5 is primarily neuronal, the ability of FARM5 to permeate cells and reach its intracellular target is critical for its potential as a PPI disruptor. Here, we show that FARM5 exhibits superior uptake when compared to the native,

unstapled control peptide, indicating that the hydrocarbon constraint improves cell uptake [**Figure 5.3**].

Previous work has shown that overexpression of mutant LRRK2 (G2019S or other pathogenic mutants) in primary cortical cultures neurons results in apoptotic death of the neurons[193, 197]. Our previous work characterizing the pathologic interaction between LRRK2 and FADD has demonstrated the importance of this PPI in transducing neuronal death induced by mutant LRRK2[112, 193]. Disruption of this interaction by dominant negative fragments of both FADD[112] and LRRK2[109], or by deletion of the predicted FADD-binding domain[109], is neuroprotective against over-expression of mutant LRRK2. To determine if FARM5, which shows efficacy in disrupting the interaction between LRRK2 and FADD, is also able to block apoptotic death of primary neurons, we treated mouse embryonic cortical neurons transiently transfected with G2019S LRRK2 with increasing concentrations of peptide. When treated with 10 μM FARM5, neurons expressing G2019S-LRRK2 lack evidence of chromatic condensation or other apoptotic features such as caspase-3 activation. The lowest concentration, 0.1 μM of FARM5 was unable to significantly block apoptotic neuronal death; however, at higher concentrations, 1 and 10 μM, the percentage of neurons with apoptotic profiles was significantly reduced [**Figure 5.4**]. This indicates that disrupting the LRRK2-FADD interaction using small, constrained peptides can effectively protect primary neurons from the cell death pathway triggered by expression of mutant LRRK2.

By allosterically regulating LRRK2, we aim to disrupt mutant LRRK2-dependent apoptotic death signaling without altering other key functions of the protein, such as its kinase activity. To determine if the PPI-disrupting stapled peptides alter LRRK2 kinase activity in cells, we cotransfected HEK293T cells with WT or G2019S-LRRK2 together with Rab10. Cells

expressing mutant LRRK2 and Rab10 were treated with our FARM5 compound and cell extracts were probed for multiple indication of LRRK2 kinase activity, including phosphorylated Rab10 and autophosphorylation of S1292 on LRRK2. As a positive control for inhibition of LRRK2 activity, parallel cells were treated with the potent inhibitor of LRRK2, ML2-2[83]. Cells co-expressing G2019S-LRRK2 and Rab10 exhibited a robust increase in pRab10 levels, compared to WT-LRRK2 expressing cells, or cells treated with MLi-2, indicating increased kinase activity. Additionally, levels of pS1292-LRRK2 were increased as expected in cells expressing G2019S-LRRK2, which was prevented by treatment with MLi-2. In contrast to the inhibition of autophosphorylation and phosphorylation of Rab10 by MLi-2, we could not detect any loss in phosphorylation upon FARM5 treatment [**Figure 5.5**]. There is an unexpected increase in the phosphorylation of Rab10 in G2019S-expressing cells treated with FARM5, which does not appear to be dose-dependent; however, the reasons for this are unclear. Rab10 phosphorylation could be an adverse result of peptide uptake or mislocalization of LRRK2 upon peptide treatment, but elucidating the precise reasoning is beyond the scope of this work. In a cellular setting, disruption of the interaction between LRRK2 and FADD using constrained peptides does not alter the kinase activity of LRRK2.

Until recently, the precise mechanism by which LRRK2 contributed to neuronal apoptosis in Parkinson's Disease was unclear. The identification of the interaction between LRRK2 and FADD, which allows mutant pathogenic LRRK2 to hijack the extrinsic death pathway and trigger increased levels of apoptosis, was essential for highlighting the crucial role of the protein-protein interaction in LRRK2-mediated pathogenesis[109]. The interaction between LRRK2 and FADD exists in endogenous levels but is significantly upregulated by pathogenic mutations exhibiting an increase in kinase activity, and kinase inhibition normalized

the PPI to wild-type levels [112]. Given the discrepancy of kinase activity across different pathogenic mutants and cell lines, we sought to determine how allosteric inhibition of the PPI would regulate apoptosis and whether this interaction is kinase independent[65]. Further, due to the adverse side effects seen with some LRRK2 kinase inhibitors[86, 87], subtler regulation of LRRK2-mediated apoptosis represents an area of therapeutic interest.

Here, we sought to disrupt this clinically relevant PPI by mimicking the LRRK2-binding region of FADD to outcompete FADD *in vitro*. We designed a library of all-hydrocarbon stapled peptides and identified a lead compound, FARM5, that can permeate cells, disrupt the interaction between LRRK2 and FADD, and downregulate apoptosis in neurons. Further, while inhibition of the interaction between LRRK2 and FADD provided neuronal protection, disruption of this PPI was not associated with a decrease in kinase activity. This work serves as a proof of concept that neuronal apoptosis triggered by mutant LRRK2 is, in part, independent of its kinase activity and identifies the FADD:LRRK2 PPI as a major contributor to neuronal apoptosis.

5.4 Methods

Plasmids and cell culture. Plasmids used for the assessment of the LRRK2-FADD PPI, as well as the over-expression of mutant LRRK2 in primary cortical neurons, were as previously described[109]. Human LRRK2 cDNA[112] was PCR-amplified and sub-cloned into pcDNA3.1(+) with an N-terminal Flag epitope tag. The G2019S and R1441C pathogenic mutations were introduced using site-directed mutagenesis (QuikChange; Agilent Technologies) as per the manufacturer's instructions, and fully sequenced to ensure no errors were introduced. N-terminal V5-tagged FADD expression constructs were used as previously described[109, 197].

Design and Synthesis of Peptide Library. Peptides were designed based on a previously generated homology model of the FADD:LRRK2 interaction[109] using a combination of

PepCalc, ClusPro, Pep-Fold, BUDE Ala Scan, and rational design. Peptide synthesis was performed via standard solid phase peptide synthesis (SPPS) with N-a-Fmoc protected amino acids on rink amide MBHA resin. All reagents and solvents were purchased from Sigma-Aldrich, Fisher, or Acros unless otherwise stated. Deprotection was performed using 25% (v/v) piperidine in 75% (v/v) N-methylpyrrolidinone (NMP) for 25 minutes with agitation. After deprotection, resin was washed 3x for 30 seconds with NMP before coupling standard amino acids by adding 10 equiv of amino acid, 9.9 equiv 2-(6-chloro-1H-benzotriazole-1-yl)-1,1,3,3-tetramethylaminium (HCTU in NMP), and 20 equiv of N,N-diisopropyl ethylamine (DIEA). The coupling solution was agitated for 45 minutes. For the olefinic amino acid S_5 ((S)-N-Fmoc-2-(4-pentenyl) alanine) and PEG_3 (Fmoc-11-amino-3,6,9-trioxaundecanoic acid), we added 4 equiv of S_5 or PEG_3, 3.9 equiv HCTU, and 20 equiv of DIEA.

After coupling all amino acids, before coupling of PEG_3, the peptides were cyclized using ring closing metathesis (RCM) using first generation Grubbs Catalyst. RCM was performed on resin with 1,2-dichloroethane (DCE) using 0.4 equiv of Grubbs for one hour. This process was repeated for another 1 hr. Upon completion of RCM, PEG_3 was coupled as previously described[107] and labels were added. The peptides were labelled with either 5,6-carboxyfluorescein or D-Biotin depending on experimental needs. When completed with synthesis, the peptides were cleaved from the resin using 95% (v/v) trifluoroacetic acid (TFA), 2.5% (v/v) triisopropylsilane, and 2.5% water and 5 hr rotation at room temperature. Crude peptides were then separated in methyl-*tert*-butyl ether at 4C via centrifugation. The peptide pellet was dried over night with continuous air flow.

Peptide Characterization. Peptides were separated from byproducts using a Zorbax analytical SB-C18 column and RP-HPLC (Agilent 1200). The mobile phase gradient for RP-

HPLC was 10-100% water to acetonitrile with 0.1%TFA at a linear gradient and flow rath of 0.5mL/min. Peptides were characterized using ESI-MS (Agilent 6120 Single Quadrupole). Peptides were purified using the same mobile phase gradient conditions over a semipreparatory column with a flow rate of 4mL/min. Final verification of peptide purity was done via ESI-MS over a Zorbax analytical SB-C18 column.

Peptide quantification was done using methods dependent on the N-terminal label of the peptide of interest. For FAM labeled peptides, quantification was based on peptide fluorescence, which was quantified using absorbance at 495 nm using an extinction coefficient of 69,000 $M^{-1}cm^{-1}$. Biotin-labeled peptide were quantified by measuring decreased absorbance of the 2-hydroxyazobenzene-4'-carboxylic acid (HABA)-avidin complex at 500nm. In the following peptide sequences, * indicates olefinic amino acid S_5 ((S)-N-Fmoc-2-(4-pentenyl) alanine).

The sequence for FAM-FARM Native is FAM- PEG_3-KVADLVQEVQQARDLQNRSK and the mass is 2871.3 (expected = 2872.1).

The sequence for FAM-FARM1 is FAM- PEG_3-K*ADL*QEVQQARDLQNRSK and the mass is 2924.4 (expected = 2924.2).

The sequence for FAM-FARM2 is FAM- PEG_3-KVADL*QEV*QARDLQNRSK and the mass is 2895.0 (expected = 2895.2).

The sequence for FAM-FARM3 is FAM- PEG_3-KVADLVQE*QQA*DLQNRSK and the mass is 2866.8 (expected = 2867.1).

The sequence for FAM-FARM4 is FAM- PEG_3-KVADLVQEVQQ*RDL*NRSK and the mass is 2922.6 (expected = 2923.2).

The sequence for FAM-FARM5 is FAM- PEG_3-KVADLVQEVQQA*DLQ*RSK and the mass is 2851.8 (expected = 2852.2).

The sequence for Biotin-FARM5 is Biotin-PEG_3-KVADLVQEVQQA*DLQ*RSK and the mass is 2719.2 (expected = 2720.2).

Coimmunoprecipitation of LRRK2 and FADD. Briefly, 10 cm plates of HEK293T cells transiently expressing Flag-WT or mutant LRRK2 and V5-FADD (at a 3:1 ratio) and treated with different concentrations of FARM peptides (as indicated in the Figure legends). After 72 hours of treatment, cells were washed and lysed in co-IP buffer for 30 min on ice followed by 15 strokes with a Dounce glass homogenizer, and cleared by centrifugation at 13000 rpm for 15 min. Following pre-clearing with IgG-coupled beads, 40 µl of washed anti-Flag resin (Sigma-Aldrich) per mg of protein was added and the samples incubated under rotation overnight at 4˚C. The following morning, the beads were centrifuged and washed a total of 5X with coIP buffer, before elution in 2X SDS sample buffer at 95˚C for 5 min. The eluate (and input) was separated by SDS-PAGE and membranes probed with anti-Flag (LRRK2) and V5 (FADD).

Cell Uptake. HEK293T cells were seeded at 20,000 cells/well on 8-well chamber slides (BD Biosciences). Cells were grown overnight in complete DMEM (10% Fetal Bovine Serum and 1% Penicillin Streptomycin). 5µM of FAM labelled peptides were added once cells reached 70% confluence and incubated at 37 °C for 24 hours before staining with Hoechst and fixation with 2% paraformaldehyde. Slides were imaged using an Olympus 1X71 microscope, and three independent uptake experiments were completed.

Assessment of Neuronal Death. Embryonic day 16 (E16) pregnant C57BL mice were used in this study, with primary cortical neurons prepared as described (Antoniou 2018). Briefly, cortices were removed and cut into small pieces followed by enzymatic digestion (trypsin 0.05%

and 100 μg/ml DNAse) and mechanical dissociation. Cells were centrifuged and counted and plated on poly-D-lysine coated glass coverslips at a density of 150,000/cm^2 in BrainPhys neuronal culture medium (StemCell Technologies) supplemented with SM1 Neuronal Supplement (StemCell Technologies), L-glutamine (0.5 mM) and penicillin/streptavidin. After 3-4 DIV, neurons were transfected using Lipofectamine 2000 (ThermoScientific) as per the manufacturer's instructions. Neurons were transfected with Flag-tagged WT or mutant (G2019S) human LRRK2 (as described previously[109]), or un-tagged LRRK2 expressed from the EGFP-pcms vector expressing EGFP under a separate promoter. The following day after transfection, we initiated the treatment of neurons with biotinylated (or fluorescent-tagged) stapled peptides (at 0.1 - 10 μM final concentration). We replenished the peptides in the neuronal medium after 24hr at the indicated concentrations. After three days following transfection, and two days of treatment, the coverslips were washed in PBS and fixed in 3.7% paraformaldehyde for 20min at 4˚C. The neurons were processed for immunofluorescence labeling with the following antibodies: GFP (chicken; Abcam), Flag (M2 mouse; Sigma-Aldrich), active caspase-3 (rabbit; R&D Systems), and DAPI nuclear stain. In the cases where biotinylated peptides were used, we labeled taken up peptide using Alexa647-streptavidin (ThermoScientific). Mounted coverslips were imaged on a Leica TSP5 multi-photon confocal microscope, and the Z-stacks processed in FIJI/ImageJ, and Adobe Photoshop. For quantification of apoptotic neuronal profiles, we used the approach described by Antoniou and colleagues[109].

Assessment of LRRK2 kinase function. To determine whether peptides targeting the LRRK2-FADD PPI could also alter kinase function, we assessed LRRK2 activity in a cellular setting, through the phosphorylation of an endogenous substrate (pT73-Rab10), as well as auto-phosphorylation (pS1292-LRRK2). HEK293T cells were transiently co-transfected (WT,

G2019S-LRRK2 & Flag-Rab10) as above and treated with increasing concentrations of stapled peptide, or as a control, the selective kinase inhibitor MLi-2 (100nM, overnight). Following 72hr of total expression, the cells were washed in cold PBS and collected. Cell lysis was performed, and cell extracts stored at -80˚C until use. The extracts were separated by SDS-PAGE and proteins transferred to nitrocellulose membranes, which were probed for total/pS1292-LRRK2, total/pT73-Rab10, or β-actin. For quantification, the band intensities for phosphorylated Rab10 or LRRK2 were normalized to total expression of the respective protein.

5.5 Chapter 5 Figures

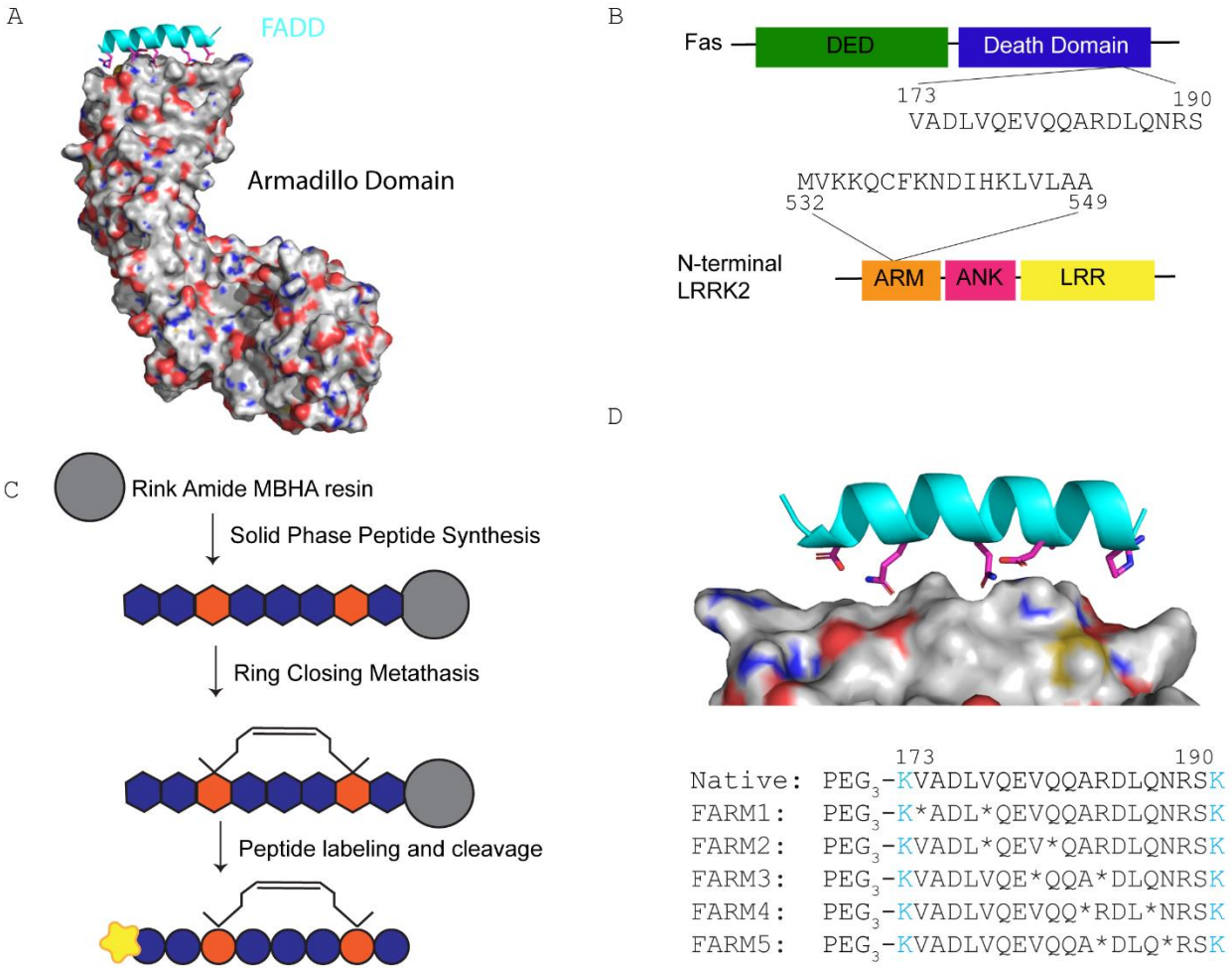

Figure 5.1 Design and synthesis of stapled peptide disruptors of LRRK2-FADD interaction

a, Homology model of LRRK2 Armadillo domain interaction interface with Fas Associated Death Domain (FADD)[109]. **b**, Identification of peptide sequences with Fas (top) and LRRK2 (bottom) responsible for driving the interaction. **c**, Schematic of Fmoc-based Solid Phase Peptide Synthesis (SPPS) and ring-closing metathesis. **d**, Peptide library sequences were designed to preserve amino acids at the predicted interface (magenta). Non-natural amino acids (denoted by *) were substituted on the predicted non-binding interface.

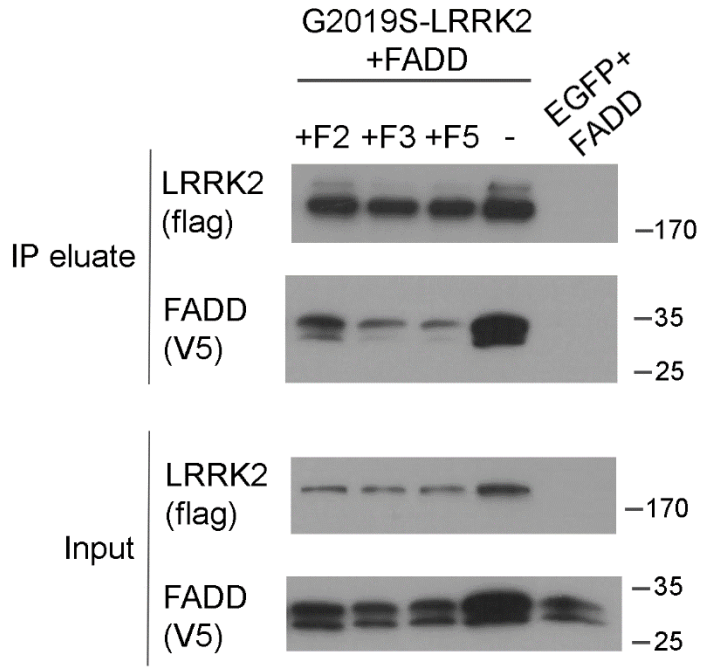

Figure 5.2 Coimmunoprecipitation identifies FARM5 as the lead compound. HEK293T cells transiently expressing Flag-G2019S LRRK2 and V5-FADD were treated with 10μM peptide for 48 hours prior to lysis. While both FARM2 and FARM3 disrupted the interaction, FARM5 had the most pronounced and consistent effect.

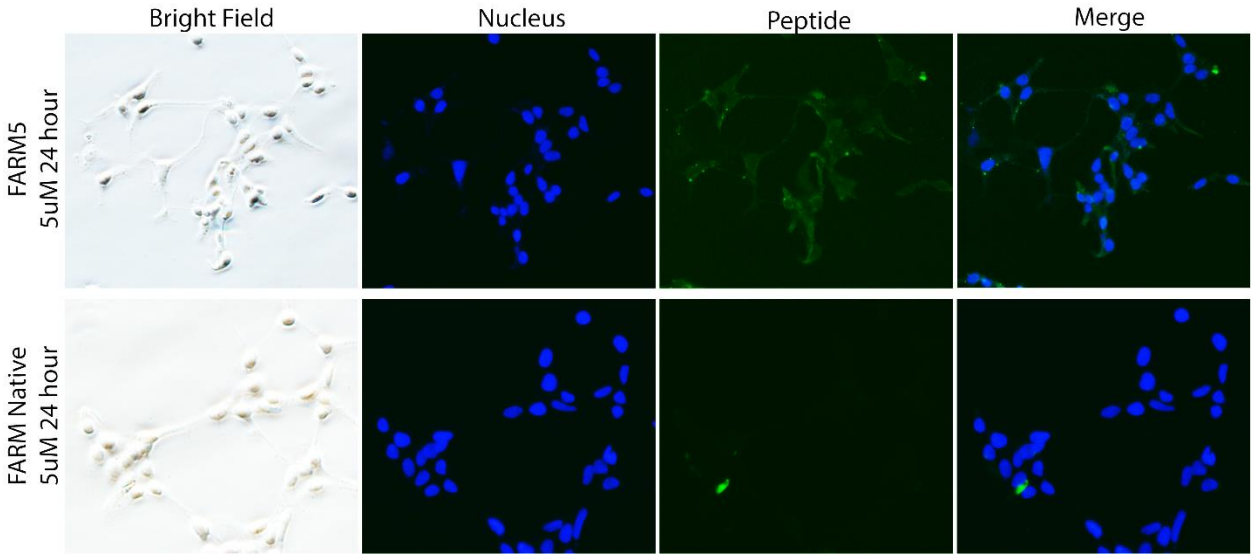

Figure 5.3 FARM5 exhibits superior uptake when compared to Native peptide. HEK293T cells were treated with 5μM of fluorescently labelled peptide for 24 hours. After 24 hours, peptides were stained with Hoechst and fixed before imaging.

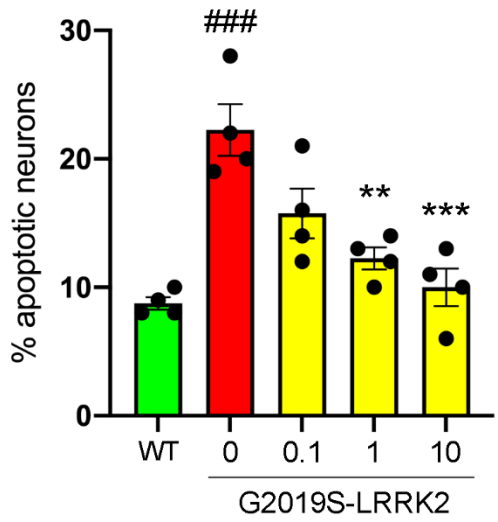

Figure 5.4 FARM5 effectively downregulates apoptosis in neuronal cells. Primary cortical cultures neurons were transfected with mutant LRRK2 then treated with biotinylated peptides (0.1, 1, and 10μM) for 72 hours. The cells were then fixed and processed for immunofluorescence labeling. Dose response of neuroprotection by FARM5 was determined by counting the percentage of transfected neurons expressing chromatin condensation or other apoptotic features such as caspase-3 activation. # n.s.; ** $p<0.01$; *** $p< 0.001$

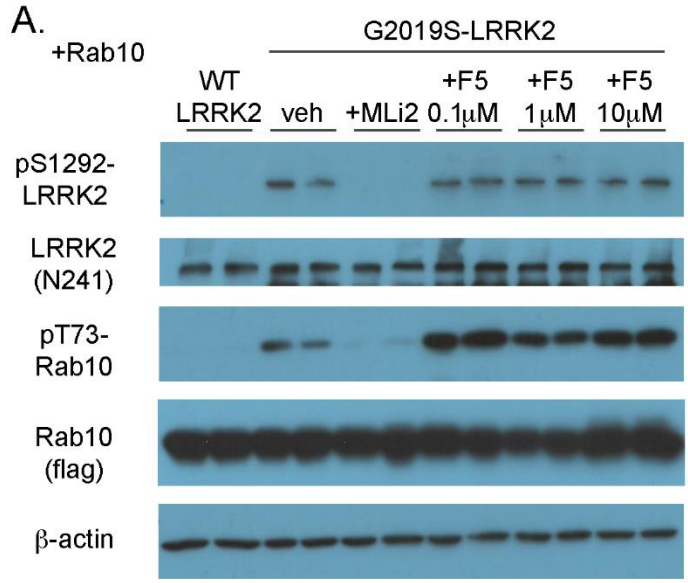

Figure 5.5 FARM5 downregulation of apoptosis is kinase independent. HEK293T cells co-expressing G2019S-LRRK2 and Rab10 exhibit robust increase in both pS1292-LRRK2 and pRab10 levels, which is abolished upon treatment with MLi-2 (100nM, overnight). Upon FARM5 treatment (72 hours), there is no decrease in autophosphorylation, indicating the impact of FARM5 on apoptosis is kinase independent.

CHAPTER 6

ALLOSTERIC SITES FOR LRRK2 REGULATION: PRELIMINARY WORK DESIGNING CONSTRAINED PEPTIDES TO ALTER LRRK2 ACTIVITY AND LOCALIZATION[6]

[6] Helton, L.G., Soliman, A.M., Barbour, K., Kortholt, A. and Kennedy, E.J. (In preparation; To be submitted to *ACS Chem Biol)* **2022**

- Portions of the work to characterize Rab-based inhibitors of LRRK2 were done in collaboration with Soliman, A.M. and Kortholt, A. from the University of Groningen

6.1 Abstract

Efforts to understand how pathogenic LRRK2 is regulated by both itself and upstream proteins has resulted in the identification of Rab29 as an upstream regulator of LRRK2 and multiple helices within LRRK2 itself as potential mediators of activity and localization. Rab29 recruits LRRK2 to the Trans Golgi Network (TGN) via a direct PPI, where it acts on downstream substrates in the area. Some pathogenic LRRK2 mutations are more readily recruited by Rab29 to the TGN, which is directly associated with an increase in kinase activity. Here we show the design and early-stage characterization of constrained peptides designed to disrupt this interaction and return LRRK2 activity to wild type levels. In addition to modulation extramolecular PPIs, we also examine interfaces within LRRK2 that contribute elongated binding interfaces poised to intramolecular modulate LRRK2 structure and function. Specifically, the C-terminal helix of the WD40 domain has been reported to drive LRRK2 association with the microtubules, and it also mediates cross-domain intramolecular interactions within LRRK2. In addition to the C-terminal helix, there is a helix within the COR domain of LRRK2 that is embedded between the COR and kinase domains to potential play a role in modulating kinase activity. Here we report the design and early-stage characterization of multiple constrained peptides targeted at allosteric regulation of LRRK2 activity.

6.2 Introduction: Association between LRRK2 and Rab29

A subset of Rab GTPases, which are master regulators of cell trafficking, have been identified as downstream substrates of LRRK2[61, 66]. Pathogenic LRRK2 mutations within the Roc and COR domains (R1441G/C and Y1699C) do not have the same stimulating effect on LRRK2 kinase activity as pathogenic mutations within the kinase domain (G2019S, I2020T)[62, 125]. Early studies to identify proteins acting upstream of LRRK2 identified Rab29 as operating

in a pathway common to LRRK2[198], and this association was later identified as a direct interaction[72]. Rab29 binds to LRRK2 via its Ankyrin domain to recruit LRRK2 to the trans Golgi Network, and pathogenic mutations that promote GTP binding (R1441C/G and Y1699C) exhibit increased levels of this recruitment[72]. Later work to characterize this pathway in mice tissues and cell lines revealed Rab29 expression or lack-thereof had no significant impact on LRRK2 activity, which is in direct contrast to previous *in vitro* analysis[199].

Here, we sought to design constrained peptides to mimic the LRRK2-binding region of Rab29 to determine the prevalence of this interaction across multiple cell lines and model systems. Given the homology of Rab GTPases, we created a library of homologous Rab-mimicking peptides for Rab29, Rab32, and Rab10 to identify how small changes in sequence could alter the association with LRRK2 and potential effect on downstream activity. Here we show that these peptides permeate cells and, in some cases, bind to LRRK2. Future work to characterize these peptides will focus on determining how treatment impacts downstream kinase activity and cellular activity *in vitro*.

6.3 Results and Discussion: Association between LRRK2 and Rab29

While previous work identified Rab29 as an upstream regulator of LRRK2, there is not currently a crystal structure available of this interaction[72]. Thus, to design peptides, we examined the structure of the interaction between Varp and Rab32[200], which is a homologous interaction. Using this structure, we identified a helical region of Rab32 that greatly contributes to the protein-protein interface [**Figure 6.1**]. We then ran sequence alignment to compare the Rab32 sequence with Rab29 and Rab10 [**Figure 6.1**]. After identifying the sequences of interest, we then designed a library of peptides for each Rab GTPase with shifting staple positions and improved charge [**Figure 6.1**].

Early-stage characterization of these compounds revealed that stapled placement greatly impacted the cellular uptake of Rab29 and Rab32 compounds, while Rab32 compounds seemed localized to vesicles within the cell [**Figure 6.2**]. Both Rab29 and Rab32 libraries were able to bind to LRRK2 in vitro, while Rab10 peptides did not [**Figure 6.3**]. This work lays the foundation for the design of Rab mimetics to bind LRRK2, and future work could focus on elucidating how regulation of LRRK2:Rab with constrained peptides alters downstream pathways.

6.5 Results and Discussion: Embedded helices regulating LRRK2

LRRK2 is a large, complex protein kinase with multiple domains contributing to distant interdomain contacts that likely regulate the overall secondary structure of the protein[92]. With the recent release of the full-length structure of LRRK2[75], we identified multiple helices embedded within LRRK2 that facilitate interdomain contact, as discussed in Chapter 2. Here we discuss the design and early-stage characterization of two peptide libraries based on helices within LRRK2 that could play a critical role in self-regulating LRRK2 activity.

We first identified a helix within the COR domain of LRRK2, termed “NCIP”, which is composed of amino acid residues 1771 through 1791. Recently structure information highlighted the role of this peptide in stabilizing the COR domain, directly interacting with the Roc domain, and forming an elongated interface with the kinase domain [**Figure 6.4A**]. Due to the diverse contacts involving the NCIP peptide, we sought to develop a library of mimetics to better understand how it regulates LRRK2 structure and downstream function. We designed peptides to conserve critical amino acids and incorporated olefinic amino acids along the non-binding interface using the previously described rational design method [**Figure 6.4B]** (chapter 4).

We first sought to determine if the NCIP peptides could permeate cells, and all constrained peptides were able to effectively permeate cells at a concentration of 10μM in 8 hours [**Figure 6.4C**]. We next aimed to identify whether the NCIP peptides could effectively downregulate LRRK2 kinase activity due to binding the kinase domain by measuring downstream substrate phosphorylation of Rab10 in A549 cells. While NCIP4 was able to partially inhibit substrate phosphorylation in A549 cells, this effect was inconsistent [**Figure 6.4D**]. Due to the drawbacks of the cell systems in place to measure endogenous LRRK2 phosphorylation, identification of an alternate method of measuring LRRK2 kinase activity could be useful for better characterization of the NCIP compounds.

Another helix we were interested in mimicking was the C-terminal helix of the WD40 domain, which is largely distant from the WD40 domain itself in favor of binding directly onto the kinase domain[75]. Further, point mutations within this region of the WD40 domain have been linked to altered 14-3-3 binding and microtubule association, further identifying this helix as a regulator of LRRK2 activity and localization[74, 121].

To maintain the physiological functions of the peptide, we preserved amino acids contributing with both the kinase protein-protein interaction interface and C-terminal residues linked to localization [**Figure 6.5A**]. We further performed an *in silico* alanine scan and designed a library of three peptides with shifting staple positions along the non-binding interface [**Figure 6.5A**]. The WD40 peptides exhibited extensive uptake, but the peptide often aggregated within the cell, which is likely due to the long, hydrophobic characteristics of the peptide [**Figure 6.5B**].

Moving forward, we truncated the WD40 helices into three different sections to decrease both the size and hydrophobicity of the compounds [**Figure 6.5C**], which yielded three truncated peptides. Preliminary work to characterize these compounds showed improved uptake when

compared to full length WD1-3 helices and slight downregulation of kinase activity [**Figure 6.5D**]. Work to optimize and characterize these compounds is ongoing.

6.5 Methods

Peptide synthesis, purification, characterization, and quantification was performed as previously described [107] (chapter 3). Cell uptake and pulldowns for Rab peptides were performed as previously described in the lab of Arjan Kortholt[107] (chapter 3). Cell uptake and phosphorylation assays for NCIP and WD40 peptides were performed as previously described in the lab of Eileen Kennedy (chapter 3).

6.6 Chapter 6 Figures

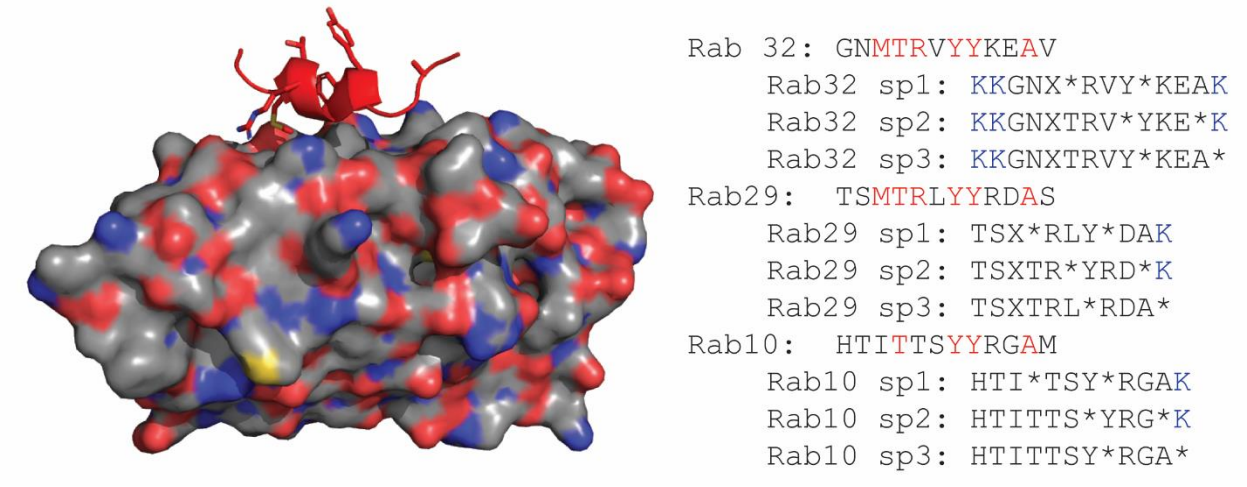

Figure 6.1 Designing Rab-mimicking peptide library. Structure of the interaction between VARP(grey, colored by charge) and Rab32 (red) is shown on the left (PDB: 4CYM)[200]. Side chains of residues conserved between Rab32 and Rab29 are shown as sticks. On the right, native sequences for Rab32, Rab29, and Rab10 are shown, with any matching residues shown in red. Below each Native Rab sequence is a list of peptides designed to mimic the Rab sequence with olefinic amino acids depicted as * and Norleucine depicted as X. Additionally, Lysines (denoted K) were added to some sequences to improve overall charge and solubility.

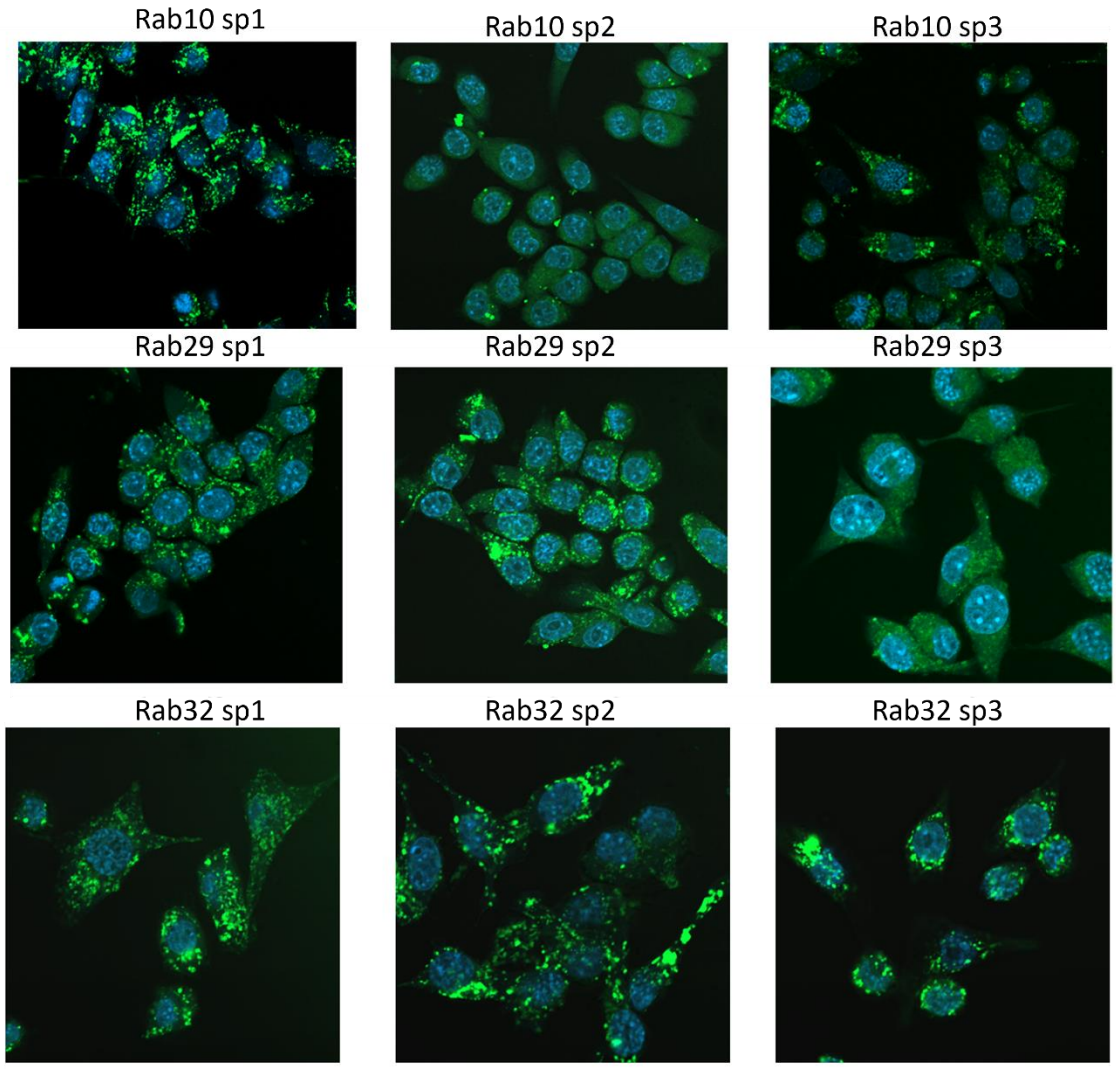

Figure 6.2 Rab-mimicking peptides permeate cells. RAW264.7 cells were treated with 10μM peptide for 6 hours; at which time they were DAPI stained and imaged via fluorescence microscopy.

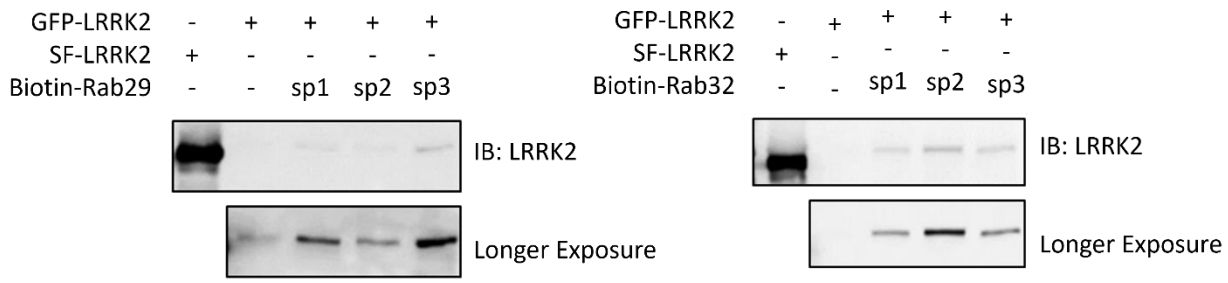

Figure 6.3. Rab29 and Rab32 peptides bind LRRK2 *in cellulo*. HEK293T cells were transiently transfected with GFP-LRRK2 and SF-LRRK2. Cells were then lysed, and lysate was incubated with biotin-labelled peptide at 4C overnight. Pulldowns were performed with streptavidin resin, and the peptide-protein complex was separated from supernatant as described in Chapter 3.

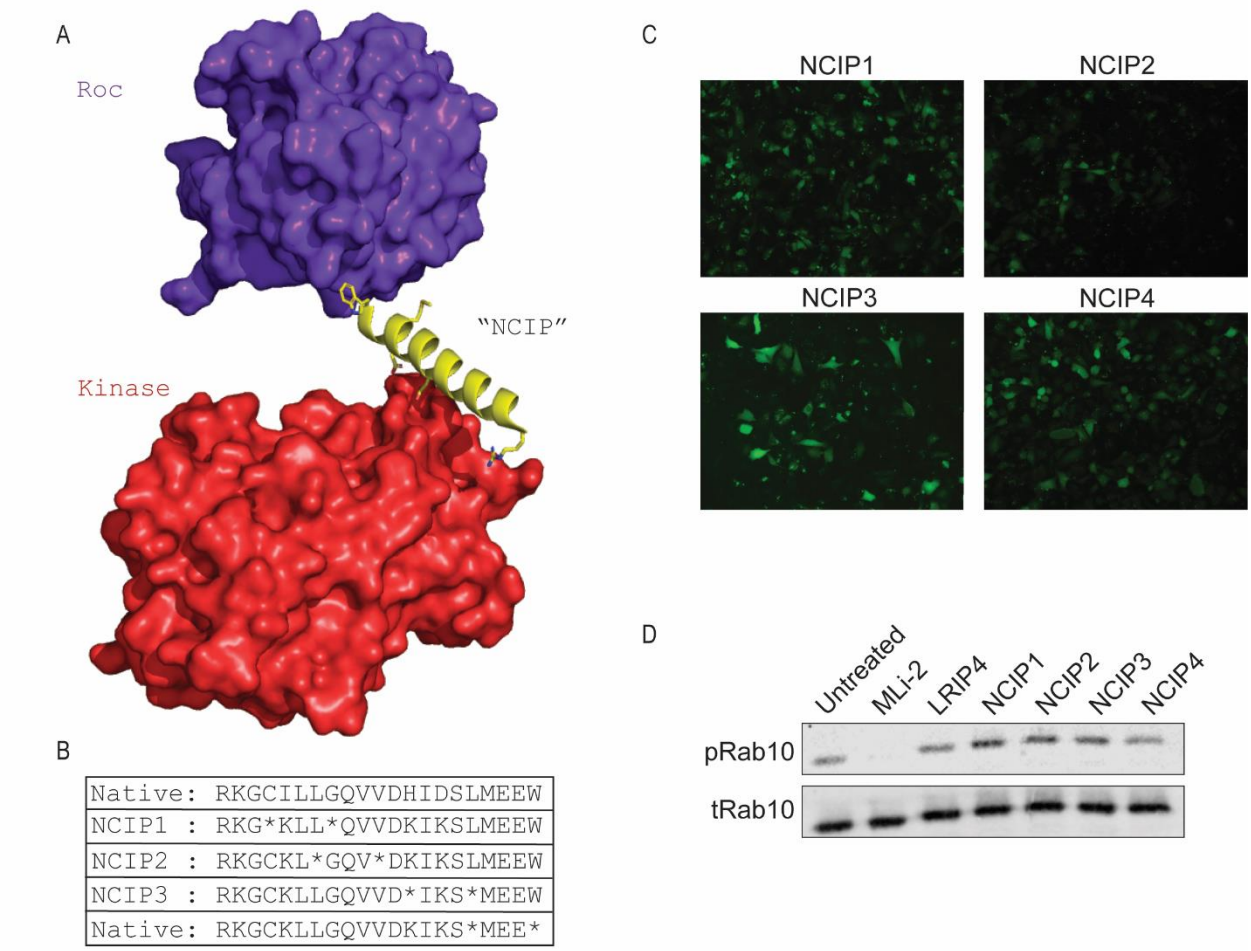

Figure 6.4 Design and Characterization of NCIP Peptides. a, NCIP (yellow) forms an elongated interface with the kinase domain (red) and hydrophobic contacts with the Roc domain (purple). Generated with PDB:7LHT[75]. **b**, NCIP peptide library compared to native sequence. Lysines (K) were introduced to promote solubility. **c**, HEK293 cells were treated with 10μM FAM labelled peptide for 8 hours prior to fixation. Cells were imaged using confocal microscopy. **d**, A549 cells were treated overnight with 10μM peptide in complete DMEM. After 16 hours, cells were lysed in 1x Laemmeli, boiled, and proteins separated via SDS-PAGE.

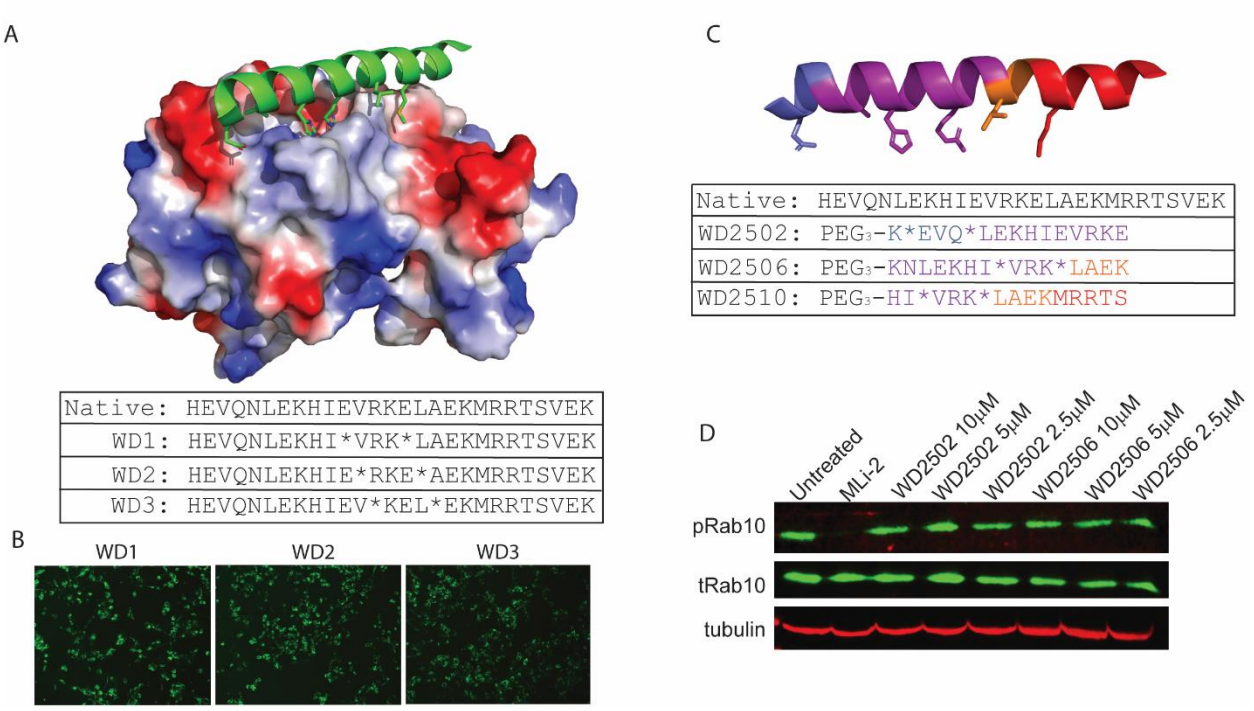

***Figure 6.5 Design and Characterization of WD40 Peptides*. a,** Initial full-length C-terminal helix design and library. WD40 helix is shown in green and electrostatic potential of the kinase domain is shown as surface. Peptide library is listed. **b,** RAW Macrophages were treated with FAM labelled peptide for 8 hours prior to fixation and imaging via fluorescence microscopy. **c,** Truncated WD40 helices were designed to improve hydrophilicity of the compounds. Shared residues are color coded. **d,** A549 cells were treated with truncated peptides for 8 hours prior to cell lysis and separation via SDS-PAGE. Neither WD2502 nor WD2506 showed significant impact on kinase activity. Synthesis of WD2510 was not successful.

CHAPTER 7

CONCLUSIONS

7.1 Summary of Results

In summary, we have utilized all-hydrocarbon stapled peptides to effectively disrupt multiple protein-protein interactions that drive LRRK2-mediated Parkinson's Disease pathogenesis. This work serves as a proof of concept that allosteric inhibition of LRRK2 can reverse PD-related activity to wild type levels without directly inhibiting the catalytic core of the kinase domain. While kinase inhibition of LRRK2 is still widely being pursued due to its therapeutic potential[84, 98, 101], we have now verified allosteric targeting of PPIs involving LRRK2 as a research area with therapeutic promise.

The association of LRRK2 dimerization and its catalytic activity has long been a point of interest in understanding how dimerization contributes to disease pathogenesis. Prior to this work, efforts to discern the role of dimerization were difficult due to the complex signaling network and sheer size of LRRK2 (reviewed here [190]). Due to the difficulty in purifying full-length LRRK2, work do understand how LRRK2 dimerization alters activity was primarily reliant on either bacterial homologs or *in vitro* analysis of endogenous or exogenous LRRK2 expression[70, 162, 201]. Our aim was to develop a tool that would allow for direct disruption of LRRK2 dimerization via an allosteric binding site, which would allow researchers to draw more direct conclusions regarding how dimerization contributes to pathogenesis. With the design and development of LRIP4[107] and ECOR peptides (Chapter 4), we have successfully designed allosteric inhibitors of LRRK2 dimerization that validate this PPI as a potential therapeutic target and validate constrained peptides as a potential therapeutic approach.

Looking beyond the dimerization interface, we also developed a lead constrained peptide candidate to disrupt the interaction between LRRK2 and Fas Associated Death Domain (FADD), an association that's made more prevalent with the introduction of pathogenic LRRK2 mutations[109]. By disrupting this interaction, we can decrease levels of apoptosis *in vitro* in a kinase-independent manner (chapter 5). This work highlights the importance of PPIs in driving LRRK2 pathogenesis and identifies the need for more specific forms of LRRK2 regulation.

Since its identification as a major contributor to the genetic form of Parkinson's Disease in 2002, the work surround LRRK2 has evolved as a rapid pace. In 2016, a homology model was developed to help identify how interdomain contacts were working to regulate LRRK2 structure and function[92]. Five years later, multiple crystal structures of LRRK2 have been solved, with each structure highlighting new and unique interfaces[73-75]. These structures revealed interfaces composed of elongated helices, which allowed us to utilize constrained peptides. In this dissertation, we report the design and development of constrained peptides as first-in-class allosteric inhibitors of LRRK2.

7.2 Future Directions

With the recent development of new tools to study LRRK2, new downstream substrates, interacting proteins, and associated signaling pathways are still being discovered. In addition to LRRK2 Dimerization and interaction with FADD, Rab29 may also serve as a master upstream regulator of LRRK2 and further identification of the role of this pathway *in vivo* could highlight a unique potential target (chapter 7). Continuing to develop the constrained peptides described herein, both *in vitro* and *in vivo,* can help elucidate the precise pathways by which LRRK2 mediates PD pathogenesis. By better characterizing how PPIs drive LRRK2 pathogenesis, we

can identify new drug targets with therapeutic potential for both LRRK2-mediated PD and potentially the idiopathic form of the disease.

More broadly, this work has further highlighted the opportunity for constrained peptides as both cellular tools and potential therapeutics. The combination of their ability to target previously “undruggable” interfaces, permeate cells to bind intracellular targets, and outcompete PPIs makes constrained peptides a unique class of therapeutics. With multiple constrained peptides currently in the therapeutic pipeline[196], this work identifies LRRK2 as a prime target for future therapeutic development.

References

1. Arkin, M.R., Y. Tang, and J.A. Wells, *Small-molecule inhibitors of protein-protein interactions: progressing toward the reality.* Chem Biol, 2014. **21**(9): p. 1102-14.
2. Nero, T.L., et al., *Oncogenic protein interfaces: small molecules, big challenges.* Nat Rev Cancer, 2014. **14**(4): p. 248-62.
3. Thompson, T.B., et al., *Protein-protein interactions in neurodegenerative diseases: A conspiracy theory.* PLoS Comput Biol, 2020. **16**(10): p. e1008267.
4. Lu, H., et al., *Recent advances in the development of protein-protein interactions modulators: mechanisms and clinical trials.* Signal Transduct Target Ther, 2020. **5**(1): p. 213.
5. Ran, X. and J.E. Gestwicki, *Inhibitors of protein-protein interactions (PPIs): an analysis of scaffold choices and buried surface area.* Curr Opin Chem Biol, 2018. **44**: p. 75-86.
6. Bullock, B.N., A.L. Jochim, and P.S. Arora, *Assessing helical protein interfaces for inhibitor design.* J Am Chem Soc, 2011. **133**(36): p. 14220-3.
7. Azzarito, V., et al., *Inhibition of alpha-helix-mediated protein-protein interactions using designed molecules.* Nat Chem, 2013. **5**(3): p. 161-73.
8. Walensky, L.D. and G.H. Bird, *Hydrocarbon-stapled peptides: principles, practice, and progress.* J Med Chem, 2014. **57**(15): p. 6275-88.
9. Verdine, G.L. and G.J. Hilinski, *Stapled peptides for intracellular drug targets.* Methods Enzymol, 2012. **503**: p. 3-33.
10. Dharanipragada, R., *New modalities in conformationally constrained peptides for potency, selectivity and cell permeation.* Future Med Chem, 2013. **5**(7): p. 831-49.

11. Rosell, M. and J. Fernandez-Recio, *Hot-spot analysis for drug discovery targeting protein-protein interactions.* Expert Opin Drug Discov, 2018. **13**(4): p. 327-338.

12. Stelzl, U., et al., *A human protein-protein interaction network: a resource for annotating the proteome.* Cell, 2005. **122**(6): p. 957-68.

13. Rual, J.F., et al., *Towards a proteome-scale map of the human protein-protein interaction network.* Nature, 2005. **437**(7062): p. 1173-8.

14. Buchwald, P., *Small-molecule protein-protein interaction inhibitors: therapeutic potential in light of molecular size, chemical space, and ligand binding efficiency considerations.* IUBMB Life, 2010. **62**(10): p. 724-31.

15. Linhares, B.M., J. Grembecka, and T. Cierpicki, *Targeting epigenetic protein-protein interactions with small-molecule inhibitors.* Future Med Chem, 2020. **12**(14): p. 1305-1326.

16. Chames, P., et al., *Therapeutic antibodies: successes, limitations and hopes for the future.* Br J Pharmacol, 2009. **157**(2): p. 220-33.

17. Di, L., *Strategic approaches to optimizing peptide ADME properties.* AAPS J, 2015. **17**(1): p. 134-43.

18. Banting, F.G., et al., *Pancreatic Extracts in the Treatment of Diabetes Mellitus.* Can Med Assoc J, 1922. **12**(3): p. 141-6.

19. Elkinton, J.R. and A.D. Hunt, Jr., *Effects of pituitary adrenocorticotropic hormone therapy.* J Am Med Assoc, 1949. **141**(18): p. 1273-9.

20. Lau, J.L. and M.K. Dunn, *Therapeutic peptides: Historical perspectives, current development trends, and future directions.* Bioorg Med Chem, 2018. **26**(10): p. 2700-2707.

21. Walensky, L.D., et al., *Activation of apoptosis in vivo by a hydrocarbon-stapled BH3 helix.* Science, 2004. **305**(5689): p. 1466-70.

22. Shim, S.Y., Y.W. Kim, and G.L. Verdine, *A new i, i + 3 peptide stapling system for alpha-helix stabilization.* Chem Biol Drug Des, 2013. **82**(6): p. 635-42.

23. Walensky, L.D., et al., *A stapled BID BH3 helix directly binds and activates BAX.* Mol Cell, 2006. **24**(2): p. 199-210.

24. Cowell, J.K., et al., *Suppression of Breast Cancer Metastasis Using Stapled Peptides Targeting the WASF Regulatory Complex.* Cancer Growth Metastasis, 2017. **10**: p. 1179064417713197.

25. Manning, G., et al., *The protein kinase complement of the human genome.* Science, 2002. **298**(5600): p. 1912-34.

26. Roskoski, R., Jr., *Properties of FDA-approved small molecule protein kinase inhibitors: A 2022 update.* Pharmacol Res, 2022. **175**: p. 106037.

27. Roskoski, R., Jr., *Classification of small molecule protein kinase inhibitors based upon the structures of their drug-enzyme complexes.* Pharmacol Res, 2016. **103**: p. 26-48.

28. Modi, V. and R.L. Dunbrack, *Kincore: a web resource for structural classification of protein kinases and their inhibitors.* Nucleic Acids Res, 2022. **50**(D1): p. D654-D664.

29. Cromm, P.M., J. Spiegel, and T.N. Grossmann, *Hydrocarbon stapled peptides as modulators of biological function.* ACS Chem Biol, 2015. **10**(6): p. 1362-75.

30. Wu, Y., et al., *Toolbox of Diverse Linkers for Navigating the Cellular Efficacy Landscape of Stapled Peptides.* ACS Chem Biol, 2019. **14**(3): p. 526-533.

31. Blackwell, H.E., et al., *Ring-closing metathesis of olefinic peptides: design, synthesis, and structural characterization of macrocyclic helical peptides.* J Org Chem, 2001. **66**(16): p. 5291-302.

32. Connolly, B.S. and A.E. Lang, *Pharmacological treatment of Parkinson disease: a review.* JAMA, 2014. **311**(16): p. 1670-83.

33. Schekman, R. and E.A. Riley, *Coordinating a new approach to basic research into Parkinson's disease.* Elife, 2019. **8**.

34. Marin, I., *The Parkinson disease gene LRRK2: evolutionary and structural insights.* Mol Biol Evol, 2006. **23**(12): p. 2423-33.

35. Funayama, M., et al., *A new locus for Parkinson's disease (PARK8) maps to chromosome 12p11.2-q13.1.* Ann Neurol, 2002. **51**(3): p. 296-301.

36. Zimprich, A., et al., *The PARK8 locus in autosomal dominant parkinsonism: confirmation of linkage and further delineation of the disease-containing interval.* Am J Hum Genet, 2004. **74**(1): p. 11-9.

37. Paisan-Ruiz, C., et al., *Cloning of the gene containing mutations that cause PARK8-linked Parkinson's disease.* Neuron, 2004. **44**(4): p. 595-600.

38. Di Maio, R., et al., *LRRK2 activation in idiopathic Parkinson's disease.* Sci Transl Med, 2018. **10**(451).

39. Barrett, J.C., et al., *Genome-wide association defines more than 30 distinct susceptibility loci for Crohn's disease.* Nat Genet, 2008. **40**(8): p. 955-62.

40. Hui, K.Y., et al., *Functional variants in the LRRK2 gene confer shared effects on risk for Crohn's disease and Parkinson's disease.* Sci Transl Med, 2018. **10**(423).

41. Witoelar, A., et al., *Genome-wide Pleiotropy Between Parkinson Disease and Autoimmune Diseases.* JAMA Neurol, 2017. **74**(7): p. 780-792.

42. Fava, V.M., et al., *Pleiotropic effects for Parkin and LRRK2 in leprosy type-1 reactions and Parkinson's disease.* Proc Natl Acad Sci U S A, 2019. **116**(31): p. 15616-15624.

43. Wang, D., et al., *Association of the LRRK2 genetic polymorphisms with leprosy in Han Chinese from Southwest China.* Genes Immun, 2015. **16**(2): p. 112-9.

44. Zhang, F.R., et al., *Genomewide association study of leprosy.* N Engl J Med, 2009. **361**(27): p. 2609-18.

45. Zhang, D.F., et al., *Is there an antagonistic pleiotropic effect of a LRRK2 mutation on leprosy and Parkinson's disease?* Proc Natl Acad Sci U S A, 2020. **117**(19): p. 10122-10123.

46. Hartlova, A., et al., *LRRK2 is a negative regulator of Mycobacterium tuberculosis phagosome maturation in macrophages.* EMBO J, 2018. **37**(12).

47. Saunders-Pullman, R., et al., *LRRK2 G2019S mutations are associated with an increased cancer risk in Parkinson disease.* Mov Disord, 2010. **25**(15): p. 2536-41.

48. Inzelberg, R., et al., *The LRRK2 G2019S mutation is associated with Parkinson disease and concomitant non-skin cancers.* Neurology, 2012. **78**(11): p. 781-6.

49. Agalliu, I., et al., *Higher frequency of certain cancers in LRRK2 G2019S mutation carriers with Parkinson disease: a pooled analysis.* JAMA Neurol, 2015. **72**(1): p. 58-65.

50. Berwick, D.C., et al., *LRRK2 Biology from structure to dysfunction: research progresses, but the themes remain the same.* Mol Neurodegener, 2019. **14**(1): p. 49.

51. Rolli-Derkinderen, M., et al., *Is Parkinson's disease a chronic low-grade inflammatory bowel disease?* J Neurol, 2020. **267**(8): p. 2207-2213.

52. Allegra, R., et al., *LRRK2-G2019S mutation is not associated with an increased cancer risk: a kin-cohort study.* Mov Disord, 2014. **29**(10): p. 1325-6.

53. Ruiz-Martinez, J., et al., *Prevalence of cancer in Parkinson's disease related to R1441G and G2019S mutations in LRRK2.* Mov Disord, 2014. **29**(6): p. 750-5.

54. Feng, D.D., W. Cai, and X. Chen, *The associations between Parkinson's disease and cancer: the plot thickens.* Transl Neurodegener, 2015. **4**: p. 20.

55. Gotthardt, K., et al., *Structure of the Roc-COR domain tandem of C. tepidum, a prokaryotic homologue of the human LRRK2 Parkinson kinase.* EMBO J, 2008. **27**(16): p. 2239-49.

56. Terheyden, S., et al., *Revisiting the Roco G-protein cycle.* Biochem J, 2015. **465**(1): p. 139-47.

57. Marin, I., W.N. van Egmond, and P.J. van Haastert, *The Roco protein family: a functional perspective.* FASEB J, 2008. **22**(9): p. 3103-10.

58. Alessi, D.R. and E. Sammler, *LRRK2 kinase in Parkinson's disease.* Science, 2018. **360**(6384): p. 36-37.

59. Schmidt, S.H., et al., *Conformation and dynamics of the kinase domain drive subcellular location and activation of LRRK2.* Proc Natl Acad Sci U S A, 2021. **118**(23).

60. Taylor, S.S., et al., *Kinase Domain Is a Dynamic Hub for Driving LRRK2 Allostery.* Front Mol Neurosci, 2020. **13**: p. 538219.

61. Steger, M., et al., *Phosphoproteomics reveals that Parkinson's disease kinase LRRK2 regulates a subset of Rab GTPases.* Elife, 2016. **5**.

62. Jaleel, M., et al., *LRRK2 phosphorylates moesin at threonine-558: characterization of how Parkinson's disease mutants affect kinase activity.* Biochem J, 2007. **405**(2): p. 307-17.

63. Nichols, R.J., et al., *Substrate specificity and inhibitors of LRRK2, a protein kinase mutated in Parkinson's disease.* Biochem J, 2009. **424**(1): p. 47-60.

64. Rideout, H.J., et al., *The Current State-of-the Art of LRRK2-Based Biomarker Assay Development in Parkinson's Disease.* Front Neurosci, 2020. **14**: p. 865.

65. Taylor, M. and D.R. Alessi, *Advances in elucidating the function of leucine-rich repeat protein kinase-2 in normal cells and Parkinson's disease.* Curr Opin Cell Biol, 2020. **63**: p. 102-113.

66. Steger, M., et al., *Systematic proteomic analysis of LRRK2-mediated Rab GTPase phosphorylation establishes a connection to ciliogenesis.* Elife, 2017. **6**.

67. Cookson, M.R., *The role of leucine-rich repeat kinase 2 (LRRK2) in Parkinson's disease.* Nat Rev Neurosci, 2010. **11**(12): p. 791-7.

68. Kluss, J.H., et al., *Detection of endogenous S1292 LRRK2 autophosphorylation in mouse tissue as a readout for kinase activity.* NPJ Parkinsons Dis, 2018. **4**: p. 13.

69. Sheng, Z., et al., *Ser1292 autophosphorylation is an indicator of LRRK2 kinase activity and contributes to the cellular effects of PD mutations.* Sci Transl Med, 2012. **4**(164): p. 164ra161.

70. Gloeckner, C.J., et al., *The Parkinson disease causing LRRK2 mutation I2020T is associated with increased kinase activity.* Hum Mol Genet, 2006. **15**(2): p. 223-32.

71. Ray, S., et al., *The Parkinson disease-linked LRRK2 protein mutation I2020T stabilizes an active state conformation leading to increased kinase activity.* J Biol Chem, 2014. **289**(19): p. 13042-53.

72. Purlyte, E., et al., *Rab29 activation of the Parkinson's disease-associated LRRK2 kinase.* EMBO J, 2018. **37**(1): p. 1-18.

73. Watanabe, R., et al., *The In Situ Structure of Parkinson's Disease-Linked LRRK2.* Cell, 2020. **182**(6): p. 1508-1518 e16.

74. Deniston, C.K., et al., *Structure of LRRK2 in Parkinson's disease and model for microtubule interaction.* Nature, 2020. **588**(7837): p. 344-349.

75. Myasnikov, A., et al., *Structural analysis of the full-length human LRRK2.* Cell, 2021. **184**(13): p. 3519-3527 e10.

76. Deng, X., et al., *Characterization of a selective inhibitor of the Parkinson's disease kinase LRRK2.* Nat Chem Biol, 2011. **7**(4): p. 203-5.

77. Luerman, G.C., et al., *Phosphoproteomic evaluation of pharmacological inhibition of leucine-rich repeat kinase 2 reveals significant off-target effects of LRRK-2-IN-1.* J Neurochem, 2014. **128**(4): p. 561-76.

78. Ramsden, N., et al., *Chemoproteomics-based design of potent LRRK2-selective lead compounds that attenuate Parkinson's disease-related toxicity in human neurons.* ACS Chem Biol, 2011. **6**(10): p. 1021-8.

79. Zhang, J., et al., *Characterization of TAE684 as a potent LRRK2 kinase inhibitor.* Bioorg Med Chem Lett, 2012. **22**(5): p. 1864-9.

80. Estrada, A.A., et al., *Discovery of highly potent, selective, and brain-penetrant aminopyrazole leucine-rich repeat kinase 2 (LRRK2) small molecule inhibitors.* J Med Chem, 2014. **57**(3): p. 921-36.

81. Chan, B.K., et al., *Discovery of a Highly Selective, Brain-Penetrant Aminopyrazole LRRK2 Inhibitor.* ACS Med Chem Lett, 2013. **4**(1): p. 85-90.

82. Estrada, A.A., et al., *Discovery of highly potent, selective, and brain-penetrable leucine-rich repeat kinase 2 (LRRK2) small molecule inhibitors.* J Med Chem, 2012. **55**(22): p. 9416-33.

83. Fell, M.J., et al., *MLi-2, a Potent, Selective, and Centrally Active Compound for Exploring the Therapeutic Potential and Safety of LRRK2 Kinase Inhibition.* J Pharmacol Exp Ther, 2015. **355**(3): p. 397-409.

84. Henderson, J.L., et al., *Discovery and preclinical profiling of 3-[4-(morpholin-4-yl)-7H-pyrrolo[2,3-d]pyrimidin-5-yl]benzonitrile (PF-06447475), a highly potent, selective, brain penetrant, and in vivo active LRRK2 kinase inhibitor.* J Med Chem, 2015. **58**(1): p. 419-32.

85. Daher, J.P., et al., *Leucine-rich Repeat Kinase 2 (LRRK2) Pharmacological Inhibition Abates alpha-Synuclein Gene-induced Neurodegeneration.* J Biol Chem, 2015. **290**(32): p. 19433-44.

86. Fuji, R.N., et al., *Effect of selective LRRK2 kinase inhibition on nonhuman primate lung.* Sci Transl Med, 2015. **7**(273): p. 273ra15.

87. Baptista, M.A.S., et al., *LRRK2 inhibitors induce reversible changes in nonhuman primate lungs without measurable pulmonary deficits.* Sci Transl Med, 2020. **12**(540).

88. Kett, L.R., et al., *LRRK2 Parkinson disease mutations enhance its microtubule association.* Hum Mol Genet, 2012. **21**(4): p. 890-9.

89. Usmani, A., F. Shavarebi, and A. Hiniker, *The Cell Biology of LRRK2 in Parkinson's Disease.* Mol Cell Biol, 2021. **41**(5).

90. Scott, J.D., et al., *Discovery of a 3-(4-Pyrimidinyl) Indazole (MLi-2), an Orally Available and Selective Leucine-Rich Repeat Kinase 2 (LRRK2) Inhibitor that Reduces Brain Kinase Activity.* J Med Chem, 2017. **60**(7): p. 2983-2992.

91. Wauters, L., W. Versees, and A. Kortholt, *Roco Proteins: GTPases with a Baroque Structure and Mechanism.* Int J Mol Sci, 2019. **20**(1).

92. Guaitoli, G., et al., *Structural model of the dimeric Parkinson's protein LRRK2 reveals a compact architecture involving distant interdomain contacts.* Proc Natl Acad Sci U S A, 2016. **113**(30): p. E4357-66.

93. Gloeckner, C.J., et al., *Phosphopeptide analysis reveals two discrete clusters of phosphorylation in the N-terminus and the Roc domain of the Parkinson-disease associated protein kinase LRRK2.* J Proteome Res, 2010. **9**(4): p. 1738-45.

94. Deyaert, E., A. Kortholt, and W. Versees, *The LRR-Roc-COR module of the Chlorobium tepidum Roco protein: crystallization and X-ray crystallographic analysis.* Acta Crystallogr F Struct Biol Commun, 2017. **73**(Pt 9): p. 520-524.

95. Deng, J., et al., *Structure of the ROC domain from the Parkinson's disease-associated leucine-rich repeat kinase 2 reveals a dimeric GTPase.* Proc Natl Acad Sci U S A, 2008. **105**(5): p. 1499-504.

96. Zhang, P., et al., *Crystal structure of the WD40 domain dimer of LRRK2.* Proc Natl Acad Sci U S A, 2019. **116**(5): p. 1579-1584.

97. Leandrou, E., et al., *Kinase activity of mutant LRRK2 manifests differently in hetero-dimeric vs. homo-dimeric complexes.* Biochem J, 2019. **476**(3): p. 559-579.

98. Deng, X., et al., *Leucine-rich repeat kinase 2 inhibitors: a patent review (2006 - 2011).* Expert Opin Ther Pat, 2012. **22**(12): p. 1415-26.

99. Rocha, E.M., et al., *LRRK2 inhibition prevents endolysosomal deficits seen in human Parkinson's disease.* Neurobiol Dis, 2020. **134**: p. 104626.

100. Wojewska, D.N. and A. Kortholt, *LRRK2 Targeting Strategies as Potential Treatment of Parkinson's Disease.* Biomolecules, 2021. **11**(8).

101. Tasegian, A., et al., *Impact of Type II LRRK2 inhibitors on signaling and mitophagy.* Biochem J, 2021. **478**(19): p. 3555-3573.

102. Garofalo, A.W., et al., *Selective Inhibitors of G2019S-LRRK2 Kinase Activity.* J Med Chem, 2020. **63**(23): p. 14821-14839.

103. Muller, S., et al., *The ins and outs of selective kinase inhibitor development.* Nat Chem Biol, 2015. **11**(11): p. 818-21.

104. Lahiry, P., et al., *Kinase mutations in human disease: interpreting genotype-phenotype relationships.* Nat Rev Genet, 2010. **11**(1): p. 60-74.

105. Schmidt, S.H., et al., *The dynamic switch mechanism that leads to activation of LRRK2 is embedded in the DFGpsi motif in the kinase domain.* Proc Natl Acad Sci U S A, 2019. **116**(30): p. 14979-14988.

106. Mills, R.D., et al., *The Roc-COR tandem domain of leucine-rich repeat kinase 2 forms dimers and exhibits conventional Ras-like GTPase properties.* J Neurochem, 2018. **147**(3): p. 409-428.

107. Helton, L.G., et al., *Allosteric Inhibition of Parkinson's-Linked LRRK2 by Constrained Peptides.* ACS Chem Biol, 2021. **16**(11): p. 2326-2338.

108. Marku, A., et al., *The LRRK2 N-terminal domain influences vesicle trafficking: impact of the E193K variant.* Sci Rep, 2020. **10**(1): p. 3799.

109. Antoniou, N., et al., *A motif within the armadillo repeat of Parkinson's-linked LRRK2 interacts with FADD to hijack the extrinsic death pathway.* Sci Rep, 2018. **8**(1): p. 3455.

110. McGrath, E., et al., *LRRK2 binds to the Rab32 subfamily in a GTP-dependent manner via its armadillo domain.* Small GTPases, 2021. **12**(2): p. 133-146.

111. Haile, Y., et al., *Rab32 connects ER stress to mitochondrial defects in multiple sclerosis.* J Neuroinflammation, 2017. **14**(1): p. 19.

112. Ho, C.C., et al., *The Parkinson disease protein leucine-rich repeat kinase 2 transduces death signals via Fas-associated protein with death domain and caspase-8 in a cellular model of neurodegeneration.* J Neurosci, 2009. **29**(4): p. 1011-6.

113. Deyaert, E., et al., *A homologue of the Parkinson's disease-associated protein LRRK2 undergoes a monomer-dimer transition during GTP turnover.* Nat Commun, 2017. **8**(1): p. 1008.

114. Soliman, A., F.N. Cankara, and A. Kortholt, *Allosteric inhibition of LRRK2, where are we now.* Biochem Soc Trans, 2020. **48**(5): p. 2185-2194.

115. Dong, C.Z., et al., *Identification of peptides interfering with the LRRK2/PP1 interaction.* PLoS One, 2020. **15**(8): p. e0237110.

116. Liu, Z., et al., *LRRK2 phosphorylates membrane-bound Rabs and is activated by GTP-bound Rab7L1 to promote recruitment to the trans-Golgi network.* Hum Mol Genet, 2018. **27**(2): p. 385-395.

117. Eguchi, T., et al., *LRRK2 and its substrate Rab GTPases are sequentially targeted onto stressed lysosomes and maintain their homeostasis.* Proc Natl Acad Sci U S A, 2018. **115**(39): p. E9115-E9124.

118. Gomez, R.C., et al., *Membrane association but not identity is required for LRRK2 activation and phosphorylation of Rab GTPases.* J Cell Biol, 2019. **218**(12): p. 4157-4170.

119. Rosenquist, M., et al., *Evolution of the 14-3-3 protein family: does the large number of isoforms in multicellular organisms reflect functional specificity?* J Mol Evol, 2000. **51**(5): p. 446-58.

120. Aitken, A., *14-3-3 proteins on the MAP*. Trends Biochem Sci, 1995. **20**(3): p. 95-7.

121. Manschwetus, J.T., et al., *Binding of the Human 14-3-3 Isoforms to Distinct Sites in the Leucine-Rich Repeat Kinase 2.* Front Neurosci, 2020. **14**: p. 302.

122. Furukawa, Y., et al., *Demonstration of the phosphorylation-dependent interaction of tryptophan hydroxylase with the 14-3-3 protein.* Biochem Biophys Res Commun, 1993. **194**(1): p. 144-9.

123. Fu, H., R.R. Subramanian, and S.C. Masters, *14-3-3 proteins: structure, function, and regulation.* Annu Rev Pharmacol Toxicol, 2000. **40**: p. 617-47.

124. Li, X., et al., *Phosphorylation-dependent 14-3-3 binding to LRRK2 is impaired by common mutations of familial Parkinson's disease.* PLoS One, 2011. **6**(3): p. e17153.

125. Nichols, R.J., et al., *14-3-3 binding to LRRK2 is disrupted by multiple Parkinson's disease-associated mutations and regulates cytoplasmic localization.* Biochem J, 2010. **430**(3): p. 393-404.

126. Stevers, L.M., et al., *Structural interface between LRRK2 and 14-3-3 protein.* Biochem J, 2017. **474**(7): p. 1273-1287.

127. Ballone, A., F. Centorrino, and C. Ottmann, *14-3-3: A Case Study in PPI Modulation.* Molecules, 2018. **23**(6).

128. Muda, K., et al., *Parkinson-related LRRK2 mutation R1441C/G/H impairs PKA phosphorylation of LRRK2 and disrupts its interaction with 14-3-3.* Proc Natl Acad Sci U S A, 2014. **111**(1): p. E34-43.

129. Foote, M. and Y. Zhou, *14-3-3 proteins in neurological disorders.* Int J Biochem Mol Biol, 2012. **3**(2): p. 152-64.

130. Slone, S.R., et al., *Increased 14-3-3 phosphorylation observed in Parkinson's disease reduces neuroprotective potential of 14-3-3 proteins.* Neurobiol Dis, 2015. **79**: p. 1-13.

131. Mabonga, L. and A.P. Kappo, *Protein-protein interaction modulators: advances, successes and remaining challenges.* Biophys Rev, 2019. **11**(4): p. 559-581.

132. Helton, L.G. and E.J. Kennedy, *Targeting Plasmodium with constrained peptides and peptidomimetics.* IUBMB Life, 2020. **72**(6): p. 1103-1114.

133. Ikenoue, T., et al., *A rationally designed bicyclic peptide remodels Abeta42 aggregation in vitro and reduces its toxicity in a worm model of Alzheimer's disease.* Sci Rep, 2020. **10**(1): p. 15280.

134. Ribaric, S., *Peptides as Potential Therapeutics for Alzheimer's Disease.* Molecules, 2018. **23**(2).

135. Bouvier, B., *Protein-Protein Interface Topology as a Predictor of Secondary Structure and Molecular Function Using Convolutional Deep Learning.* J Chem Inf Model, 2021. **61**(7): p. 3292-3303.

136. Fulton, M.D., et al., *Conformationally constrained peptides target the allosteric kinase dimer interface and inhibit EGFR activation.* Bioorg Med Chem, 2018. **26**(6): p. 1167-1173.

137. Laxio Arenas, J., J. Kaffy, and S. Ongeri, *Peptides and peptidomimetics as inhibitors of protein-protein interactions involving beta-sheet secondary structures.* Curr Opin Chem Biol, 2019. **52**: p. 157-167.

138. Wendt, M., et al., *Bicyclic beta-Sheet Mimetics that Target the Transcriptional Coactivator beta-Catenin and Inhibit Wnt Signaling.* Angew Chem Int Ed Engl, 2021. **60**(25): p. 13937-13944.

139. Bird, G.H., et al., *Stapled HIV-1 peptides recapitulate antigenic structures and engage broadly neutralizing antibodies.* Nat Struct Mol Biol, 2014. **21**(12): p. 1058-67.

140. Muppidi, A., et al., *Rational design of proteolytically stable, cell-permeable peptide-based selective Mcl-1 inhibitors.* J Am Chem Soc, 2012. **134**(36): p. 14734-7.

141. Baggio, C., et al., *N-locking stabilization of covalent helical peptides: Application to Bfl-1 antagonists.* Chem Biol Drug Des, 2020. **95**(4): p. 412-426.

142. Fasan, R., et al., *Using a beta-hairpin to mimic an alpha-helix: cyclic peptidomimetic inhibitors of the p53-HDM2 protein-protein interaction.* Angew Chem Int Ed Engl, 2004. **43**(16): p. 2109-12.

143. White, A.M., et al., *Application and Structural Analysis of Triazole-Bridged Disulfide Mimetics in Cyclic Peptides.* Angew Chem Int Ed Engl, 2020. **59**(28): p. 11273-11277.

144. Kruger, D.M., et al., *Structure-Based Design of Non-natural Macrocyclic Peptides That Inhibit Protein-Protein Interactions.* J Med Chem, 2017. **60**(21): p. 8982-8988.

145. Dorsey, E.R., et al., *Projected number of people with Parkinson disease in the most populous nations, 2005 through 2030.* Neurology, 2007. **68**(5): p. 384-6.

146. Dauer, W. and S. Przedborski, *Parkinson's disease: mechanisms and models.* Neuron, 2003. **39**(6): p. 889-909.

147. Klein, C. and A. Westenberger, *Genetics of Parkinson's disease.* Cold Spring Harb Perspect Med, 2012. **2**(1): p. a008888.

148. Duvoisin, R.C., *Recent advances in the genetics of Parkinson's disease.* Adv Neurol, 1996. **69**: p. 33-40.

149. Polymeropoulos, M.H., et al., *Mutation in the alpha-synuclein gene identified in families with Parkinson's disease.* Science, 1997. **276**(5321): p. 2045-7.

150. Kruger, R., et al., *Ala30Pro mutation in the gene encoding alpha-synuclein in Parkinson's disease.* Nat Genet, 1998. **18**(2): p. 106-8.

151. Farrer, M., et al., *A chromosome 4p haplotype segregating with Parkinson's disease and postural tremor.* Hum Mol Genet, 1999. **8**(1): p. 81-5.

152. Gasser, T., et al., *A susceptibility locus for Parkinson's disease maps to chromosome 2p13.* Nat Genet, 1998. **18**(3): p. 262-5.

153. Simon-Sanchez, J., et al., *Genome-wide association study reveals genetic risk underlying Parkinson's disease.* Nat Genet, 2009. **41**(12): p. 1308-12.

154. Zimprich, A., et al., *Mutations in LRRK2 cause autosomal-dominant parkinsonism with pleomorphic pathology.* Neuron, 2004. **44**(4): p. 601-7.

155. Verstraeten, A., J. Theuns, and C. Van Broeckhoven, *Progress in unraveling the genetic etiology of Parkinson disease in a genomic era.* Trends Genet, 2015. **31**(3): p. 140-9.

156. Biosa, A., et al., *GTPase activity regulates kinase activity and cellular phenotypes of Parkinson's disease-associated LRRK2.* Hum Mol Genet, 2013. **22**(6): p. 1140-56.

157. Mata, I.F., et al., *LRRK2 in Parkinson's disease: protein domains and functional insights.* Trends Neurosci, 2006. **29**(5): p. 286-93.

158. Li, J.Q., L. Tan, and J.T. Yu, *The role of the LRRK2 gene in Parkinsonism.* Mol Neurodegener, 2014. **9**: p. 47.

159. Tolosa, E., et al., *LRRK2 in Parkinson disease: challenges of clinical trials.* Nat Rev Neurol, 2020. **16**(2): p. 97-107.

160. Berger, Z., K.A. Smith, and M.J. Lavoie, *Membrane localization of LRRK2 is associated with increased formation of the highly active LRRK2 dimer and changes in its phosphorylation.* Biochemistry, 2010. **49**(26): p. 5511-23.

161. James, N.G., et al., *Number and brightness analysis of LRRK2 oligomerization in live cells.* Biophys J, 2012. **102**(11): p. L41-3.

162. Greggio, E., et al., *The Parkinson disease-associated leucine-rich repeat kinase 2 (LRRK2) is a dimer that undergoes intramolecular autophosphorylation.* J Biol Chem, 2008. **283**(24): p. 16906-14.

163. Nichols, W.C., et al., *Genetic screening for a single common LRRK2 mutation in familial Parkinson's disease.* Lancet, 2005. **365**(9457): p. 410-2.

164. Kachergus, J., et al., *Identification of a novel LRRK2 mutation linked to autosomal dominant parkinsonism: evidence of a common founder across European populations.* Am J Hum Genet, 2005. **76**(4): p. 672-80.

165. Bonifati, V., *Parkinson's disease: the LRRK2-G2019S mutation: opening a novel era in Parkinson's disease genetics.* Eur J Hum Genet, 2006. **14**(10): p. 1061-2.

166. West, A.B., et al., *Parkinson's disease-associated mutations in leucine-rich repeat kinase 2 augment kinase activity.* Proc Natl Acad Sci U S A, 2005. **102**(46): p. 16842-7.

167. Bendzunas, N.G., et al., *Investigating PKA-RII specificity using analogs of the PKA:AKAP peptide inhibitor STAD-2.* Bioorg Med Chem, 2018. **26**(6): p. 1174-1178.

168. Manschwetus, J.T., et al., *A Stapled Peptide Mimic of the Pseudosubstrate Inhibitor PKI Inhibits Protein Kinase A.* Molecules, 2019. **24**(8).

169. Hanold, L.E., M.D. Fulton, and E.J. Kennedy, *Targeting kinase signaling pathways with constrained peptide scaffolds.* Pharmacol Ther, 2017. **173**: p. 159-170.

170. Gilsbach, B.K., et al., *Roco kinase structures give insights into the mechanism of Parkinson disease-related leucine-rich-repeat kinase 2 mutations.* Proc Natl Acad Sci U S A, 2012. **109**(26): p. 10322-7.

171. Deyaert, E., et al., *Structure and nucleotide-induced conformational dynamics of the Chlorobium tepidum Roco protein.* Biochem J, 2019. **476**(1): p. 51-66.

172. Nguyen, A.P. and D.J. Moore, *Understanding the GTPase Activity of LRRK2: Regulation, Function, and Neurotoxicity.* Adv Neurobiol, 2017. **14**: p. 71-88.

173. Wu, C.X., et al., *Parkinson's disease-associated mutations in the GTPase domain of LRRK2 impair its nucleotide-dependent conformational dynamics.* J Biol Chem, 2019. **294**(15): p. 5907-5913.

174. Blackwell, H.E. and R.H. Grubbs, *Highly Efficient Synthesis of Covalently Cross-Linked Peptide Helices by Ring-Closing Metathesis.* Angew Chem Int Ed Engl, 1998. **37**(23): p. 3281-3284.

175. Yin, G., et al., *alpha-Synuclein interacts with the switch region of Rab8a in a Ser129 phosphorylation-dependent manner.* Neurobiol Dis, 2014. **70**: p. 149-61.

176. Saez-Atienzar, S., et al., *The LRRK2 inhibitor GSK2578215A induces protective autophagy in SH-SY5Y cells: involvement of Drp-1-mediated mitochondrial fission and mitochondrial-derived ROS signaling.* Cell Death Dis, 2014. **5**: p. e1368.

177. Heo, H.Y., et al., *LRRK2 enhances oxidative stress-induced neurotoxicity via its kinase activity.* Exp Cell Res, 2010. **316**(4): p. 649-56.

178. Kim, J., et al., *LRRK2 kinase plays a critical role in manganese-induced inflammation and apoptosis in microglia.* PLoS One, 2019. **14**(1): p. e0210248.

179. Gardet, A., et al., *LRRK2 is involved in the IFN-gamma response and host response to pathogens.* J Immunol, 2010. **185**(9): p. 5577-85.

180. Nguyen, A.P.T., et al., *Dopaminergic neurodegeneration induced by Parkinson's disease-linked G2019S LRRK2 is dependent on kinase and GTPase activity.* Proc Natl Acad Sci U S A, 2020. **117**(29): p. 17296-17307.

181. Skibinski, G., et al., *Mutant LRRK2 toxicity in neurons depends on LRRK2 levels and synuclein but not kinase activity or inclusion bodies.* J Neurosci, 2014. **34**(2): p. 418-33.

182. Herzig, M.C., et al., *LRRK2 protein levels are determined by kinase function and are crucial for kidney and lung homeostasis in mice.* Hum Mol Genet, 2011. **20**(21): p. 4209-23.

183. Baptista, M.A., et al., *Loss of leucine-rich repeat kinase 2 (LRRK2) in rats leads to progressive abnormal phenotypes in peripheral organs.* PLoS One, 2013. **8**(11): p. e80705.

184. Sen, S., P.J. Webber, and A.B. West, *Dependence of leucine-rich repeat kinase 2 (LRRK2) kinase activity on dimerization.* J Biol Chem, 2009. **284**(52): p. 36346-36356.

185. Daniels, V., et al., *Insight into the mode of action of the LRRK2 Y1699C pathogenic mutant.* J Neurochem, 2011. **116**(2): p. 304-15.

186. Leemans, M., et al., *Allosteric modulation of the GTPase activity of a bacterial LRRK2 homolog by conformation-specific Nanobodies.* Biochem J, 2020. **477**(7): p. 1203-1218.

187. Civiero, L., et al., *Biochemical characterization of highly purified leucine-rich repeat kinases 1 and 2 demonstrates formation of homodimers.* PLoS One, 2012. **7**(8): p. e43472.

188. Carrion, M.D.P., et al., *The LRRK2 G2385R variant is a partial loss-of-function mutation that affects synaptic vesicle trafficking through altered protein interactions.* Sci Rep, 2017. **7**(1): p. 5377.

189. Fernandez-Suarez, M., T.S. Chen, and A.Y. Ting, *Protein-protein interaction detection in vitro and in cells by proximity biotinylation.* J Am Chem Soc, 2008. **130**(29): p. 9251-3.

190. Civiero, L., et al., *Molecular Insights and Functional Implication of LRRK2 Dimerization.* Adv Neurobiol, 2017. **14**: p. 107-121.

191. Bird, G.H., et al., *Hydrocarbon double-stapling remedies the proteolytic instability of a lengthy peptide therapeutic.* Proc Natl Acad Sci U S A, 2010. **107**(32): p. 14093-8.

192. Hanold, L.E., et al., *Design of a selenylsulfide-bridged EGFR dimerization arm mimic.* Bioorg Med Chem, 2015. **23**(12): p. 2761-6.

193. Rideout, H.J., *Neuronal death signaling pathways triggered by mutant LRRK2.* Biochem Soc Trans, 2017. **45**(1): p. 123-129.

194. Smith, W.W., et al., *Kinase activity of mutant LRRK2 mediates neuronal toxicity.* Nat Neurosci, 2006. **9**(10): p. 1231-3.

195. Greggio, E., et al., *Kinase activity is required for the toxic effects of mutant LRRK2/dardarin.* Neurobiol Dis, 2006. **23**(2): p. 329-41.

196. Morrison, C., *Constrained peptides' time to shine?* Nat Rev Drug Discov, 2018. **17**(8): p. 531-533.

197. Melachroinou, K., et al., *Activation of FADD-Dependent Neuronal Death Pathways as a Predictor of Pathogenicity for LRRK2 Mutations.* PLoS One, 2016. **11**(11): p. e0166053.

198. Kuwahara, T., et al., *LRRK2 and RAB7L1 coordinately regulate axonal morphology and lysosome integrity in diverse cellular contexts.* Sci Rep, 2016. **6**: p. 29945.

199. Kalogeropulou, A.F., et al., *Endogenous Rab29 does not impact basal or stimulated LRRK2 pathway activity.* Biochem J, 2020. **477**(22): p. 4397-4423.

200. Hesketh, G.G., et al., *VARP is recruited on to endosomes by direct interaction with retromer, where together they function in export to the cell surface.* Dev Cell, 2014. **29**(5): p. 591-606.

201. Klein, C.L., et al., *Homo- and heterodimerization of ROCO kinases: LRRK2 kinase inhibition by the LRRK2 ROCO fragment.* J Neurochem, 2009. **111**(3): p. 703-15.